Studies on Microcrystalline Cellulose, Cellulose Nanocrystals from Sago Seed Shells and their Composites

Thesis submitted to the
University of Calicut
in partial fulfilment of the requirements
for the award of the degree of

Doctor of Philosophy
in
Chemistry

by

SUBAIR NADUPARAMBATH

DEPARTMENT OF CHEMISTRY
UNIVERSITY OF CALICUT
KERALA

NOVEMBER, 2017

DEPARTMENT OF CHEMISTRY
UNIVERSITY OF CALICUT
THENJIPALAM, MALAPPURAM
KERALA-673 635

Dr. E.Purushothaman **Tel: +91-9447683351**
Professor (Retd.) **E-mail: epurushot@yahoo.com**

Date: …….

CERTIFICATE

This is to certify that the thesis entitled "Studies on Microcrystalline Cellulose, Cellulose Nanocrystals from Sago Seed Shells and their Composites" is an authentic record of the research work carried out by Mr. Subair Naduparambath under my supervision and guidance in partial fulfillment of the requirements for the award of the degree of Doctor of Philosophy in Chemistry under the faculty of Science, University of Calicut, Kerala. The work presented in this thesis has not been presented/ reported earlier for any degree or diploma of any University/Institute.

Calicut University **Dr. E. Purushothaman**

DECLARATION

I hereby declare that the thesis entitled "Studies on Microcrystalline Cellulose, Cellulose Nanocrystals from Sago Seed Shells and their Composites" is an authentic record of the research work carried out by me under the supervision and guidance of Dr. E. Purushothaman, Professor (Retd.) and KSCSTE Emeritus Scientist, Department of Chemistry, University of Calicut, Kerala and that no part of this work has been presented/reported earlier for any degree or diploma of any University/Institute.

Calicut University Subair Naduparambath

……

ACKNOWLEDGEMENTS

There are a number of important people who contributed immensely in making this PhD thesis a reality. It is a pleasure for me to express my sincere gratitude and affection to them in words of acknowledgements. First and foremost, it gives me immense pleasure to express my deep sense of gratitude to my supervisor ***Dr. E. Purushothaman,*** *Professor (Retd.) and KSCSTE Emeritus Scientist, Department of Chemistry, University of Calicut, Kerala for his invaluable advice, instruction, guidance, motivation, constant inspiration and above all for his co-operation and support throughout this research programme.*

I express sincere thanks and gratitude to Prof. P. Raveendran, Head, Dept. of Chemistry, University of Calicut, for his help and co-operation. I am also thankful to the former Head Prof. K. Muraleedharan for help and support during my PhD. Programme.

Also, I am grateful to Dr. M. T. Ramesan, for fruitful suggestions and encouragement.

I also express sincere thanks to Prof. V. M. Abdul Mujeeb, Prof. Abraham Joseph, Dr. N. K. Renuka, Dr. Yahya A. I, Prof. D. Bahulayan, Prof. K. K. Aravindakshan, and Prof. P. Mohammed Shafi for their support and encouragements.

I take this opportunity to express my sincere thanks to my groupmates Sreejith M.P, Aparna K Balan, Shaniba.V, Jinitha T.V and Dipin for their valuable suggestions, help, making pleasant working atmosphere and exchanging their ideas.

I express sincere thanks to Prof. P. Ramakrishnan former Principal Govt. College, Madappally for his help in making FIP a reality and also to Prof. M. Chitralekha Principal Govt. College Madappally. I express my sincere thanks to former Head, Prof. K. P. Jamaluddin, Dept. of Chemistry, Govt. College,

Madappally, Dr. B. Preetha and other faculties. I would like to express my thanks to the University Grant Commission (UGC) and the Collegiate Education Department for giving me the opportunity to complete the research work under FIP scheme.

I express my sincere thanks to my friends Dr. Mujeeb Rahman, Dr. Sanjay Gopal, Binu Noufal, Jithesh, Jasna, Nihmath, Jayakrishnan, Suhailath, Safna Hussain, Shabeer and Jamshihas. My sincere thanks are also to Dr.C. Sareena and Dr. Mehar Al Minnath.

I express my gratitude to my labmates Soumya, Jithin, Jency, Rejeena. Thasnim, Shyam, Shamsiya and other research scholars in the department.

I express my sincere gratitude to all non-teaching staff of the Dept. of Chemistry, University of Calicut.

I also express sincere thanks to Prof. Praydumnan P. P and Dr. Shahin, Dept. of Physics, University of Calicut. I remain very much indebted to Dr. A. Sujith, Asst. Professor of NITC, Calicut, Kerala for providing their facilities and help. A special thanks to Dr. Tania Francis, Asst. Professor, St. Joseph's College, Devagiri, for her help.

I thank the STIC Cochin and SAIF, M.G University for providing instrument facilities.

My deepest gratitude also goes to my family for their love and support. Finally, I would like to thank everybody who was important to the successful realization of this thesis. Above all, I thank almighty Allah

University of Calicut *Subair Naduparambath*

In the memory of my dear Father

CONTENTS

LIST OF TABLES

LIST OF FIGURES

LIST OF SCHEMES

GLOSSARY OF TERMS

ΔH_f	-	Heat of fusion of PVA
ΔH^o_f	-	Heat of fusion of 100% crystalline PVA
θ	-	Diffraction angle
AFM	-	Atomic force microscopy
ASTM	-	American society for testing and materials
ATR-FTIR	-	Attenuated total reflectance FTIR
CI	-	Crystallinity index
CNC	-	Cellulose nanocrystals
CNW	-	Cellulose nanowhiskers
CW	-	Cellulose whiskers
DLS	-	Dynamic light scattering
DSC	-	Differential scanning calorimetry
FTIR	-	Fourier transform infrared
MCC	-	Microcrystalline cellulose
MFC	-	Microfibrillated cellulose
MU	-	Moisture uptake
NFC	-	Nanofibrillated cellulose
nm	-	Nanometer
OTR	-	Oxygen transmission rate
PHA	-	Poly (hydroxy alkanoate)
PVA	-	Poly (vinyl alcohol)
PLA	-	Poly (lactic acid)
PP	-	Polypropylene
RH	-	Relative humidity

SEM	-	Scanning electron microscopy
Tg	-	Glass transition temperature
TG	-	Thermogravimetry
$\mathbf{T_{max}}$	-	Temperature at maximum weight loss
$\mathbf{T_m}$	-	Melting temperature
$\mathbf{T_{on}}$	-	Onset degradation temperature
TEM	-	Tunneling electron microscopy
TEMPO	-	2,2,6,6-tetramethylpiperidine-1-oxyl
UV	-	Ultra-violet
WVTR	-	Water vapor transmission rate
WAXD	-	Wide angle X-ray diffraction
XRD	-	X-ray diffraction.
$\mathbf{X_P}$	-	Degree of crystallinity
ZP	-	Zeta potential

PREFACE

Sago (*Cycas circinalis*) seed shells are unexplored agricultural waste, which are thrown out after taking the pith. The use of seed shells as reinforcement in polymers has been well documented. Hoewever, reports on the isolation of microcrystalline cellulose and cellulose nanocrystals from seed shells are very rare. The main aim of this investigation is the isolation of microcrystalline cellulose, cellulose nanocrystals from sago seed shells and their characterization. Moreover, the utilization of microcrystalline cellulose and cellulose nanocrystals as reinforcements in poly (vinyl alcohol) has also been investigated.

Chapter 1 deals with the general background of composites, natural fiber reinforced composites and nanocomposites. Special reference is given to cellulose nanomaterials. The selections of PVA as potential matrix for the fabrication bio-nanocomposites are justified. A review on microcrystalline cellulose reinforced composites, isolation of nanocellulose and cellulose nanomaterial reinforced composites are given in Chapter 2. The materials, methods and various experimental techniques used in the investigations are briefly discussed in Chapter 3. Establishing the composition of sago seed shells, isolation of microcrystalline cellulose and their characterisation are included in Chapter 4. Development of green composites of MCC reinforced PVA and their optimisations for better properties are described in Chapter 5. Isolation of cellulose nanocrystals from sago seed shells and their characterizations are given in Chapter 6. The fabrication of bio-nanocomposites of PVA reinforced with cellulose nanocrystals and their properties are presented in Chapter 7. In Chapter 8, the development of bio-nanocomposites as barrier membrane for packaging application is explored. The thesis concludes with a summary of the results obtained in the present work and a brief mention on the future prospects.

CHAPTER 1
INTRODUCTION AND OBJECTIVES

Abstract

This chapter gives an account of composites including natural fibre reinforced composites, biocomposites, green composites, nanocomposites and bio-nanocomposites with special relevance to their merits and demerits. The use of PVA as potential biodegradable matrix is discussed. Emphasis is also given to cellulose nanomaterials like microfibrillated cellulose and cellulose nanocrystals. The scope and objectives of the present work have also been highlighted.

1.1 BRIEF BACKGROUND OF COMPOSITES

Polymers or macromolecules are large molecules with very high molecular weight. Polymers can be either natural or synthetic. Synthetic polymers, compared to their natural counterparts have provided undeniable benefits for the development of the society due to their desirable properties having wide range of applications in diverse fields such as packaging, agriculture, food, consumer products, medical appliances, building materials, aerospace materials etc. These polymers have superseded the use of other traditional materials such as metals, glasses and ceramics in a number of fields. Among these, plastics can be moulded into desired article by the application of heat and pressure. Therefore, the attractiveness of plastics lies in their versatility and ability to offer a broad variety of properties, low cost, easy processability and transformation into a myriad of shapes and sizes [1].

Eventhough, polymers are widely used; virgin polymers alone cannot find much use. In fact they are mixed with other materials to get the desired properties. Therefore, when we incorporate materials other than polymers, composites having desired properties in which polymer is the continuous phase (matrix) and added substance as the discontinuous phase (reinforcement) are developed. They are fabricated by the judicious mixing of two or more distinct materials or multiphase materials [2]. Many naturally occurring materials, like wood fibres consist of cellulose microfibrils embedded in an amorphous matrix of lignin and hemicellulose. Bone and teeth composed of inorganic crystals in a matrix of collagen are also composites [3]. Composites can also be made by using metals or ceramics and they are called metal matrix composites and ceramic matrix composites. But here we are concerned with polymer matrix composites. Additives are incorporated into the polymers in order to achieve benefits like reduction in

materials cost, improvement in properties, performance and service life of the end product, ease of processing, reduction in processing cost, minimising degradation during processing and above all the end use. The above properties can be achieved by the use of the following class of materials referred to as fillers, plasticizers, stabilisers, colouring matters, lubricants, flow promoters, cross linking agents etc [4].

Polymer composites, to a greater extent can fulfil many properties like low densities, high tensile strength, high stiffness, resistance to abrasion and corrosion, which are difficult to find in any of the conventional polymers. The main constituents in any composites are matrix, reinforcement and the interface region. Since the interface region is responsible for interaction between the matrix and filler, it is having property different from the bulk matrix because of its closeness to the surface of the filler. Therefore, the adhesion between the reinforcement and the matrix in composite materials play an important role in the final properties of the material, like stress transfer between reinforcement and matrix [5].

1.1.1 Role of fillers

Fillers are the main class of materials which are added either in large/small quantities depending on the requirement; fillers can be either inert or reinforcing. Inert fillers are added to reduce the material cost, without giving any disadvantage to polymer matrix. On the other hand reinforcing fillers have a definite function on the polymer matrix. Most of it will improve the properties of matrix. Improvements can be observed in physical properties like tensile strength, modulus, tear strength, abrasion resistance etc [4]. For any filler, its shape, size, orientation and concentration has a profound effect on the final enhancement in properties of composites. Some examples of common fillers used are presented in **Table 1.1** [6].

Table1.1 Examples of common fillers used.

Type	Examples
Inorganics	Oxides:- Glass (fibres, spheres, hollow spheres, flakes), MgO, SiO_2, Sb_2O_3, Al_2O_3 Hydroxides:-$Al(OH)_3$, $Mg(OH)_2$ Salts:- $CaCO_3$, $BaSO_4$, $CaSO_4$, Phosphates Silicates:-Talc, mica, kaolin, wollastonite, montmorillonite, nanoclays, feldspar, asbestos Metals:-Boron, steel
Organics	Carbon fibres, graphite fibres and flakes, carbon nanotubes, carbon black
Natural polymers	Cellulose fibres, wood flour, flax, cotton, sisal and starch
Synthetic polymers	Polyamide, polyester, aramid, poly (vinyl alcohol) fibres

Fillers are classified as particulate fillers like carbon black, silica, clays, $CaCO_3$, Al_2O_3, $Mg(OH)_2$ etc., and fibrous fillers, which can be either natural like wood flour, wood pulp, cotton flock, glass, mica and asbestos or synthetic like polyesters, nylons, rayons, SiC, boron, aramid fibres etc. Other way of classification is continuous fibres, short fibres, whiskers and flakes. The dispersed phase can be further classified according to particle dimensions as platelets, ellipsoids and spheres. The particles can be of organic or inorganic origin and possess flexible or rigid characteristics [7]. There are different techniques usually employed for composite fabrication, which are listed in **Table 1.2**

Table1.2 Processing methods for composites fabrication [4].

Moulding	Forming	Other
Compression moulding Transfer moulding Injection/jet moulding Blow moulding	Extrusion Spinning Calendaring Thermoforming Casting, slush moulding, Rotomoulding	Lamination Reinforcement and coating

Many polymers including thermoplastics, thermosets and elastomers, can function as matrices. Some common polymers and fillers generally used are presented in **Table1.3**

Table1.3 Polymers and fillers generally used.

Polymers	Fillers
Poly vinyl chloride (PVC)	$CaCO_3$ and kaoline clay
Polypropylene (PP)	$CaCO_3$, talc and wollastonite,
Nylon	Glass fibre, kaoline, talc and wollastonite
Polyformaldehyde	Glass fibre, $CaCO_3$
Polyethylene (PE)	$CaCO_3$ and kaoline
Polyester	Glass fiber
Epoxy	Graphite, kevlar and boron
Rubbers	Carbon black

Polymer matrix composites (PMC) are popular due to their versatility, used in diverse fields for many applications. Moreover, they have low-cost and are made by simple fabrication methods. Polymers reinforced by strong fibrous network permits fabrication of PMCs having, high specific strength, high specific stiffness, high fracture resistance, abrasion resistance,

impact resistance, corrosion resistance, fatigue resistance along with low thermal resistance and high coefficient of thermal expansion [8]. The properties of composites depend up on (i) nature of the matrix (thermosetting, thermoplastic and rubbers) (ii) nature of the reinforcement (iii) interaction between matrix, reinforcement and their compatibility (iv) the orientation, dispersion and shape of reinforcement (particles, flakes, fibres, and laminates).

Glass fibre reinforced plastics (GRP), a typical composite, has excellent tensile strength, compressive strength, light-weight and resistance to chemicals. So it is widely used in aircraft, automobiles, boats, storage tanks, construction, piping, electronics, and sports. Moreover, glass fibres are often substituted by high performance and costly fibres, such as carbon (aramids) or polymeric fibres [3,9]. There are hybrid composites consisting of more than one filler like carbon fibre and aramid, in which carbon fibre provides compressive strength and aramid improves the toughness of the material. Another popular hybrid is a mixture of the carbon fibre and glass fibre. Carbon fibre provides high specific strength, specific modulus and glass fibre provides better toughness and lower material cost [10].

Fibre reinforced plastic composites (FRP) play an important role in vast areas of applications due to their high specific strength and modulus. The manufacture, use and removal of traditional fibre reinforced plastics, usually made of glass, carbon or aramid fibres in thermoplastic and thermoset resins are considered critical because of environmental problems. Composites made from thermosetting resins cannot be reprocessed or recycled. However, a small amount of these thermosetting composites are crushed into powder and used as filler or incinerated to obtain energy in the form of heat. But most of them end up in landfills at the end of their life, though incineration and

dumping in landfills are environmentally undesirable as well as expensive [11].

1.2 NATURAL FIBRE REINFORCED COMPOSITES

For structural and non-structural applications, glass, carbon, kevlar, boron fibre etc., have been used as reinforcing materials in fibre reinforced plastics such as epoxy, unsaturated polyester resins, polyurethanes, or phenolics etc. But these materials are resistant to biodegradation and can create environmental problems [8]. Due to the indiscriminate use of plastic products, their disposal caused damages to the environment. Moreover, the shortage of landfill space, the depletion of petroleum resources and the entrapment by the ingestion of packaging plastics by marine and land animals necessitated efforts for better alternatives [5]. Thus, the current environmental problems, the incomplete combustibility, and demand for recycling methods etc., resulted in the replacement of synthetic fillers or inorganic fillers by natural-organic ones such as natural fibres, wood fibres, starch, etc. The natural fibre reinforced polymer composites have attracted considerable interest as a potential structural material as well as in other applications in the past decades. The attractive features of natural fibres are their low-cost, light-weight, high specific modulus, renewability and biodegradability, no abrasion of the processing equipment, similar moduli and good thermal properties [12]. Vegetable fibres used for composite application are obtained from stem, leaves or fruits etc. Specific stiffness and specific strength of natural fibres and glass fibres are comparable, but they have to be compromised in the mechanical properties of composite constructed from each of these fibres. Great attention is being paid to develop environment-friendly materials by replacing reinforcement like glass, carbon, aramid fibres etc., using natural reinforcing fibres like jute, flax, hemp, etc.,

in synthetic composite matrices. Therefore, the term ‘‘biocomposite’’ came in place of simple composite [13]. Biocomposites derived from renewable resources have been the subject of attention since 1942 when Ford applied soy based plastics in their cars [14].

1.2.1 Biocomposites

Biocomposites can be fabricated using biofibres and petroleum derived polymers like PP, PE, PVC, polyester etc. The advantages of biocomposites include good specific strength, renewable nature, biodegradability, low embodied energy, non-toxicity, bio-compatibility and low cost. However, disadvantages like high water absorption, low durability and variable mechanical properties need mention [15].

Usually the natural fibre composites do not have the same strength as glass fibre composites because of incompatibility between hydrophobic host polymer matrix and hydrophilic natural fibre combined with low thermal resistance of the cellulosic material. Natural fibres are lignocellulosics, hydrophilic in nature composed of cellulose, hemicellulose, lignin, pectin and wax therefore incompatible with hydrophobic thermoplastics such as polyolefin. The major drawback of using these fibres as reinforcements in such matrices results in poor interfacial adhesion between polar hydrophilic fibre and nonpolar hydrophobic matrix and difficulties in mixing due to poor wetting of the fibre with the matrix [16]. Moreover, the processing temperatures of composites to be restricted to 200 ^{0}C as vegetable fibres undergo degradation at higher temperatures which can reduce the choice of matrix. Other problems using natural fibres are, high moisture absorption leading to swelling which manifests in poor mechanical properties further leading to reduction in the dimensional stability of composites, low microbial resistance, susceptibility to rotting, non-uniformity, variation in dimensions

of fibres and their mechanical properties [17]. There are physical treatments such as corona, plasma discharge, γ-ray, UV-bombardment, laser and chemical reactions like alkali treatment, silane treatment, acetylation, peroxide, graft copolymerisation, permanganate treatment, solvent extraction, that are used to modify natural fibre to increase its compatibility with matrix[18–21]. Good compatibility with matrix is essential for getting better properties.

1.2.1.1 *Thermoset biocomposites*

Biofibres are reinforced in polymers like phenolic, epoxies, and polyester resins to form composite materials. These polymers contain reactive groups, which can develop the interfacial interaction. [11].

1.2.1.2. *Thermoplastic biocomposites*

In order to enhance the compatibility, compatibilisers such as maleated ethylene, maleated propylene, acrylic grafted linear polymers or coupling agents are used in hydrophobic matrix composites [11]. Automobile applications represent one of the best opportunities for natural fibre filled thermoplastics due to some distinctive advantages over glass fibre composites [3]. They find applications as seat backs, door panels, pillar cover panels and boot linings [22].

1.2.2 Composition of natural fibres

All plant fibres are composed of cellulose, including bast (stem or soft sclerenchyma) fibres, leaf or hard fibres, seed, fruit, wood, cereal straw, and other grass fibres. Natural fibres can be considered as naturally occurring composites consisting mainly of cellulose fibrils embedded in lignin matrix. Natural fibres are composed of α-cellulose, hemicellulose, lignin, pectins, and

waxes, For this reason, natural fibres are also referred to as cellulosic or lignocellulosic fibres [23]. Not only natural fibres, but agricultural residues are also composed of α-cellulose, hemicellulose, lignin, pectin, and waxes. The composition of different natural fibres are presented in **Table 1.4** [24]

Table 1.4 Composition of different natural fibres

Fibre	Cellulose (wt%)	Hemicellulose (wt%)	Lignin (wt%)	Waxes (wt%)
Bamboo	26–43	30	21–31	-
Flax	71	18.6–20.6	2.2	1.5
Kenaf	72	20.3	9	-
Jute	61–71	14–20	12–13	0.5
Hemp	68	15	10	0.8
Abaca	56–63	20–25	7–9	3
Ramie	68.6–76.2	13–16	0.6–0.7	0.3
Sisal	65	12	9.9	2
Coir	32–43	0.15–0.25	40–45	-
Oil palm	65	-	29	-
Pineapple	81	-	12.7	-
Curaua	73.6	9.9	7.5	-
Wheat straw	38–45	15–31	12–20	-

Cellulose extraction from biomass has been a subject of intense research because there is urgent need for application of green chemistry principles in modern life [25].

The discovery of cellulose dates back to 1838, introduced and isolated by Anselme Payen. Since then extensive studies including its biosynthesis, structure analysis, chemical modification, regeneration of cellulosic materials and applications in various fields are in progress. The

enthusiasm on the research of cellulose had once lost with the emergence of polymer based on fossil fuels. However, the environmental problems and the exhausting fossil resources revived the interests in the research in full swing [26]. Cellulose, being the most abundant natural biopolymer in the world, is a linear homo polymer composed of D-anhydroglucopyranose units (AGU) which are linked together by β-(1→4) glycosidic bonds.

Microcrystalline cellulose (MCC) has been known since late 1800s, also called hydrocellulose, produced by the controlled acid hydrolysis of high purity cellulose fibres and used as commercial product in number of applications. Any source containing cellulose can be used to isolate MCC.

Hemicellulose comprises a group of polysaccharides composed of a combination of 5 and 6 carbon ring sugars. Cellulose microfrbrils are embedded in hemicellulose matrix; they are very hydrophilic, soluble in alkali and hydrolysed by acids. They are composed of β-(1→4) linked D-xylopyranosyl units with side chains containing L-arabinose, D-glucuronic acid, or its 4-O-methyl ether, D-galactose and D-glucose. They act as a compatibilizer between cellulose and lignin. Lignins are found to have five hydroxyl and five methoxyl groups per building unit, the structural unit of lignin molecule are derivatives of 4-hydroxy-3-methoxy phenylpropane, complex hydrocarbon polymer with both aliphatic and aromatic constituents. It is totally amorphous, hydrophobic and imparts rigidity to the plants. Lignin behaves like thermoplastic polymer having glass transition temperature of around 90 ^{0}C and melting temperature of around 170 ^{0}C. Pectins are heteropolysaccharide whose main chain is a modified polymer of glucuronic acid and rhamnose residue. Waxes consist of different types of alcohols [17]. The matrix of natural fibres is provided by lignin, hemicelluloses, and the pectin to hold the cellulosic framework.

1.3 GREEN COMPOSITES

Green composites contain both the matrix and reinforcement biodegradable for enhanced biodegradability. The reinforcement may be biofibres or biopolymers like cellulose, starch etc. Biopolymers are biodegradable and the main products are obtained from renewable resources such as agro resources. They represent interesting alternative route to common nondegradable polymers for short life applications like packaging, agriculture, and biomedical etc. Nevertheless, until now, some of the biopolymers like polylactic acid (PLA), which are fully biodegradable are costly compared to conventional thermoplastic and they are sometimes too weak for practical uses [27].

Synthetic polymers, in general, are non-biodegradable. However, polymers with hydrolysable backbones such as polyesters, polycaprolactone, polyamides, polyurethanes, polyureas, polyanhydrides poly (amide enamine)s, poly (ester amide)s, poly (orthoesters), poly (phosphoesters) and vinyl polymers containing easily oxidisable functional groups like poly (vinyl alcohol), poly (vinyl esters) and polyacrylates are susceptible to hydrolysis and enzymatic biodegradation [9,28]. Biodegradable polymers are classified as biosynthetic, semi-biosynthetic, and chemosynthetic. Almost all polymers which are readily available from renewable resources are biodegradable. Semi-biosynthetic and chemosynthetic polymers are also biodegradable if they contain chemical bonds which occur in natural compounds. Biodegradability is not only a function of origin but also of chemical structure and depends also on degrading environments [29]. The classifications of biodegradable polymers are diagrammatically represented in **Scheme 1.1** [25].

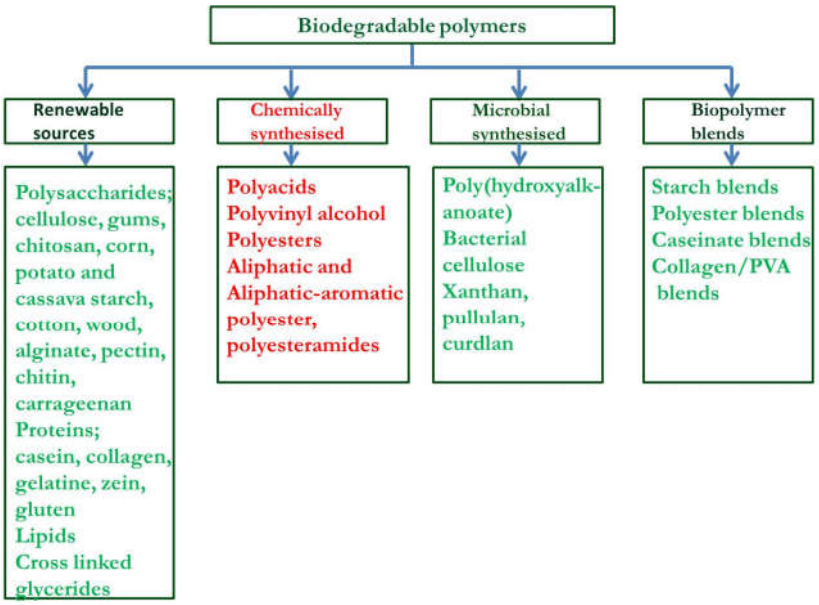

Scheme 1.1 Classification of biodegradable polymers

It is known that resins from natural oils like soy bean, castor, linseed, etc., can be used as substitute for petrochemical-derived thermosetting resins such as unsaturated polyesters, vinyl esters, and epoxy resins, resulting to thermosetting green composites [30]. In green composites both matrix and reinforcement are biodegradable. However, the use of biopolymer as matrix has also been associated with some disadvantages. In order to overcome this, synthetic polymers which are biodegradable such as PVA has been used as potential matrix to develop green composites.

1.4. POLY (VINYL ALCOHOL) (PVA)

The discovery of PVA dates back to 1924, obtained by saponifying poly (vinyl ester) with caustic soda to produce PVA solution [31]. Poly (vinyl alcohol) is the widely known water soluble and biodegradable synthetic polymer worldwide. PVA has been produced industrially by the hydrolysis of

poly (vinyl acetate), as the vinyl alcohol monomer cannot exist due to its tautomerisation into acetaldehyde. **Scheme 1.2** represents the chemical structure of fully hydrolysed form and **Scheme 1.3** that of partially hydrolysed PVA.

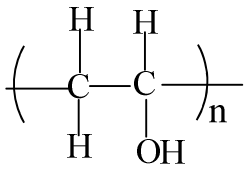

Scheme 1.2 Chemical structure of fully hydrolysed PVA

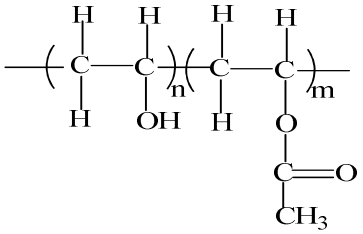

Scheme 1.3 Chemical structure of partially hydrolysed PVA

The polymerization of vinyl acetate occurs *via* a free-radical mechanism, usually in an alcoholic solution of methanol or ethanol; sometimes suspension polymerization technique can also be used. Polymerization reactions can be carried out in batch or in continuous processes, the latter being used mostly for large-scale productions. In the continuous industrial process, the free radical polymerization of vinyl acetate is followed by alkaline alcoholysis of poly (vinyl acetate) [32]. The most suitable renewable base material is ethanol [33]. Articles from PVA are usually obtained using casting techniques, also by melt processing technology. The main difficulty in producing PVA articles by thermal extrusion process is the close proximity of its melting point and

decomposition temperature [32]. PVA has a two dimensional hydrogen bonded network sheet structure, they are stacked and bonded together by weak van der Waal's forces [34].

1.4.1 Properties of PVA

Its properties depend to a greater extent on molecular weight, total degree of hydrolysis, sequence distribution of the monomer and tacticity. Its water solubility and biodegradability also depend on the degree of hydrolysis and molecular weight. PVA can be easily esterified or etherified and it undergoes reactions as that of molecular alcohols [35]. Moreover, it is little affected by grease, hydrocarbons, and animal or vegetable oils [36]. The partially hydrolysed PVA has better adhesion to hydrophobic surfaces, its water resistance being increased with increasing hydrolysis. The super hydrolysed grades of PVA are used when maximum water resistance and humidity resistance are desired [37]. PVA biodegrades in microbial-active environments within 5–6 weeks and the degradation of PVA also depends upon degree of hydrolysis [33,37]. The melting point of PVA ranges from 180-240 ^{0}C depending on its degree of hydrolysis [37].

1.4.2 Uses of PVA

Over 4 million ton of PVA are produced each year, in many grades, for use in diverse applications. PVA has been widely used in the production of adhesives for wood, textiles and leather, paper coatings, manufacturing of biodegradable polymer films, textile sizing and finishing agent, emulsifier and photosensitive coating. It has excellent gas barrier properties owing to small dense and closely packed monoclinic crystallite nature. High transparency, high dielectric strength, flexibility, toughness, dopant dependent electrical and optical properties, resistance to oil, grease, solvent and comparable cost etc are the added attractions of PVA [37–39]. PVA has

been most widely used as a membrane for the separation of aqueous organic mixtures [40]. Because of their oleophobic properties, PVA membranes are useful in waste water treatment, separation of organic compounds from one another or from water by pervaporation. In biotechnology PVA membranes have been used for protein recovery. PVA gels have been studied as biomaterials for artificial kidney and pancreas, glucose sensors, immune isolation membranes, artificial cartilage, contact lenses and drug delivery [41]. PVA has also been developed in biomedical applications such as, synthetic vitreous body, wound dressings, artificial skin and cardiovascular devices [42]. PVA based fibres have been considered as an attractive choice in tissue scaffolding, filtration materials, membranes, optics, protective clothing, enzyme immobilization, drug release, and so on [43]. PVA based composites have been successfully used in studies including biotechnology, pharmaceutical applications, safe and compatible material used in drugs coating formulation, surgical suture and controlled drug delivery system [44,45].

1.4.3 Microbial degradation of PVA

Nowadays, PVA has been attracting renewed interest since PVA with its carbon–carbon backbone, being water soluble can be biodegraded under both aerobic, anaerobic conditions and environment friendly materials are developed from it [46]. Eventhough, PVA has been considered as a truly biodegradable synthetic polymer since the early 1930s, the number of PVA degrading microorganisms are limited in comparison to the widespread species capable of degrading aliphatic polyesters, such as poly (hydroxyl alkanoate) (PHA) and PLA [37]. In 1973, it was shown that PVA is completely degraded using bacterial strain *Pseudomonas O-3*. Since then, several PVA degrading bacterial strains were reported, almost all of the degrading strains belong to the genus *Pseudomonas*, although some do belong to other genera. PVA microbial attack can only occur in the presence

of selected microorganisms that can be found almost exclusively in environments involving a continuous contamination by the polymer [47]. PVA with an average molecular weight as high as 10^6 were completely degraded by soil bacteria, especially by *Pseudomonads* and the degradation rate strongly depended on the residual acetate groups [48,49]. Along with the various *Pseudomonas* species, other PVA degrading aerobic bacteria, such as *Alcaligenes* and *Bacillus* were isolated from PVA contaminated environments [32].

1.5 NANOCOMPOSITES

Materials having at least one dimension in the range from 1 to 100 nm are called nanomaterials. Nanocomposite show unique properties, because of the nanometer size effect compared to conventional composite even at low filler content [50]. Polymer nanocomposites (PNC) include polymers, which can be thermoplastics, thermosets or elastomers, reinforced with small quantities (less than 5% by weight) of nano sized particles. The reinforcing nano material can be made up of particles like minerals, sheets like exfoliated clay stacks or fibres like carbon nanotubes, electrospun fibres or cellulose nanofibres. Because of their nano dimensions, the surface is important for nano fillers, the magnitude of specific surface area is higher than conventional fillers. Therefore nano fillers can be used at lower volume fractions than the conventional macroscopic fillers and they present much higher surface in composites. Due to this the composites can show an increase in the properties like tensile strength, Young's modulus, thermal properties, electrical properties, optical properties etc [51]. As a result nano fillers have a significant role in tailoring the properties of polymeric materials for technological application.

Because of the nano size of the nanoparticles and the high surface to volume ratio; the properties of nanocomposites are influenced by the extent of mixing between the two phases. In conventionally filled polymers, the

constituents may be immiscible, and this results in poorly blended macrocomposite with chemically separated phases. This results in lower physical interaction between the organic and inorganic components, leading to the agglomeration of the latter and ultimately results in weaker materials. Moreover, the macro scale particles can also act as stress concentrators [52]. By introducing inorganic nano fillers into polymers, thermal resistance of host polymers has been significantly improved. Compared to virgin polymers, polymeric/inorganic nanocomposites usually degrade at comparatively higher temperatures and demonstrate a substantial decrease in the degradation rate [53]. The advantages and disadvantages of polymer nanocomposites are listed in **Scheme 1.4** [54].

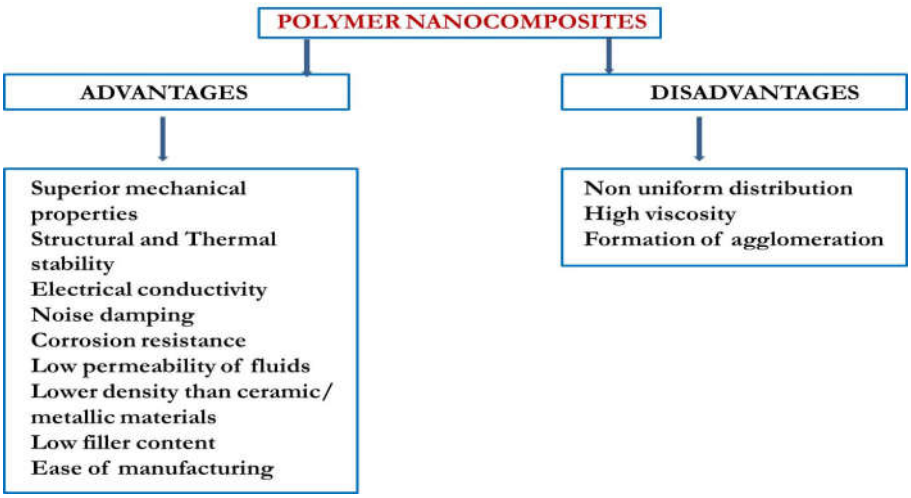

Scheme 1.4 Advantages and disadvantages of polymer nanocomposites

1.5.1 Bio-nanocomposites

Bio-nanocomposites are bio-based nanocomposites; consist of nanomaterials made from renewable nanoparticles like cellulose whiskers or microfibrillated cellulose as fillers and petroleum derived polymers like PP, PE, epoxies etc., as matrix. Nanocomposites derived from biopolymers like

PLA, PHA as matrix and synthetic or inorganic nano fillers like carbon nanotubes, nanoclay also come under bio-nanocomposites [23].

1.6 CELLULOSE BASED NANOMATERIALS

Each anhydroglucose unit of cellulose chain possesses three hydroxyl groups at C-2, C-3, and C-6 positions as shown in **Scheme 1.5** and it can form hydrogen bonds.

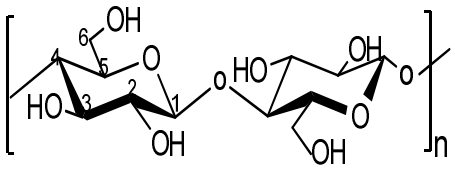

Scheme 1.5 Anhydroglucose unit of cellulose

An extended network of hydrogen bonds consisting of inter- and intra-molecular bonds are responsible for the aggregation of cellulose chains, which in turn form the crystalline and amorphous regions [55]. This is pictorially represented in **Figure 1.1**

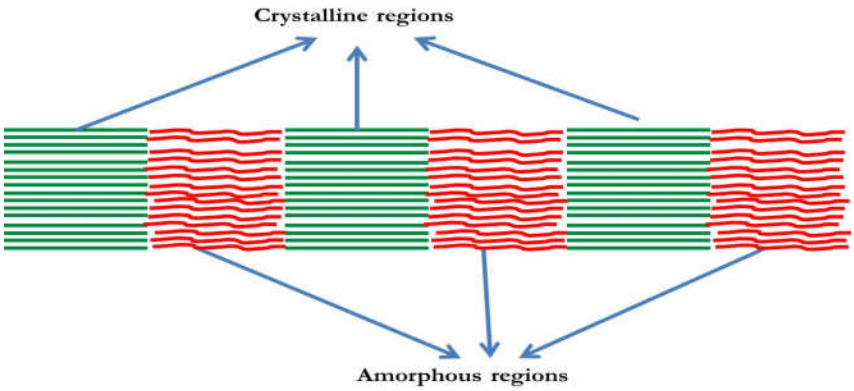

Figure 1.1 Crystalline and amorphous region in cellulose

During biosynthesis, van der Waals and inter-molecular hydrogen bonds between hydroxyl groups and oxygens of adjacent molecules promote parallel stacking of multiple cellulose chains forming elementary fibrils that further aggregate into larger microfibrils having 5–50 nm in diameter and several microns in length [56]. Thus cellulose contains linear chain aggregates transformed into highly ordered structures referred to as nano fibrils or elementary fibrils, which are then packed into larger units called microfibrils and in turn are assembled into cellulose fibres [57].

The high mechanical properties of cellulose fibres are due to the complicated hydrogen bonding networks among cellulose chains. The Young's modulus of the crystalline cellulose is very high, compared with stainless steel and the strength-to-weight ratio of cellulose nanocrystals is eight times higher [58]. The pictorial representation of cellulose fibres is shown in **Figure 1.2** [59]**.**

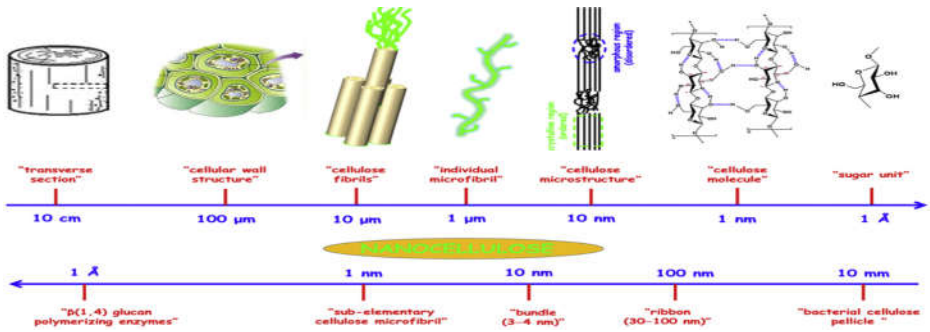

Figure 1.2 Pictorial representations of cellulose fibres

Nanomaterials obtained from cellulose are commonly described as microfibrillated cellulose (MFC) or nanofibrillated cellulose (NFC), cellulose whiskers (CW) or nanocrystalline cellulose (NCC) and bacterially produced cellulose or bacterial cellulose [60]. Several processes have been used to extract nanomaterials from lignocellulosic materials. The usual methods

employed are chemical treatments like acid hydrolysis and mechanical treatments like cryocrushing, grinding, high-pressure homogenization, high-intensity ultrasonication, and twin-screw extrusion. Moreover, biological treatments like enzyme-assisted hydrolysis and combination of two or more methods have also often used [61]. Their renewable nature, biodegradability, low toxicity, high strength, stiffness and abundance of reactive modifiable surface hydroxyl groups render cellulose nanomaterials an attractive choice for a broad range of functional nanomaterials.

1.6.1 Microfibrillated cellulose/Nanofibrillated cellulose

Mechanical processes like high intensity homogenisation, cryocrushing, grinding, ultrasonication, twin screw extraction have been used successfully to produce NFCs. Since they require higher energy consumption during the fibre disintegration, chemical methods, like acid hydrolysis, alkaline/acid pre-treatment oxidation etc., are often employed along with mechanical processes [62]. Large number of sources have been used to isolate nanofibres like wood fibres, cotton, potato tuber cells, prickly pear fruits, lemon and maize, soy bean, wheat straw, soy hulls, coconut husk fibres, branch-barks of mulberry, pineapple leaf fibres, banana rachis, pea hull fibre and sugar beet etc [63].

1.6.2 Nanocellulose (NC)/cellulose nanowhisker (CNW)/cellulose nanocrystals (CNC)

Among the methods developed to extract nanocellulose from cellulose, acid hydrolysis is the most well-known and the widely used [64]. When subjected to acid hydrolysis, cellulose microfibrils undergo transverse cleavage along the amorphous regions. Sulphuric acid is used as hydrolysing agent. If nanocrystals are prepared using hydrochloric acid their ability to disperse in solvents is limited, the suspension is unstable and tends to

flocculate [50,65]. Acid hydrolysis, followed by sonication results in rod like material with relatively low aspect ratio referred to as cellulose nanowhiskers. It is difficult to obtain uniformly dispersed CNW from natural plant fibres because they have a strong tendency to form larger structures through agglomeration. But, when subjected to mechanical dispersion or sonication, it results in the production of stable colloidal suspensions [3]. Eventhough, acid hydrolysis with sulphuric acid give CNW with negatively charged surface due to the esterification of hydroxyl groups by sulphate ions, they will have low thermal stability than cellulose. Large number of sources have been used for the isolation of nanocellulose and some of them are microcrystalline cellulose, sugar beet, cotton, tunicate, potato peel and wheat straw etc [3]. The aspect ratio distinguishes NFC and MFC, from nanocellulose. Nanocellulose has a very low aspect ratio (10–100), while NFC and MFC have a high aspect ratio of >1000 [66].

1.6.2.1 Nanocellulose as polymer reinforcement

The main attributes, which make use of nanocellulose as excellent polymer reinforcement agents are their large specific surface area of several hundreds of m^2g^{-1}, very high modulus of elasticity, approximately 150 GPa even theoretically stronger than steel and similar to Kevlar and low density of about 1.566 g cm^{-3}, along with biocompatibility and biodegradability [67]. Therefore, NCs are considered as one of the ideal nano reinforcements for polymer matrices including water soluble and water insoluble polymer systems and have already been incorporated into many polymer matrices to produce reinforced composites [68]. Cellulosic nanocomposites can be prepared by taking into consideration the stability of nanowhisker suspension in water. Therefore, hydrophilic matrices are the most important choice as the host polymer matrix. Hydrophobic matrices can also be used by modifying

the cellulose nanowhiskers. The three most used techniques to prepare composites films are casting followed by solvent evaporation, freeze drying and hot pressing, extrusion and hot pressing of the mixtures [69,70]. Compared to traditional composites they possess better thermal, mechanical and barrier properties at low reinforcement levels along with better recyclability, transparency and low weight.

1.6.2.2 Uses of nanocellulose

Apart from being used as excellent reinforcement in various polymer matrixes, NC has great potential application in many fields. Depending on the nature of application they can be converted into different forms like solids, films, aerogel and foams, therefore find application in a number of fields. Films made of NCs can be used in various areas such as barriers for packaging, substrates for printed electronics, stabilizer and thickening agent for paint, food, adhesives, coatings and cement. In biomedical applications, NCs have been used as a drug carrier into human bodies and wound dressing due to its size and antibacterial properties. Since NCs are having high surface area to volume ratio, offering high sensitivity and fast response times than microcellulose, they find use in sensor applications [71,72]. Metals like Au, Ag, Pd, Ni, etc., minerals like $Ca_x(PO4)_y$, $CaCO_3$, montmorillonite, etc., carbon nanotube and graphene have been incorporated into NC substrates and examined for electrical, optical and catalytic properties of these nanocomposites extensively. NCs based composites have shown potentials for applications in drinking water filtration, catalytic degradation of organic pollutants, absorbents to remove spilt oil from water, monitoring waterborne pathogens and organic contaminants, superior energy conversion and for superior antimicrobial properties. NCs hinder nanoparticle aggregation typically acting as a catalyst support when used for catalysis. Gold

nanoparticle/nanocellulose composites are employed as biosensors. Moreover, NC based nanocomposite can also be applied in fuel cell, solar cell and Li-ion battery manufacturing [60,73,74].

1.7 SCOPE AND OBJECTIVES OF THE PRESENT STUDY

Lignocellulosic materials like sugarcane bagasse, rice hulls, peanut shells, and other agricultural and agro industrial residues are world's widely available low-cost renewable resources used for the production of a number of value added products. Since lignocellulosic materials may differ in their composition, each area of application needs specific requirement based on the composition. Traditionally they are used for production of energy, charcoal, ethanol, paper and pulp, potential reinforcement in composites etc [17].

Another important product obtained from lignocellulose is microcrystlline cellulose (MCC), wood definitely being the most important principal source. MCC is a commercially important product, used in a number of applications. It is obtained by the acid hydrolysis of cellulose using relatively low concentration like 2.5 N HCl for lower time like 15 min at boiling temperature, so that some of the amorphous regions are cleaved. Number of other sources has also been studied as source for isolating MCC. Therefore, utilisation of agricultural residues like sago seed shells (*Cycas circinalis*) for MCC production in a way gives value addition to agricultural waste materials. Moreover, since there are no documents available on the composition of sago seed shells, the characterization of sago seed shell is also important.

The growing search for green and sustainable materials made from natural and renewable raw materials has created interest in the development of high performance and high value cellulose nanomaterials. Like other

nanomaterials, cellulose nanomaterials such as microfibrillated cellulose and cellulose nanocrystals are credited with unique properties, with potentials to develop new products or significantly enhance the performance of existing products. One important difference from many other nanomaterial is that cellulose nanomaterial products are made from natural raw materials that have the potential to be harvested in a sustainable manner [75]. Cellulose has been extracted from number of sources and subsequently converted to cellulose nanocrystals by acid hydrolysis. Any source containing cellulose can be potentially used as sources for extraction of cellulose. Thus the isolation, characterization and search for applications of novel forms of cellulose, like nanocrystals, whiskers, nanofibrils, and nanofibres, are getting much attention. Eventhough, a number of sources are known for the isolation of cellulose and the use of seed shells as potential reinforcement in polymers has been well studied, the cellulose extraction from the seed shell is not exploited well. Moreover, obtaining value added products from agricultural waste material is another thrust area.

When cellulose fibres undergo mechanical process involving defibrillation by various methods it produces microfibrillated cellulose, whereas acid hydrolysis gives cellulose nanocrystals. Cellulose nanocrystal aqueous suspensions are highly stable and therefore water is chosen as the preferred processing medium. Hydro-soluble polymers will be well adapted for the processing of cellulose nanocrystals to produce reinforced nanocomposites. Since PVA is water soluble it can be processed along with cellulose nanocrystals in water medium. Films are obtained by casting and evaporating the aqueous polymer solution [76]. Therefore, the main objectives of the present investigation are

- *To establish the composition of sago seed shells*
- *To isolate microcrystalline cellulose from sago seed shells*
- *To characterise MCC by FTIR, TG, XRD, SEM, TEM and AFM*
- *To develop green composites of MCC reinforced PVA.*
- *To characterise the green composites by FTIR, ATR-FTIR, XRD, TG, DSC, UV-Visible, SEM, AFM, and determine their mechanical properties.*
- *To isolate cellulose nanocrystals (CNCs) from sago seed shells.*
- *To characterise the isolated CNCs by FTIR, XRD, SEM, TEM, AFM, DLS, Zeta (ζ) potential and TG.*
- *To develop bio-nanocomposites of PVA reinforced with CNC.*
- *To characterise bio-nanocomposites by FTIR, ATR-FTIR, XRD, DSC, TG, UV-Visible, SEM, AFM, determine the mechanical properties and assess the biodegradability.*
- *To exploit the possibility of prepared bio-nanocomposite for packaging application by studying the properties such as water vapour transmission rate, moisture uptake and gas barrier.*

REFERENCES

1. Lagaron, J. M.; Catala, R.; Gavara, R. Structural characteristics defining high barrier properties in polymeric materials. *Mater. Sci. Technol.* **2004**, *20*, 1–7.

2. Feldman, D. Cellulose nanocomposites. *J. Macromol. Sci. Part A* **2015**, *52*, 322–329.

3. Miao, C.; Hamad, W. Y. Cellulose reinforced polymer composites and nanocomposites: A critical review. *Cellulose* **2013**, *20*, 2221–2262.

4. Ghosh, P. *Polymer science and technology plastics, rubber, blends and composites*; Third.; mcGraw hill education (India) Private limited, 2014;

5. Eslami-farsani, R. Effect of fiber treatment on the mechanical properties of date palm fiber reinforced PP/EPDM composites. *Adv. Compos. Mater.* **2015**, *24*, 27–40.

6. Xanthos, M. *Functional fillers for plastics*; 2nd ed.; Wiley-vch verlag gmbh & co kgaa, 2005;

7. Spoljaric, S.; Genovese, A.; Shanks, R. A. Polypropylene-microcrystalline cellulose composites with enhanced compatibility and properties. *Compos. Part A* **2009**, *40*, 791–799.

8. Thomas, S.; Joseph, K.; Malhotra; Kumar, S.; Goda, K.; Sreekala, M. S. *Introduction to polymer composites*; Wiley-vch verlag gmbh & co. kgaa., 2012;

9. Zini, E.; Scandola, M. Green composites: An overview. *Polym. Compos.* **2011**, *32*, 1905–1915.

10. Wang, R. M.; Zheng, S. R.; Ya Ping, Z. *Polymer matrix composites and technology*; Woodhead Publishing, 2011;

11. Mitra, B. C. Environment friendly composite materials: Biocomposites and green composites. *Def. Sci. J.* **2014**, *64*, 244–261.

12. Bhatnagar, A.; Sain, M. Processing of cellulose nanofiber-reinforced composites. *J. Reinf. Plast. Compos.* **2005**, *24*, 1259–1267.

13. Islam, R.; Islam, T.; Nigar, F.; Saha, S.; Sharmin, N.; Dey, K.; Mustafa, A. I.; Khan, R. A.; Khan, M. A.; Zaman, H. U. Fabrication and mechanical characterization of jute fabrics: Reinforced poly (vinyl chloride)/polypropylene hybrid Composites. *Int. J. Polym. Mater. Polym. Biomater.* **2011**, *60:*, 576–590.

14. Pandey, J. K.; Ahn, S. H.; Lee, C. S.; Mohanty, A. K.; Misra, M. Recent advances in the application of natural fiber based composites. *Macromol. Mater. Eng.* **2010**, *295*, 975–989.

15. Dicker, M. P. M.; Duckworth, P. F.; Baker, A. B.; Francois, G.; Hazzard, M. K.; Weaver, P. M. Green Composites: A review of material attributes and complementary applications. *Compos. Part A. Appl. Sci. Manuf.* **2014**, *56*, 280–289.

16. John, M. J.; Anandjiwala, R. D. Recent developments in chemical modification and characterization of natural fiber-reinforced composites. *Polym. Compos.* **2008**, *29*, 187–207.

17. John, M. J.; Thomas, S. Biofibres and biocomposites. *Carbohydr. Polym.* **2008**, *71*, 343–364.

18. Zaman, H.; Khan, M. A.; Khan, R. A.; Mollah, M. Z. I.; Pervin, S.; AL-Mamun, M. A comparative study between gamma and UV radiation of jute fabrics/polypropylene composites:Effect of starch. *J. Reinf. Plast. Compos.* **2010**, *29*, 1930–1939.

19. Ayma, A. Effect of gamma radiation on the properties of jute reinforced polyester matrix composites. *J. Text. Sci. Eng.* **2017**, *6*, 294.

20. Khan, M. A.; Haque, N.; Al-kafi, A.; Alam, M. N.; Abedin, M. Z. Jute reinforced polymer composite by gamma radiation :Effect of surface treatment with UV radiation. *Polym. Plast. Tech. Engi.* **2006**, *45*, 607–613.

21. Khan, M. A.; Shehrzade, S.; Hassan, M. M. Effect of alkali and ultraviolet (UV) radiation pretreatment on physical and mechanical Properties of 1,6-Hexanediol Diacrylate-grafted jute yarn by UV radiation. *J. Appl. Polym. Sci.* **2004**, *92*, 18–24.

22. Juntaro, J.; Pommet, M.; Mantalaris, A.; Shaffer, M.; Bismarck, A. Nanocellulose enhanced interfaces in truly green unidirectional fibre reinforced composites. *Compos. Interfaces* **2007**, *14*, 753–762.

23. Siqueira, G.; Bras, J.; Dufresne, A. Cellulosic bionanocomposites: A review of preparation, properties and applications. *Polym.* **2010**, *2*, 728–765.

24. Faruk, O.; Bledzki, A. K.; Fink, H.; Sain, M. Biocomposites reinforced with natural fibers:2000-2010. *Prog. Polym. Sci.* **2012**, *37*, 1552–1596.

25. Rehman, N.; Inez, M. G.; Miranda, D.; L, S. M.; Rosa; Pimentel, D. M.; B, S. M.; Nachtigall; Bica, C. I. D. Cellulose and nanocellulose from maize straw: An insight on the crystal properties. *J. Polym. Env.* **2014**, *22*, 252–259.

26. Kang, H.; Liu, R.; Huang, Y. Graft modification of cellulose: Methods, properties and applications. *Polym.* **2015**, *70*, A1–A16.

27. Abraham, E.; Elbi, P. A.; Deepa, B.; Jyotishkumar, P.; Pothen, L. A.; Narine, S. S.; Thomas, S. X-ray diffraction and biodegradation analysis of green composites of natural rubber/nanocellulose. *Polym. Degrad. Stab.* **2012**, *97*, 2378–2387.

28. Luckachan, G. E.; Pillai, C. K. S. Biodegradable polymers-A review on recent trends and emerging perspectives. *J.Polym.Env.* **2011**, *19*, 637–676.

29. Mohanty, A. K.; Misra, M.; Hinrichsen, G. Biofibres, biodegradable polymers and biocomposites: An overview. *Macromol. Mater. Eng.* **2000**, *276*, 1–24.

30. Khot, S. N.; Lascala, J. J.; Can, E.; Morye, S. S.; Williams, G. I.; Palmese, G. R.; Kusefoglu, S. H.; Wool, R. P. Development and application of triglyceride-based polymers and composites. *J. Appl. Polym. Sci.* **2001**, *82*, 703–723.

31. W, H.; Herrmann WO German Patent 450:286 1924.

32. Chiellini, E.; Corti, A.; Antone, S. D.; Solaro, R. Biodegradation of poly (vinyl alcohol) based materials. *Prog. Polym. Sci.* **2003**, *28*, 963–1014.

33. FLieger, M.; Antorová, M. K.; Prell, A.; Rezanka, T.; Votruba, J. Biodegradable plastics from renewable sources. *Folia Microbiol.* **2003**, *48*, 27–44.

34. El-Zaher, N. A.; Osiris, W. G. Thermal and structural properties of poly (vinyl alcohol) doped with hydroxypropyl cellulose. *J. Appl. Polym. Sci.* **2005**, *96*, 1914–1923.

35. Bana, R.; Banthia, A. K. Green composites: Development of poly (vinyl alcohol)- wood dust composites. *Polym. Plast. Technol. Eng.* **2007**, *46*, 821–829.

36. Lang, K.; Sourirajan, S.; Matsuura, T.; Chowdhury, G. A study on the preparation of poly (vinyl alcohol) thin-film composite membranes and reverse osmosis testing. *Desalination* **1996**, *104*, 185–196.

37. Tang, X.; Alavi, S. Recent advances in starch, poly (vinyl alcohol) based polymer blends, nanocomposites and their biodegradability. *Carbohydr. Polym.* **2011**, *85*, 7–16.

38. Jang, J.; Lee, D. K. Plasticizer effect on the melting and crystallization behavior of poly (vinyl alcohol). *Polym.* **2003**, *44*, 8139–8146.

39. Silva, G. G. D.; Sobral, P. J. A.; Carvalho, R. A.; Bergo, P. V. A.; Mendieta-Taboada, O.; Habitante, A. M. Q. B. Biodegradable films based on blends of gelatin and poly (vinyl alcohol): Effect of PVA type or concentration on some physical properties of films. *J .Polym. Environ.* **2008**, *16*, 276–285.

40. Adoor, S. G.; Manjeshwar, L. S.; Naidu, B. V. K.; Sairam, M.; Aminabhavi, T. M. Poly (vinyl alcohol)/poly (methyl methacrylate) blend membranes for pervaporation separation of water+isopropanol and water+1,4-dioxane mixtures. *J. Memb. Sci.* **2006**, *280*, 594–602.

41. Bolto, B.; Tran, T.; Hoang, M.; Xie, Z. Crosslinked poly (vinyl alcohol) membranes. *Prog. Polym. Sci.* **2009**, *34*, 969–981.

42. Chhatri, A.; Bajpai, J.; Bajpai, A. K.; Sandhu, S. S.; Jain, N.; Biswas, J. Cryogenic fabrication of savlon loaded macroporous blends of alginate and poly (vinyl alcohol) (PVA). swelling, deswelling and antibacterial behaviors. *Carbohydr. Polym.* **2011**, *83*, 876–882.

43. Peresin, M. S.; Habibi, Y.; Zoppe, J. O.; Pawlak, J. J.; Rojas, O. J. Nanofiber composites of poly (vinyl alcohol) and cellulose nanocrystals: Manufacture and characterization. *Biomacromolecules* **2010**, *11*, 674–681.

44. Abdulkhani, A.; Marvasta, E. H.; Ashorib, A.; Hamzeha, Y.; Karimia, A. N. Preparation of cellulose/poly (vinyl alcohol) biocomposite films

using 1-n-butyl-3-methylimidazolium chloride. *Int. J. Biol. Macromol.* **2013**, *62*, 379–386.

45. Chen, J.; Li, Y.; Zhang, Y.; Zhu, Y. Preparation and characterization of graphene oxide reinforced PVA film with boric acid as crosslinker. *J. Appl. Polym. Sci.* **2015**, *132*, 1–8.

46. Raghul, S. S.; Bhat, S. G.; Chandrasekaran, M.; Francis, V.; Thachil, E. T. Biodegradation of poly (vinyl alcohol)-low linear density polyethylene-blended plastic film by consortium of marine benthic vibrios. *Int. J. Environ. Sci. Technol.* **2013**, *11*, 1827–1834.

47. Chiellini, E.; Corti, A.; Solaro, R. Biodegradation of poly (vinyl alcohol) based blown films under different environmental conditions. *Polym. Degrad. Stab.* **1999**, *64*, 305–312.

48. Lenz, R. W. Biodegradable polymers. *Adv. Polym. Sci.* **1993**, *107*, 33–39.

49. Chen, Y.; Cao, X.; Chang, P. R.; Huneault, M. A. Comparative study on the films of poly (vinyl alcohol)/pea starch nanocrystals and poly (vinyl alcohol)/native pea starch. *Carbohydr. Polym.* **2008**, *73*, 8–17.

50. Mariano, M.; Kissi, N. El; Dufresne, A. Cellulose nanocrystals and related nanocomposites: Review of some properties and challenges. *J. Polym. Sci. Part B. Polym. Phys.* **2014**, *52*, 791–806.

51. Rothon, R. N.; DeArmitt, C. *Particulate-filled polymer composites*; second.; ismithers rapra Publishing, 2003;

52. Ishida, H.; Campbell, S.; Blackwell, J. General approach to nanocomposite preparation. *Chem. Mater* **2000**, *12*, 1260–1267.

53. Peng, Z.; Kong, L. X. A thermal degradation mechanism of poly (vinyl alcohol)/silica nanocomposites. *Polym. Degrad. Stab.* **2007**, *92*, 1061–1071.

54. Abdullah, Z. W.; Dong, Y.; Davies, I. J.; Barbhuiya, S. PVA, PVA blends, and their nanocomposites for biodegradable packaging application. *Polym. Plast. Technol. Eng.* **2017**, 1–38.

55. Khalil, H. P. S. A.; Bhat, A. H.; Yusra, A. F. I. Green composites from sustainable cellulose nanofibrils: A review. *Carbohydr. Polym.* **2012**, *87*, 963–979.

56. Moon, R. J.; Martini, A.; Nairn; Simonsen, J.; Jeff, Y. Cellulose nanomaterials review: Structure, properties and nanocomposites. *Chem. Soc. Rev.* **2011**, *40*, 3941–3994.

57. Chakraborty, A.; Sain, M.; Kortschot, M. Cellulose microfibrils: A novel method of preparation using high shear refining and cryocrushing. *Holzforschung* **2005**, *59*, 102–107.

58. Peng, Y.; Gardner, D. J.; Han, Y.; Kiziltas, A.; Cai, Z.; Tshabalala, M. A. Influence of drying method on the material properties of nanocellulose I: Thermostability and crystallinity. *Cellulose* **2013**, *20*, 2379–2392.

59. Lin, N.; Dufresne, A. Nanocellulose in biomedicine: Current status and future prospect. *Eur. Polym. J.* **2014**, *59*, 302–325.

60. Wei, H.; Rodriguez, K.; Renneckar, S.; Vikesland, P. J. Environmental science and engineering applications of nanocellulose-based nanocomposites. *Environ. Sci. Nano* **2014**, *1*, 302–316.

61. Li, Y.; Liu, Y.; Chen, W.; Wang, Q.; Liu, Y.; Li, J.; Yu, H. Facile extraction of cellulose nanocrystals from wood using ethanol and peroxide solvothermal pretreatment followed by ultrasonic nanofibrillation. *Green Chem.* **2016**, *18*, 1010–1018.

62. Soni, B.; Barbary, E.; Mahmoud, B. Chemical isolation and characterization of different cellulose nanofibers from cotton stalks. *Carbohydr. Polym.* **2015**, *134*, 581–589.

63. Khawas, P.; Deka, S. C. Isolation and characterization of cellulose nanofibers from culinary banana peel using high-intensity ultrasonication combined with chemical treatment. *Carbohydr. Polym.* **2016**, *137*, 608–616.

64. Bondeson, D.; Mathew, A.; Oksman, K. Optimization of the isolation of nanocrystals from microcrystalline cellulose by acid hydrolysis. *Cellulose* **2006**, *13*, 171–180.

65. Jonoobi, M.; Oladi, R.; Davoudpour, Y.; Oksman, K.; Dufresne, A.; Hamzeh, Y.; Davoodi, R. Different preparation methods and properties of nanostructured cellulose from various natural resources and residues: A review. *Cellulose* **2015**, *22*, 935–969.

66. Osong, S. H.; Norgren, S.; Engstrand, P. Processing of wood-based microfibrillated cellulose and nanofibrillated cellulose, and

applications relating to papermaking: A review. *Cellulose* **2016**, *23*, 93–123.

67. Fortunati, E.; Puglia, D.; Luzi, F.; Santulli, C.; Kenny, J. M.; Torre, L. Binary PVA bio-nanocomposites containing cellulose nanocrystals extracted from different natural sources: Part I. *Carbohydr. Polym.* **2013**, *97*, 825–836.

68. Klemm, D.; Kramer, F.; Moritz, S.; Lindström, T.; Ankerfors, M.; Gray, D.; Dorris, A. Nanocelluloses: A new family of nature-based materials. *Angew. Chem.* **2011**, *50*, 5438–5466.

69. Cheng, Q.; Wang, S.; Rials, T. G. Poly (vinyl alcohol) nanocomposites reinforced with cellulose fibrils isolated by high intensity ultrasonication. *Compos. Part A* **2009**, *40*, 218–224.

70. Teboho Clement, M. Preparation and characteriztion of vinyl silane croslinked thermoplastic composites filled with natural fibers, University of the free state (Qwaqwa campus), 2012.

71. Kumar, V.; Bollstro, R.; Yang, A.; Chen, Q.; Chen, G.; Salminen, P.; Bousfield, D.; Toivakka, M. Comparison of nano-and microfibrillated cellulose films. *Cellulose* **2014**, *21*, 3443–3456.

72. Mohaiyiddin, M. S.; Lin, O. H.; Owi, W. T.; Chan, C. H.; Chia, C. H.; Zakaria, S.; Villagracia, A. R.; Akil, H. M. Characterization of nanocellulose recovery from Elaeis guineensis frond for sustainable development. *Clean Technol. Environ. Policy* **2016**, *18*, 2503–2512.

73. Lam, E.; Male, K. B.; Chong, J. H.; Leung, A. C. W.; Luong, J. H. T. Applications of functionalized and nanoparticle-modified nanocrystalline cellulose. *Trends Biotechnol.* **2012**, *30*, 283–290.

74. Fortunati, E.; Puglia, D.; Monti, M.; Santulli, C.; Maniruzzaman, M.; Kenny, J. M. Cellulose nanocrystals extracted from Okra fibers in PVA nanocomposites. *J. Appl. Polym. Sci.* **2013**, *128*, 3220–3230.

75. Aspler, J. O. E.; Bouchard, J.; Hamad, W.; Berry, R.; Beck, S.; Drolet, F.; Zou, X. *Biopolymer nanocomposites: Processing, properties, and applications*; John Wiley & Sons, Inc, 2013;

76. Roohani, M.; Habibi, Y.; Belgacem, N. M.; Ebrahim, G.; Naghi, A.; Dufresne, A. Cellulose whiskers reinforced poly (vinyl alcohol) copolymers nanocomposites. *Eur. Polym. J.* **2008**, *44*, 2489–2498.

CHAPTER 2

MICROCRYSTALLINE CELLULOSE AND CELLULOSE NANOMATERIAL REINFORCED POLYMER COMPOSITES –A REVIEW

Abstract

This chapter discusses the review of the earlier investigations on microcrystalline cellulose filled composites and cellulose nanomaterials reinforced composites, with special reference to PVA as matrix. Their current status has also been discussed.

2.1 INTRODUCTION

Polymer composites with enhanced properties and versatility made their ubiquitous presence in many industrial applications, including automotive, aerospace, construction, furniture, packaging etc. Fibres like aramid, carbon and glass have been extensively used as reinforcement in these composites. Eventhough, these composites are invested with favourable properties such as high strength, heat resistance and other desirable properties but they are associated with limited recyclability and above all nonbiodegradability. Therefore environmental, economic and performance issues ended in the use of natural fibres as alternative to their synthetic counterparts, without compromising performance. Not only natural fibres, but other sources like wood flour/fibres, recycled fibre-based products like newspaper, agricultural residues such as rice husks and sugarcane bagasse have also been used [1]. Since agricultural residues are rich in cellulose, they can be effectively used as reinforcement in polymer composites.

Cellulose is the most abundant natural biopolymer in the world, which is renewable and biodegradable. A number of new functional materials from cellulose have been developed for broad range of applications, due to increasing demand for environment friendly and biocompatible [2,3]. MCC, is a commercial product with over a half century of history, obtained from purified, partially depolymerised cellulose and prepared by treating cellulose with mineral acids such as 2.5 N HCl [4]. Since cellulose from different sources differ in properties like crystallinity, moisture content, surface area, porous structure, molecular mass etc., obviously MCC obtained from different sources also may vary in their properties. Moreover, physical pre-treatments can also be used significantly to modify MCC [5]. The average particle size of commercial MCC is between 50 and 350 μm.

Eventhough, wood and cotton are the principal sources to obtain MCC, a number of other source like soy bean, sugar beet pulp, bagasse, corn cob, ground nut shell, rice husks, cereal straw, Indian bamboo and luffa cylindrica etc., have also been studied as potential sources for the production of MCC [6]. Common uses of MCC include as pharmaceutical excipient, binder and texturizer, food additive, edible coatings etc. Apart from the common uses of MCC it has also been used as potential reinforcement in polymer matrix [7]. Since MCC is hydrophilic in nature, better compatibility will be obtained by hydrophilic matrices. Hydrophobic matrices can also be used by proper modification of MCC.

Physical properties of PVA depend on factors like degree of hydrolysis that is available in partially and fully hydrolysed grades, the molecular mass and water content. Partially hydrolysed PVA contains residual acetate groups with reduced crystallinity, lower melting points, easy processability, lower strength and lower water dissolution temperatures than fully hydrolysed [8]. Since PVA is water soluble, it can be processed in water medium resulting in the formation of film. Apart from being used in a number of fields, PVA has been developed for biodegradable packaging due to its biodegradability, film forming ability, flexibility, good tensile strength, as well as high oxygen and aroma barrier properties [9,10]. Since MCC is hydrophilic, the use of hydrophilic matrices like PVA enhances the compatibility, dispersion of filler, interaction between the matrix and MCC. Moreover, the composite will be environmentally benign. A number of studies dealing with the fabrication of composites of PVA reinforced with MCC, its importance and properties had appeared in the literature.

2.2 MICROCRYSTALLINE CELLULOSE (MCC) REINFORCED COMPOSITES

Blends of cellulose with PVA, prepared from mixed solutions of N,N-Dimethylacetamide-Lithium chloride by coagulation in a nonsolvent was studied by Nishiot and Manley in 1988. The results indicated that when the cellulose content increases crystallinity of PVA decreased [11].

Laka and Chernyavskaya 1996 developed thermocatalytic method for obtaining MCC (Thermocell) and studied the effect of thermocell in polystyrene. The results showed increase in density, tensile strength, bending strength than pure polystyrene [12]. The strength-deformation characteristics of low density polyethylene filled with thermocell was studied by Maskavs *et al*.1999. The results showed that as filler content increases, increase in elastic modulus and tensile strength was observed [13].

Hydroxypropyl cellulose (HPC), modified cellulose in different weight % was doped in PVA to produce composites. Its structural properties were studied by Zaher and Osiris in 2005. The results indicated that PVA became more thermally stable when 12 wt.% HPC were added [14]. MCC has been used as the reinforcement in PLA matrix by Mathew *et al*. in 2005. The composites were prepared with varying MCC contents up to 25 wt.%, wood flour (WF) and wood pulp (WP) as reference materials. The MCC-PLA composites showed lower mechanical properties than the reference materials, SEM analysis also showed poor adhesion between MCC and matrix [15].

Chakraborty *et al*.2006 studied the reinforcing potential of commercial MCC along with cellulose microfibers obtained from bleached softwood kraft pulp using PVA as matrix. The tensile strength of MCC-reinforced composites increased in comparison to neat PVA [16]. Chuayjuljit

et al.2010 isolated MCC from cotton fabric waste and blended with poly (vinyl chloride). The tensile strength, Young's modulus, moisture absorption and biodegradability of the blends were increased with increasing MCC content [17].

Composites of nylon 6 and MCC containing 2.5-30 wt.% were studied by Kiziltas *et al*.2011. TG indicated that the MCC did not show significant initial degradation below 300 ^{0}C, establishing the thermal stability of composites [18]. The effect of MCC on Polypropylene (PP) and PP modified by maleic anhydride graft (PP-g-MA) and methyl acrylic acid glycidyl ester grafted PP (PP-g-GMA), using twin-screw extruder were studied by Xiuju *et al*.2011. The addition of MCC led to increase in the tensile strength, impact strength, flexural strength and showed higher thermal decomposition temperatures [19].

Osiris and Manal 2012 also studied the effect of blends containing PVA and HPC. Thermal analysis showed variations in the glass transition temperature (T_g) indicating the miscibility of the blend systems. HPC doped PVA films was found to have improved thermal stability [20]. Hatakeyama *et al*.2012 studied the effect of particle size on the properties of composites containing water absorbed polyurethane rigid foam using polyols derived from molasses and lignin [21]. Thummanukitcharoen *et al*.2012 modified MCC by silane treatement (SiMCC) and prepared (SiMCC)-polypropylene composite using twin-screw extruder. TG results revealed that, during melting process the addition of SiMCC showed thermal stability enhancement of PP matrix [22].

2.3 ISOLATION OF NANOCELLULOSE

Nanotechnology is recognized as one of the fast emerging areas of technological development in the 21st century. Development of polymer nanocomposites includes multi-disciplinary areas, which can broaden the applications of polymers to many fields. Due to synergistic and hybrid properties derived from several components, they exhibit unique mechanical, electrical, optical, thermal and other properties [23]. Enhancements in properties are caused by the interaction of the polymer with nanoparticle and their good dispersion. Most of the nano fillers used, like carbon nanotubes, silica, clays, metal oxides etc., in nano composites with synthetic polymeric materials are inorganic. Their processability, biocompatibility and biodegradability are limited than those of naturally occurring organic nanomaterials [24].

Among naturally occurring, cellulose being the most abundant biopolymer gained much attention during the past few years. There are basically two categories of nano sized cellulosic particles obtained from cellulose. They are cellulose nanocrystals and microfibrillated cellulose (MFC). Mechanical treatments like cryocrushing, grinding, high-pressure homogenization, high-intensity ultrasonication, steam explosion, biological treatments like enzyme-assisted hydrolysis and chemical treatments like acid hydrolysis are often used to extract nanoobjects from lignocellulosic materials.

Cryocrushing employs the crushing of frozen pulp using liquid nitrogen, cellulose slurry is pumped at high pressure during high pressure homogenisation, grinding stones are used to breakdown the cell wall structure by shearing forces generated by the grinding stones, pre-treatment with enzyme like *endoglucanase* are often used before mechanical treatment [25].

High intensity ultrasonic generator is used in ultrasonic treatment [26], and treated fibres kept in autoclave under high pressures were released immediately in steam explosion process [27].

Since cellulose fibres and micro fibrils contain both crystalline and amorphous regions, on acid hydrolysis, the amorphous regions are susceptible to acid attack and under controlled conditions undergo cleavage, leaving crystalline regions intact [28]. Cellulose nanoparticles with advantages like low density, renewable nature, low energy consumption, high specific properties, modest abrasivity during processing, biodegradability, relatively reactive surface which can be used for grafting specific groups and almost unlimited availability make them suitable reinforcing filler. Since cellulose whiskers have polarity, it makes them difficult to disperse in non-polar medium. Nonpolar matrix has also been used by suitable chemical modification of the cellulose nanocrystals [28].

Beck-Candanedo *et al*.2005 prepared cellulose nanocrystals from soft, hardwood, and investigated the influence of hydrolysis time and acid-to-pulp ratio. Longer hydrolysis times produced shorter, less polydisperse cellulose nanocrystals. Moreover, with increase in acid-to-pulp ratio there was reduction in the dimensions of the nanocrystals produced [29]. Bondeson *et al*.2006 studied the effect of preparation conditions, concentration of sulphuric acid, hydrolysis time, temperature and the ultrasonication treatment time on cellulose nanowhiskers isolated from microcrystalline cellulose derived from Norwegian spruce (*Picea abies*). They observed a decrease in the length of MCC and an increase in the surface charge with prolonged hydrolysis. They also found that the optimum conditions to produce cellulose nanowhiskers was sulphuric acid of 63.5% (w/w) concenration [30]. After the optimisation of conditions by Bondenson *et al*.2006, a number of sources

have been used for the isolation of nanocellulose using H_2SO_4. Wang *et al.* 2007 isolated the spherical cellulose nanocrystals by hydrolysis of MCC with mixed acid consisting 30% (v/v) sulphuric acid and 10% (v/v) hydrochloric acid. The degradation occurred within a narrow temperature range and shifted to higher temperature, when neutralized with NaOH solution. Cellulose with small size showed degradation at lower temperature [31]. Moran *et al*.2008 extracted cellulose from sisal fibre, by means of two different procedures including acid hydrolysis, chlorination, alkaline extraction, and bleaching. The extraction procedures gave purified cellulose and nanocellulose, by subsequent acid hydrolysis. AFM of nanocellulose showed an average diameter of 30.9±12.5 nm [32]. Acid hydrolysis of native ramie fibres after chemical treatment was used to isolate aqueous suspension of elongated nanocrystals with high aspect ratio by Habibi *et al*.2008. The rod-like nanocrystals obtained by TEM exhibited an average diameter 6–8 nm and a length of about 150–250 nm [33]. Wang *et al*.2008 isolated spherical cellulose nanocrystals (SCNC) by acid hydrolysis of MCC using sulphuric and hydrochloric acid under ultrasonication. The authors obtained SCNC with diameters in the range of 10-180 nm, having an average diameter of 62 nm with polydispersity 49%. They observed a liquid crystalline phase under polarized optical microscope with solid contents above 3.9% [34].

Li *et al*.2009 isolated cellulose whiskers from the branch-barks of mulberry (*Morus alba L.*), by alkali treatment followed by sulphuric acid hydrolysis. AFM image showed the diameter of whiskers are in the range 20-40 nm and length 400–500 nm [35]. Pandey *et al*.2009 isolated cellulose nanowhiskers (CNW) from grass after chemical treatment followed by acid hydrolysis and mechanical treatment. The results showed that width of CNW was ~10-65 nm with a length of several nanometers [36]. Filson *et al*.2009 isolated CNCs from microcrystalline wood cellulose (Avicel) and recycled

pulp obtained from wood pulp, by sono-chemical assisted hydrolysis. CNC obtained from Avicel and recycled pulp showed different morphologies. Avicel produced cellulose nanocrystals with average diameter of 21±5 nm in deionized water, while recycled pulp produced has average diameter of 23±4 nm. CNCs having length 65±19 and width 15 nm with cylindrical shape were obtained by maleic acid sono-chemical assisted hydrolysis of Avicel at 15 ^{0}C with 90% power output for 9 min [37].

Rosa *et al*.2010 studied the effect of preparation conditions on thermal and morphological behaviour of cellulose nanowhiskers isolated from coconut husk fibres by sulphuric acid hydrolysis at different time. CNWs having diameters as low as 5 nm and aspect ratio of up to 60 were obtained. However, correlation between preparation conditions and particle size was not observed. Higher residual lignin content was found to increase thermal stability of the CNW [38]. Elanthikkal *et al*.2010 studied the effect of temperature, reaction time, and H_2SO_4 acid concentration on cellulose microfibers isolated from banana fibre waste. As the concentration of acid increases, more stable aqueous suspensions of the cellulose product were obtained; moreover the dimensions of cellulose microfibers were reduced. XRD studies revealed that cellulose prepared by acid hydrolysis has more crystallinity than the banana fibres [39]. Teixeira *et al*.2010 isolated cellulose nanofibers from white and naturally colored cotton fibres by acid hydrolysis. Suspensions of white and colored nanofibres were obtained by the acid hydrolysis of white and naturally colored cotton fibres. No significant morphological differences in shape and size were observed among them [40]. Lu and Hsieh 2010 isolated cellulose nanocrystals with rod, sphere, and network morphologies by acid hydrolysis of cotton cellulose followed by freeze-drying. Freeze drying induced mesoporosity and significantly improved specific surface than original cellulose [41].

Nanocellulose was also isolated from sugarcane bagasse (SCB) by Mandal and Chakrabarty in 2011 using acid hydrolysis. The isolated nanocellulose showed earlier onset degradation temperature compared to SCB. The results showed that the isolated nanocellulose has nano dimensions with significant conversion of cellulose I to cellulose II [42]. Teixeira *et al.* 2011 also isolated cellulose whiskers from SCB by alkaline peroxide pre-treatment followed by acid hydrolysis at 45 ^{0}C for 30 and 75 min. The results revealed that cellulose whiskers had needle like structures with an average length of 255±55 nm and diameter of 4±2 nm, giving an aspect ratio around 64. Hydrolysis for 75 min resulted in thermally less stable whiskers, caused some damage to the cellulose crystal structure [43]. Purkait *et al*.2011 isolated cellulose whiskers from sesame husk using 35% sulphuric acid. When subjected to homogenization, spherical cellulose nanoparticles (CNPs) were produced having diameters in the range of 30-120 nm [44]. Oksman *et al*.2011 isolated cellulose nanowhiskers from the residue of wood ethanol industrial production. On acid hydrolysis nanowhiskers having lower thermal stability than that obtained by ultrasonication and high-pressure homogenization were produed. The AFM study showed that ultrasonication and homogenization processes resulted in whiskers having diameters 10-20 nm [45].

Johar *et al*.2012 isolated cellulose fibres from rice husk by chemical treatment and cellulose nanocrystals by sulphuric acid hydrolysis of cellulose fibre. TEM analysis showed that most of the nanoparticles displayed a diameter and aspect ratio in the range of 15–20 nm and 10–15 respectively. X-ray diffraction analysis revealed that crystallinity increased with successive treatments [46]. Kenaf bast fibres were used for isolation of CNC, by Kargarzadeh *et al*.2012 subjecting the fibre to alkali, bleaching and subsequent hydrolysis with sulphuric acid at different hydrolysis times. The

results showed that optimum extraction time was around 40 min at 45 ^{0}C with 65% sulphuric acid. The zeta potential measured was in the range -8.7 to -95.3 mV [47]. Bamboo cellulose nanocrystals (CNCs) were successfully prepared from the sulphuric acid hydrolysis of bamboo bleached fibres by Brito *et al.* in 2012. CNCs have a width of 8±3 and length of 100±28 nm [48]. Sebe *et al*.2012 isolated cellulose II nanowhiskers (CNW-II) from microcrystalline cellulose with sulphuric acid, by controlling the amount of H_2SO_4 and the time of addition. The CNW-II showed average length of 153±66, height of 4.2±1.5 nm by AFM and width 6.3±1.7 nm by TEM, suggested ribbon shape morphology for whiskers [49]. Nanocrystalline cellulose (NCC) obtained from wood cellulose fibre by sulphuric acid hydrolysis was modified by grafting with glycidyltrimethylammonium chloride by Zaman *et al*.2012. Due to increase in cationic surface charge density, modified NCC dispersed well in aqueous media and delayed the onset of gelation in aqueous system [50]. Lu and Hsieh 2012 isolated CNCs from rice straw by using sulphuric acid for 30 minutes (CNC30) and for 45 minutes (CNC45). Analyses showed that CNC45 was smaller than CNC30 and on freeze drying of diluted CNC suspensions both assembled into long fibrous structures. Nonporous or macroporous structures formed with CNCs by self-assembly of fibres were well aligned along the fibre axis and ultrafine fibres showed extraordinary structural stability [51].

Agro industrial residue Soy hulls were used to isolate cellulose nanocrystals by Netoa *et al*.2013, using sulphuric acid for 30 and 40 minutes. The hydrolysis of 40 minutes resulted in a shorter length of nanocrystals and caused some damage on the crystal structure of the cellulose. At 30 min, the nanocrystals presented a high crystallinity of 73.5%, an average length of 122.66±39.40 nm, a diameter of 2.77±0.67 nm and an aspect ratio around 44 [52]. Peng *et al*.2013 studied the effect of air-drying, freeze-drying, spray-

drying, and supercritical-drying on properties of nanofibrillated cellulose and cellulose nanocrystals (CNC). The CNCs obtained by the three methods showed similar onset temperature of thermal degradation. The crystallinity indices differ with each drying method and cellulose II content in CNCs changes as the drying method changes [53]. Jiang and Hsieh 2013 isolated CNCs and nanofibrils (CNFs) from rice straw cellulose by sulphuric acid hydrolysis, mechanical blending and by 2,2,6,6-tetramethylpiperidine-1-oxyl (TEMPO) mediated oxidation. Sulphuric acid hydrolysis produced highly crystalline, rod-like CNCs. Mechanically defibrillated CNFs have 82.5% crystallinity. TEMPO mediated oxidation liberated the mostly uniform, finest and micrometer long, but least crystalline CNFs [54]. Morais *et al*.2013 isolated nanocellulose from cotton (*Gossypium hirsutum*) linters using sulphuric acid of 60% (w/w). The isolated nanocrystals were 177 nm long and 12 nm wide, having an aspect ratio of 19 [55]. Fortunati *et al*.2013 isolated CNC from *Phormium tenax* leaf fibres by acid hydrolysis. The morphological analysis carried out by field emission scanning electron microscope and tapping-mode atomic force microscopy confirmed typical needle-like structure of CNC, having acicular structure ranged from 100 to 200 nm in length and 15 nm in width [56].

Cellulose was extracted from corn/maize straw (Zea mays) by Rehman *et al*.2014 using alkaline treatment and total chlorine free bleaching. Partial acid hydrolysis of cellulose with sulphuric acid at 25 ^{0}C under stirring resulted aqueous suspension of cellulose whiskers, confirmed by light scattering and TEM [57]. Low intensity ultrasonic-assisted sulphuric acid hydrolysis was used by Tang *et al*.2014 to extract nanocrystalline cellulose (NCC) from MCC. NCC obtained from ultrasonic-assisted hydrolysis and conventional hydrolysis showed similar morphology having rod-like structures with width and length of 10–20 and 50–150 nm respectively. XRD

results revealed that the NCC sample from ultrasonic assisted hydrolysis contained a small amount of cellulose II [58]. Haafiz *et al*.2014 isolated CNW from MCC obtained from oil palm biomass by chemical swelling and acid hydrolysis methods. X-ray diffraction analysis indicated that chemical swelling improved the crystallinity of MCC and retained the cellulose I structure, but acid hydrolysis reduced the crystallinity of MCC and showed the co-existence of cellulose I and II [59]. Hu *et al*.2014 isolated carboxylated cellulose nanocrystals (CCN) with ammonium per sulphate and CNC with sulphuric acid from borer powder of bamboo. CCN and CNC have spherical shape with diameters of 20–50 and 20–70 nm respectively. The crystallinity of CCN and CNC were increased to 62.75 and 69.84% respectively after a series of chemical treatments [60]. Lani *et al*.2014 isolated nanocellulose fibre with diameters ranging from 4 to15 nm nanocellulose from empty fruit bunch (EFB) fibre by acid hydrolysis [61].

Different sources like banana rachis, sisal, kapok, pineapple leaf and coir were used by Deepa *et al*.2015 for isolation of nanocellulose using combination of chemical treatments like alkaline treatment, bleaching and oxalic acid hydrolysis. The results showed that isolated nanocellulose had an average diameter in the range 10–25 nm [62]. Cellulose was isolated from tomato peels using acidified sodium chlorite and chlorine free alkaline peroxide by Jiang and Hsieh 2015. Flat spindle shaped CNCs in 15.7% yield were obtained by sulphuric acid hydrolysis of isolated cellulose. CNCs from dilute aqueous suspensions were highly crystalline cellulose I_{β} fibrous mass containing mostly submicron fibres and few interconnected nanofibres. However, more uniform nanofibres assembled from CNCs were formed in 1:1 v/v *tert*-butanol/water mixture [63]. Onion skin was used to isolate CNC after isolating cellulose by Rhim *et al*.2015 using H_2SO_4 with concentrations of 45, 55, and 65%. The CNCs isolated with 45% of H_2SO_4 (CNC45) showed

the highest yield of 48.6%, crystalinity index of 0.26 and crystallite size of 2.49 nm [64]. Van Hai *et al*.2015 isolated CNCs from softwood, hardwood and non-wood plant like cotton linters, cattail and red algae by acid hydrolysis. The CNCs from cattail fibres and red algae showed higher thermal degradation temperatures and higher crystallinity indices than CNCs from wood [65]. Ghahafarrokh *et al*.2015 purified beer industrial residuals (BIR) to obtain cellulose and subsequently isolated nanocellulose (NC) using acid hydrolysis/ultrasound method. The AFM analysis showed that NCs had whisker, oval and spherical shapes having average diameters between 73 and 146 nm [66].

Goh *et al*.2016 studied the individualisation of MFCs from oil palm empty fruit bunches by ammonium persulphate oxidation and sulphuric acid hydrolysis. Long and network like fibrils were obtained by these methods having width 8 to 40 nm [67]. Velásquez *et al*.2016, isolated nanocellulose from banana plant pseudo stems harvested at 8, 16 and 24 weeks and studied the composition, morphology and structure of cellulose during plant maturation and their influence on nanocellulose performance. Nano sized bundles obtained were polydisperse and distribution changed with maturation time. The thermal stability and allomorph ratio decreased with maturation [68]. Banana pseudo stems were also used for cellulose nanocrystal isolation by Mueller *et al*. using sulphuric acid. The hydrolysis time was varied to obtain maximum length of 375±100 nm and aspect ratio of 28. The surface charge density of the CNCs thus isolated was 168 mmol kg^{-1}, the predominant crystal structure found was cellulose I with crystallinity of 74% [69]. Liu *et al*.2016 isolated nanocellulose from bleached corncob residue (CCR) using four different methods. Formic acid hydrolysis produced longer CNCs than by sulphuric acid hydrolysis, resulted in high crystallinity and thermal stability. TEMPO mediated oxidation resulted in CNFs with fine and

individualized structures [70]. Nanocellulose was isolated from kenaf core using electron beam irradiation followed by acid hydrolysis of the isolated cellulose by Kim *et al*.2016. The results revealed that the yield of nanocellulose decreased when the absorbed dose and acid hydrolysis time increased, while the size distribution became narrow [71]. Nascimento *et al.* 2016 isolated nanocrystals from unripe coconut fibre by acidic hydrolysis with high acid concentration, low acid concentration, ammonium persulfate oxidation and high-power ultrasound. All the methods used converted coconut fibre into CNCs, among these high power ultrasound showed the highest efficiency in CNC isolation [72]. Mohaiyiddin *et al*.2016 isolated nanocellulose from *Elaeis guineensis* frond (oil palm frond, OPF) through three different chemical treatments including alkaline, bleaching and acid hydrolysis processes. All results confirmed the formation of nanocellulose [73].

Since H_2SO_4 hydrolysis may introduce large number of sulphate group during hydrolysis, during pyrolysis process sulphated regions will acquire energy faster than unsulphated regions, so get eliminated quickly. Therefore, the thermal stability of nanowhisker will be comparatively less. Neutralisation with strong alkali leads to an increase in the thermal stability. Not only H_2SO_4 but other acids like HCl have been used to isolate nanocelluloses. Araki *et al*. isolated cellulose microcrystals from bleached softwood kraft pulp with 65% (w/w) sulphuric acid and 4 N HCl. Both treatments gave similar particle sizes and shapes. Conductometric titration of suspensions showed that the H_2SO_4 treated sample has surface charge due to the introduction of sulphate groups. But for HCl treated sample it was not noticed [74]. Chang *et al*. coagulated cellulose nanoparticles (CN) from NaOH/urea/water solution of microcrystalline cellulose (MC) using an ethanol/HCl aqueous solution. CNs have size about 50 to 100 nm. Compared

to MC, CN isolated has cellulose II structure [75]. Faradilla *et al*. isolated nanocellulose from banana pseudo-stem by TEMPO mediated oxidation combined with mild mechanical disintegration, the isolated nanocellulose has a tubular structure with diameter ranging from 7 to 35 nm [76].

2.4 CELLULOSE NANOMATERIAL REINFORCED COMPOSITES

The crystal modulus of cellulose was first determined in 1936 by Meyer and Lotmar and obtained a value of ~120 GPa. The value was confirmed later by experimental methods [77,78]. Sakurada *et al*. reported a value of 138 GPa for the crystal modulus of cellulose, which was determined using X-ray diffraction of deformed fibre bundles [77]. Many determinations were done for the crystal modulus of cellulose using X-ray diffraction, the theoretical predictions were almost in 100–160 GPa range [79–82]. Recent determination using inelastic X-ray scattering (IXS) showed a value of 220 GPa [83]. Since the elastic modulus of e-glass fibre was estimated to be 70 GPa, potential reinforcement by nanocellulose can be easily explained.

It is one of the strongest and stiffest natural nanomaterial, as an emerging nano material with important physico-chemical properties like, high tensile strength, stiffness, Young's modulus, aspect ratio, large surface area and other intriguing electrical and optical properties. It is amenable to modifications such as sulphonation, oxidation, cationisation and grafting. Hence nanocellulose is used in diverse applications other than their use as potential reinforcement in composites.

Favier *et al*.1995 used cellulose whiskers, extracted from sea animal as reinforcement in composite by casting a mixture of aqueous suspensions of latex obtained by copolymerization of styrene (35% w/w) and butyl acrylate (65% w/w) and whiskers. The results showed that when whisker content was

6% (w/w), mechanical properties such as shear modulus increased by two orders of magnitude in the rubbery state of the polymeric matrix [84]. Since then large number of polymers were used as matrices for the preparation of nanocomposites. Helbert *et al*.1996 incorporated cellulose microcrystals from wheat straw in poly (styrene-co-butyl acrylate) latex. The whiskers bring reinforcing effect at temperatures higher than the glass transition temperature (T_g) of the matrix and improved the thermal stability of the composite [85]. Chazeau *et al*.1998 studied nanocomposites with plasticized poly (vinyl chloride) as matrix and cellulose whiskers from tunicate as reinforcement [86]. Angles and Dufresne 2000 studied nanocomposite from glycerol plasticized waxy maize starch as the matrix and a suspension of tunicin celluloses whiskers as reinforcement [87]. Maren and William 2002 prepared nanocomposite using cellulose acetatebutyrate as matrix and modified nanocrystals from bacterial cellulose microfibrils as reinforcement. The unmodified cellulose crystals showed better reinforcement characteristics compared to modified crystals [88]. Samir *et al*.2004 studied nanocomposite using poly (oxyethylene) as the matrix and stable aqueous suspension of cellulose nanocrystals from tunicate as the reinforcing phase [89].

By using hydrophilic matrix better interaction between matrix and filler takes place leading to improvement in properties. Zimmermann *et al.* 2004 studied the effect of dispersed cellulose fibrils or fibril bundles from sulphite pulp as reinforcement in PVA. The films showed increases in modulus of elasticity and tensile strength than PVA [90]. Hydrophobic matrix like polypropylene was also studied by Ljungberg *et al*.2005 using three types of cellulose whiskers, with various surface and dispersion characteristics [91].

Bhatnagar and Sain 2005 studied the effect of nanofibers from flax bast fibers, hemp fibers, kraft pulp, and rutabaga in PVA. The tensile strength of nanocomposites developed from rutabaga containing 90% PVA and 10% nanofiber showed an increase from 69 to 118 MPa. The different nanocomposites showed four to five fold increase in Young's modulus [92]. Bruce *et al.*2005 made nanocomposites with PVA using purified cell wall fragments (PCWF) and fibrillised cell wall material (FCWM). The results showed that strength of composite at a volume fraction of 50% fibre content obtained from FCWM, increased by five times than PVA and composite stiffness also increased [93].

Wang *et al*.2006 studied nanocomposites using soy protein isolate plastics as matrix and whisker from cotton linter pulp as reinforcement. The results showed that strong interactions occurred with the addition of cellulose whisker [94]. Chakraborty *et al*. studied the reinforcing potential of cellulose microfibers obtained from bleached softwood kraft pulp in PVA. The mechanical strength measurements showed increased tensile strength by two fold and a 2.5 fold increase in stiffness with 5% microfibre loading. Decrease in strength and stiffness at higher loading was another observation [95].

Wang and Sain 2007 dispersed nanofibres from soy bean stock by chemo-mechanical treatments in PVA, up to 10% nano fiber content (SBN). The tensile strength of 5% nanofibre blend PVA film increased by five-fold [96]. The same authors also studied the reinforcing ability of nanofibre from soy bean source in three different polymers PVA, PP and PE. The tensile strength increased by fivefold at 5 wt.% fibre content for PVA composites. The DMA showed the addition of SBN improved the thermal properties of PVA and influenced the tanδ peak and storage modulus [97]. Leitner *et al.* 2007 studied reinforcement of nanofibrils from sugar beet chips using PVA

and phenol-formaldehyde as matrices. The best mechanical performance was achieved with phenol-formaldehyde resin having nanofibril content of 10% [98]. Petersson *et al*.2007 studied nanocomposites of PLA and CNW obtained from MCC [99]. Cao *et al*.2007 prepared nanocomposite films containing suspension of cellulose nanocrystals from flax fibre as filler and polycaprolactone based waterborne polyurethane (WPU) as the matrix. The films showed a significant increase in Young's modulus and tensile strength [100].

Li *et al*. isolated cellulose whiskers from cotton linter and used as reinforcement in chitosan. With increasing whisker content from 0 to 15–20 wt.%, the tensile strength increased, displayed excellent thermal stability and water resistance [101]. Lu *et al*.2008 studied the properties of PVA films reinforced with 1, 5, 10, and 15 wt.% of MFC obtained from kraft pulp. The results showed that T_g and T_m are independent on the MFC content. DMA results showed increase in the storage tensile modulus in the glassy state when the MFC content increased. Young's modulus and tensile strength of the composite increased for composites containing MFC up to10 wt.% [102]. Paralikar *et al*.2008 studied PVA barrier membrane containing cellulose nanocrystals (CNXLs) isolated from Whatman 1 filter paper with poly (acrylic acid) (PAA) as a crosslinking agent. The membrane having 10% CNXLs/10% PAA /80% PVA exhibited the highest tensile strength, tensile modulus and toughness. Differential thermogravimetric studies also supported the tensile test results. Moreover, initial degradation temperatures of composites with modified CNXL by carboxylation and unmodified CNXL increased. But composites with modified CNXL showed higher initial degradation temperature [103]. Roohani *et al*.2008 isolated cellulose whiskers from cotton linter and used as filler in PVA having different molecular weights and degrees of hydrolysis. The results showed increased

reinforcing effect when the degree of hydrolysis of the matrix increases. This leads to an increase of the glass temperature, decrease of both the melting point and degree of crystallinity of the polymeric matrix in dry atmosphere. Whisker addition increases T_g regardless the degree of hydrolysis for moist samples. Reinforcing effect was further confirmed by DMA and tensile tests [104].

Lee *et al*.2009 studied the effect of acid treatment and filler concentration of nanocellulose obtained by acid hydrolysis of MCC with different concentrations of hydrobromic acid (HBr) in PVA. The tensile strength of films with 1.5 M HBr hydrolysis showed the value 73 MPa at the loading of 1 wt.%, 49.0% higher than neat PVA film and the value decreased at higher loading. The composite film containing nanocellulose hydrolysed with 2.5 M HBr showed 8.2, 11.6 and 27.7% higher tensile strength at loading levels 1, 3, and 5 wt.% respectively than those treated with 1.5 M HBr. The thermal properties of PVA composite films were significantly improved with the increase in the nanocellulose loading [105]. Qua *et al*.2009 characterised nanocomposite of PVA reinforced with nanofiber from MCC and flax fibre using ball milling, acid hydrolysis, and ultrasound. The films showed enhanced thermal and mechanical properties with small addition of cellulose nanofibres. DMA results showed that the use of cellulose nanofibers obtained by acid hydrolysis leads to outstanding and unusual mechanical properties [106]. Cheng *et al*.2009 studied the effect of cellulose fibrils in micro and nanoscales generated through high intensity ultrasonication from regenerated cellulose fiber (RCF), pure cellulose fiber (PCF) and MCC as reinforcement in PVA. Most of the small fibers improved the mechanical properties of PVA significantly [107].

Souza *et al*.2010 isolated nanofibers from curaua fibres and studied their effect in PVA. The results indicated that with 4% of fibre loading, the stress and modulus of the composite increased by 36% and 67%, respectively and with 5% of fibre loading Young's modulus again increased [108]. Peresin *et al*.2010 prepared composite mats containing cellulose nanocrystals (CN) through electro spinning of PVA having different acetyl concentration. Cellulose nanocrystals induced 3 fold increase in the storage modulus of fully hydrolysed PVA, while this was not observed in partially hydrolysed PVA [109]. Ibrahim *et al*.2010 isolated spherical nano cellulose from cotton linter, linen and used as reinforcement in PVA. Composite film containing 20% of nano cellulose particles from linen increased the mechanical properties, while 40% and 60% resulted in decrease in the tensile strength [10]

Kamphunthong *et al*. isolated nanofibres from para rubberwood and used as reinforcing filler in PVA. The composites gave enhancement in modulus by 100% and strength by 80%, with the addition of 7 wt.% fibre. DMA and DSC also revealed the strong interaction between the fibres and PVA [110]. Zhang *et al*.2011 studied the mechanochemical activation of cellulose by pan milling on cellulose-PVA composites using melt mixing, containing formamide and water as plasticizer. The tensile strength of cellulose-PVA composites increased from 8.8 to 16.4 MPa when pan milling cycles of cellulose increased, while elongation at break increased from 76.8 to 374%. The composites exhibited enhanced thermal stability [111]. Frone *et al*.2011 prepared cellulose nanofibre reinforced PVA composites by the action of hydrodynamic force along with ultrasound. Difference in size of nanofibre was observed using different ultrasound condition, with no change in the crystalline structure of nanofibre. The tensile strength and modulus of the PVA increased significantly by the addition of nanofibre and composite showed slightly higher onset degradation temperature [112]. Bulota *et al.* 2011 prepared PVA composites film reinforced with mechanically microfibrillated (MFC) birch pulp. Increase in Young's modulus and tensile

strength were observed for MFC below 10% (w/w) content, by providing degassing. Higher strength and stiffness were showed by composites conditioned at 45% relative humidity (RH) than at 55% RH [113]. Cho and Park 2011 isolated nanocellulose (NC) from commercial MCC and added as reinforcement in different weight % in PVA. As the NC content increases the tensile modulus and strength of the nanocomposite improved, but decreased at the higher NC content of 7 wt.% [114]. Uddin *et al*.2011 prepared nanocomposite of PVA reinforced with highly oriented colloidal suspension cellulose whiskers (CWs) obtained by acid hydrolysis of commercial cotton cellulose powder in PVA. Spun fibre containing 5 wt.% CW showed higher drawability than neat PVA fibre, leading to orientation of CWs in the matrix. The 5% CW-PVA fibre has the highest tensile strength of 1.89 GPa compared to the 1.47 GPa of neat PVA fiber [115].

Kaboorani *et al*. in 2012 studied the effect of nanocrystalline cellulose (NCC) in poly (vinyl acetate) (PVAc) as a wood adhesive. The results showed that NCC can improve bonding strength, hardness, modulus of elasticity and creep of PVAc film. Thermal stability of PVAc improved significantly [116]. Martınez-Sanz *et al*. prepared ethylene-vinyl alcohol copolymer (EVA) nanocomposite, by melt compounding plant cellulose nanowhisker (CNW) and bacterial cellulose nanowhiskers (BCNW). The results showed that BCNW up to 4 wt.% can be introduced without causing significant agglomeration, but increasing the CNW concentration up to 3 wt.% induced agglomeration. DSC result revealed that poor dispersion leads to significant reduction in crystalline content [117]. Qiu and Netravali 2012 prepared PVA composites reinforced with MFC containing glyoxal as the cross linking agent. The MFC–PVA composites showed good tensile properties and thermal stabilities, get further increased by crosslinking [118]. Sharma *et al*.2012 isolated NFC from processed ryegrass and used as reinforcement in PVA. NFC-PVA composites with NFC content of 5 wt.%, exhibited enhanced Young's modulus and thermal stability by factors of 2.5

and 2 respectively than control [119]. Li *et al*.2012 isolated nanocrystalline cellulose (NCC) from MCC by high-intensity ultrasonication and used as reinforcement in PVA. The modulus of PVA with 8 wt.% NCC was found to be 2.4 times larger than that of pure PVA [120].

Liu *et al*.2013 defibrillated paper pulp into cellulose nanofiber (CNF) by mechanical grinding and high pressure homogenization, used as reinforcement in PVA to prepare transparent composite films. The addition of CNF improved the crystallinity, mechanical strength, Young's modulus, T_g and thermal stability of the PVA [121]. Li *et al*.2013 prepared nanocomposite film of PVA containing nanocellulose fibrils (NCF) from bleached hard kraft pulp through high-intensity ultrasonication. The results showed that at 4 wt.% of NCF content, tensile strength and Young's modulus of the PVA composites increased to 1.86 and 1.63 times than neat PVA and composites has excellent transparency [122]. Alves *et al*.2013 isolated CNC from corncob by sulphuric acid hydrolysis at 45 ^{0}C for 30, 60 and 90 min, and studied their reinforcing capability with PVA. The CNC-PVA composites having reinforcement of nanocellulose with 60 minute hydrolysis duration (CNC60) has showed an increase in tensile strength of 140.2%, when 9 wt.% of CNC60 was incorporated [123]. Bio-nanocomposite reinforced with CNC extracted from commercial MCC (CNC-MCC) and from two types of natural fibres, phormium tenax and flax (CNC-Flax) was prepared by Fortunati *et al.* 2013. The addition of CNC resulted in increased tensile strength for CNC-MCC and CNC-Flax compared to the PVA matrix [124].

Virtanen *et al*.2014 used chemically modified NFC by allylation and epoxidation as reinforcement in a PVA matrix. Enhancement in modulus and strength of the pure PVA film by 474% and 224% respectively was observed by the addition of 1 wt.% epoxy-NFC, film showed transmittance of 83% and improved the crystallinity of PVA. The results indicates the significant effect of chemical modification of NFC on mechanical properties of PVA [125].

Peng *et al*.2014 studied the effect of short cellulose nanofibrils (SCNF) isolated mechanically from hard wood pulp after enzymatic pre-treatment in PVA. The result revealed that when small amounts of SCNF were added, PVA crystal orientation increased and decreased as the SCNF content increased above 2 or 3%. The SCNF-PVA composite fibre with 6% SCNF showed ultimate strength and modulus 60 and 220% higher than that of neat PVA [126]. Li *et al*.2014 isolated NCFs from chemical-thermomechanical pulps (CTMP) using ultrasonication and used as reinforcement in PVA. Composites having NCF content of 6 wt.% showed better properties. The tensile strength, Young's modulus and thermal stability of composites improved significantly [127]. Zhang *et al*.2014 studied the effect of isolated CNC from MCC and compounded with PVA through melt processing along with water and formamide as plasticizer, by injection moulding. Improvement in tensile strength from 32 to 58 MPa and modulus from 175 to 1,252 MPa by the addition of 7 wt.% CNCs were observed. The presence of CNCs reduced the volume shrinkage of PVA nanocomposite on drying and their water leaching rate [128].

Kakroodi *et al*.2015 studied the effect of CNF from the skin of the beavertail cactus (*Opuntia Basilaris*) isolated by chemo-mechanical technique in PVA. The modulus and strength of the PVA matrix increased significantly by the addition of nanofibre, while the elongation at break decreased. TG showed that the inclusion of nanofibres resulted in increase in the thermal stability of composites [129]. Voronova *et al*.2015 studied the thermal stability of PVA nanocomposite using CNC from commercial MCC as reinforcement. Thermal stability of the composites improved with CNCs content of 8–12 wt.%, but decreased when more than 12 wt.% CNCs content was used [130].

REFERENCES

1. Spoljaric, S.; Genovese, A.; Shanks, R. A. Polypropylene-microcrystalline cellulose composites with enhanced compatibility and properties. *Compos. Part A* **2009**, *40*, 791–799.

2. Ibrahim, M. M.; Koschella, A.; Kadry, G.; Heinze, T. Evaluation of cellulose and carboxymethyl cellulose/poly (vinyl alcohol) membranes. *Carbohydr. Polym.* **2013**, *95*, 414–420.

3. Bana, R.; Banthia, A. K. Green composites: Development of poly (vinyl alcohol)- wood dust composites. *Polym. Plast. Technol. Eng.* **2007**, *46*, 821–829.

4. Miao, C.; Hamad, W. Y. Cellulose reinforced polymer composites and nanocomposites: A critical review. *Cellulose* **2013**, *20*, 2221–2262.

5. Uesu, N. Y.; Go, E. A.; Adelina Winkler, H. Microcrystalline cellulose from soybean husk: Effects of solvent treatments on its properties as acetylsalicylic acid carrier. *Int. J. Pharm.* **2000**, *206*, 85–96.

6. Adel, A. M.; El-wahab, Z. H. A.; Ibrahim, A. A.; Al-shemy, M. T. Characterization of microcrystalline cellulose prepared from lignocellulosic materials. Part II: Physicochemical properties. *Carbohydr. Polym.* **2011**, *83*, 676–687.

7. Sun, X.; Lu, C.; Liu, Y.; Zhang, W.; Zhang, X. Melt-processed poly (vinyl alcohol) composites filled with microcrystalline cellulose from waste cotton fabrics. *Carbohydr. Polym.* **2014**, *101*, 642–649.

8. Tang, X.; Alavi, S. Recent advances in starch, poly (vinyl alcohol) based polymer blends, nanocomposites and their biodegradability. *Carbohydr. Polym.* **2011**, *85*, 7–16.

9. Chang, J.; Jang, T.; Ihn, K. J.; Lee, W.; Sur, G. S. Poly (vinyl alcohol) nanocomposites with different clays: Pristine clays and organoclays. *J. Appl. Polym. Sci.* **2003**, *90*, 3208–3214.

10. Ibrahim, M. M.; El-zawawy, W. K.; Nassar, M. A. Synthesis and characterization of poly (vinyl alcohol)/nanospherical cellulose particle films. *Carbohydr. Polym.* **2010**, *79*, 694–699.

11. Nishiot, Y.; Manley, R. S. J. Cellulose/poly (vinyl alcohol) blends

prepared from solutions in N,N-Dimethylacetamide-Lithium Chloride. *Macromolecules* **1988**, *21*, 1270–1277.

12. Laka, M. G.; Chernyavskaya, S. A. Physicomechanical properties of composites containing "thermocell" microcrystslline cellulsoe as filler. *Mech. Compos. Mater.* **1996**, *32*, 381–385.

13. Maskavs, M.; Kalnin, M.; S, R.; Laka, M.; Chernyavskaya, S. Effect of water sorption on some mechanical paremeters of composite systems based on low density polyethylene and microcrystalline cellulose. *Mech. Compos. Mater.* **1999**, *35*, 55–62.

14. El-Zaher, N. A.; Osiris, W. G. Thermal and structural properties of poly (vinyl alcohol) doped with hydroxypropyl cellulose. *J. Appl. Polym. Sci.* **2005**, *96*, 1914–1923.

15. Mathew, A. P.; Oksman, K.; Sain, M. Mechanical properties of biodegradable composites from poly lactic acid (PLA) and microcrystalline cellulose (MCC). *J. Appl. Polym. Sci.* **2005**, *97*, 2014–2025.

16. Chakraborty, A.; Sain, M. Reinforcing potential of wood pulp-derived microfibres in a PVA matrix. *Holzforschung* **2006**, *60*, 53–58.

17. Chuayjuljit, S.; Su-Uthai, S.; Charuchinda, S. Poly (vinyl chloride) film filled with microcrystalline cellulose prepared from cotton fabric waste: Properties and biodegradability study. *Waste Manag. Res.* **2010**, *28*, 109–117.

18. Kiziltas, A.; Gardner, D. J.; Han, Y.; Yang, H. Dynamic mechanical behavior and thermal properties of microcrystalline cellulose (MCC)-filled nylon 6 composites. *Thermochim. Acta* **2011**, *519*, 38–43.

19. Xiuju, Z.; Juncai, S.; Huajun, Y.; Zidan, L.; Shaozao, T. Mechanical properties, morphology, thermal performance, crystallization behavior, and kinetics of PP/microcrystal cellulose composites compatibilized by two different compatibilizers. *J.Thermoplast. Compos.* **2011**, *24*, 735–754.

20. Guirguis, O. W.; Moselhey, M. T. H. Thermal and structural studies of poly (vinyl alcohol) and hydroxypropyl cellulose blends. *Nat. Sci.* **2012**, *4*, 57–67.

21. Hatakeyama, H.; Kato, N.; Nanbo, T.; Hatakeyama, T. Water absorbent polyurethane composites derived from molasses and lignin

filled with microcrystalline cellulose. *J.Mater.Sci.* **2012**, *47*, 7254–7261.

22. Thummanukitcharoen; Limpanart; Srikulkit. Preparation of organosilane treated microcrystalline (SiMCC) and SiMCC/polypropylene composites. *J. Met. Mater. Miner.* **2012**, *22*.

23. Schmidt, G.; Malwitz, M. M. Properties of polymer-nanoparticle composites. *Curr. Opin. Colloid Interface Sci.* **2003**, *8*, 103–108.

24. Sriupayo, J.; Supaphol, P.; Blackwell, J.; Rujiravanit, R. Preparation and characterization of alpha-chitin whisker-reinforced poly (vinyl alcohol) nanocomposite films with or without heat treatment. *Polym.* **2005**, *46*, 5637–5644.

25. Lavoine, N.; Desloges, I.; Dufresne, A.; Bras, J. Microfibrillated cellulose-Its barrier properties and applications in cellulosic materials:a review. *Carbohydr. Polym.* **2012**, *90*, 735–764.

26. Li, Y.; Liu, Y.; Chen, W.; Wang, Q.; Liu, Y.; Li, J.; Yu, H. Facile extraction of cellulose nanocrystals from wood using ethanol and peroxide solvothermal pretreatment followed by ultrasonic nanofibrillation. *Green Chem.* **2016**, *18*, 1010–1018.

27. Mathew, B.; Lopes, A.; Ferreira, S.; Souza, D.; Thomas, S.; Pothan, L. A.; Kottaisamy, M. Isolation of nanocellulose from pineapple leaf fibres by steam explosion. *Carbohydr. Polym.* **2010**, *81*, 720–725.

28. Siqueira, G.; Bras, J.; Dufresne, A. Cellulosic bionanocomposites: A review of preparation, properties and applications. *Polym.* **2010**, *2*, 728–765.

29. Beck-Candanedo, S.; Roman, M.; Gray, D. G. Effect of reaction conditions on the properties and behavior of wood cellulose nanocrystals suspensions. *Biomacromolecules* **2005**, *6*, 1048–1054.

30. Bondeson, D.; Mathew, A.; Oksman, K. Optimization of the isolation of nanocrystals from microcrystalline cellulose by acid hydrolysis. *Cellulose* **2006**, *13*, 171–180.

31. Wang, N.; Ding, E.; Cheng, R. Thermal degradation behaviors of spherical cellulose nanocrystals with sulphate groups. *Polym.* **2007**, *48*, 3486–3493.

32. Morán, J. I.; Alvarez, V. A.; Cyras, V. P.; Vázquez, A. Extraction of

cellulose and preparation of nanocellulose from sisal fibers. *Cellulose* **2008**, *15*, 149–159.

33. Habibi, Y.; Goffin, Anne, L.; Schiltz, N.; Duquesne, E.; Dubois, P.; Dufresne, A. Bionanocomposites based on poly(ε-caprolactone)-grafted cellulose nanocrystals by ring-opening polymerization. *J. Mater. Chem.* **2008**, *18*, 5002–5010.

34. Wang, N.; Ding, E.; Cheng, R. Preparation and liquid crystalline properties of spherical cellulose nanocrystals. *Langmiur* **2008**, *24*, 5–8.

35. Li, R.; Fei, J.; Cai, Y.; Li, Y.; Feng, J.; Yao, J. Cellulose whiskers extracted from mulberry: A novel biomass production. *Carbohydr. Polym.* **2009**, *76*, 94–99.

36. Pandey, J. K.; Kim, C. S.; Chu, W. S.; Lee, C. S.; Jang, D. Y.; Ahn, S. H. Evaluation of morphological architecture of cellulose chains in grass during conversion from macro to nano dimensions. *E-Polymers* **2009**, *9*, 1221–1235.

37. Paul B. Filson; Benjamin E; Dawson, A. Sono-chemical preparation of cellulose nanocrystals from lignocellulose derived materials. *Bioresour. Technol.* **2009**, *100*, 2259–2264.

38. Rosa, M. F.; Medeiros, E. S.; Malmonge, J. A.; Gregorski, K. S.; Wood, D. F.; Mattoso, L. H. C.; Glenn, G.; Orts, W. J.; Imam, S. H. Cellulose nanowhiskers from coconut husk fibers: Effect of preparation conditions on their thermal and morphological behavior. *Carbohydr. Polym.* **2010**, *81*, 83–92.

39. Elanthikkal, S.; Gopalakrishnapanicker, U.; Varghese, S.; Guthrie, J. T. Cellulose microfibres produced from banana plant wastes: Isolation and characterization. *Carbohydr. Polym.* **2010**, *80*, 852–859.

40. de Morais Teixeira, E.; Corrêa, A. C.; Manzoli, A.; de Lima Leite, F.; de Ribeiro Oliveira, C.; Mattoso, L. H. C. Cellulose nanofibers from white and naturally colored cotton fibers. *Cellulose* **2010**, *17*, 595–606.

41. Lu, P.; Hsieh, Y. L. Preparation and properties of cellulose nanocrystals: Rods, spheres, and network. *Carbohydr. Polym.* **2010**, *82*, 329–336.

42. Mandal, A.; Chakrabarty, D. Isolation of nanocellulose from waste

sugarcane bagasse (SCB) and its characterization. *Carbohydr. Polym.* **2011**, *86*, 1291–1299.

43. Teixeira, E. de M.; Bondancia, T. J.; Teodoro, K. B. R.; Corrêa, A. C.; Marconcini, J. M.; Mattoso, L. H. C. Sugarcane bagasse whiskers: Extraction and characterizations. *Ind. Crops Prod.* **2011**, *33*, 63–66.

44. Purkait, B. S.; Ray, D.; Sengupta, S.; Kar, T.; Mohanty, A.; Misra, M. Isolation of cellulose nanoparticles from sesame husk. *Ind. Eng. Chem. Res* **2011**, *50*, 871–876.

45. Oksman, K.; Etang, J. A.; Mathew, A. P.; Jonoobi, M. Cellulose nanowhiskers separated from a bio-residue from wood bioethanol production. *Biomass and Bioenergy* **2011**, *35*, 146–152.

46. Johar, N.; Ahmad, I.; Dufresne, A. Extraction, preparation and characterization of cellulose fibres and nanocrystals from rice husk. *Ind. Crops Prod.* **2012**, *37*, 93–99.

47. Kargarzadeh, H.; Ahmad, I.; Abdullah, I.; Dufresne, A.; Zainudin, S. Y.; Sheltami, R. M. Effects of hydrolysis conditions on the morphology, crystallinity, and thermal stability of cellulose nanocrystals extracted from kenaf bast fibers. *Cellulose* **2012**, *19*, 855–866.

48. Brito, B. S. L.; Pereira, F. V.; Putaux, J. L.; Jean, B. Preparation, morphology and structure of cellulose nanocrystals from bamboo fibers. *Cellulose* **2012**, *19*, 1527–1536.

49. Sèbe, G.; Frédérique Ham-Pichavant, E. I.; Koffi, A. L. C.; Tingaut, P. Supramolecular structure characterization of cellulose II nanowhiskers produced by acid hydrolysis of cellulose I substrates. *Biomacromolecules* **2012**, *13*, 570−578.

50. Zaman, M.; Xiao, H.; Chibante, F.; Ni, Y. Synthesis and characterization of cationically modified nanocrystalline cellulose. *Carbohydr. Polym.* **2012**, *89*, 163–170.

51. Lu, P.; Hsieh, You, L. Preparation and characterization of cellulose nanocrystals from rice straw. *Carbohydr. Polym.* **2012**, *87*, 564–573.

52. Flauzino Neto, W. P.; Silvério, H. A.; Dantas, N. O.; Pasquini, D. Extraction and characterization of cellulose nanocrystals from agro-industrial residue-Soy hulls. *Ind. Crops Prod.* **2013**, *42*, 480–488.

53. Peng, Y.; Gardner, D. J.; Han, Y.; Kiziltas, A.; Cai, Z.; Tshabalala, M. A. Influence of drying method on the material properties of nanocellulose I: Thermostability and crystallinity. *Cellulose* **2013**, *20*, 2379–2392.

54. Jiang, F.; Hsieh, Y. L. Chemically and mechanically isolated nanocellulose and their self-assembled structures. *Carbohydr. Polym.* **2013**, *95*, 32–40.

55. Morais, J. P. S.; Rosa, M. D. F.; De Souza Filho, M. D. S. M.; Nascimento, L. D.; Do Nascimento, D. M.; Cassales, A. R. Extraction and characterization of nanocellulose structures from raw cotton linter. *Carbohydr. Polym.* **2013**, *91*, 229–235.

56. Fortunati, E.; Puglia, D.; Monti, M.; Peponi, L.; Santulli, C.; Kenny, J. M.; Torre, L. Extraction of cellulose nanocrystals from phormium tenax fibres. *J.Polym. Env.* **2013**, *21*, 319–328.

57. Rehman, N.; Inez, M. G.; Miranda, D.; L, S. M.; Rosa; Pimentel, D. M.; B, S. M.; Nachtigall; Bica, C. I. D. Cellulose and nanocellulose from maize straw: An insight on the crystal properties. *J. Polym. Env.* **2014**, *22*, 252–259.

58. Tang, Y.; Yang, S.; Zhang, N.; Zhang, J. Preparation and characterization of nanocrystalline cellulose via low-intensity ultrasonic-assisted sulphuric acid hydrolysis. *Cellulose* **2014**, *21*, 335–346.

59. Haafiz, M. K. M.; Hassan, A.; Zakaria, Z.; Inuwa, I. M. Isolation and characterization of cellulose nanowhiskers from oil palm biomass microcrystalline cellulose. *Carbohydr. Polym.* **2014**, *103*, 119–125.

60. Hu, Y.; Tang, L.; Lu, Q.; Wang, S.; Chen, X.; Huang, B. Preparation of cellulose nanocrystals and carboxylated cellulose nanocrystals from borer powder of bamboo. *Cellulose* **2014**, *21*, 1611–1618.

61. Lani, N, S.; Nagadi, N.; Johari, A.; Jusoh, M. Isolation, characterization, and application of nanocellulose from oil palm empty fruit bunch fiber as nanocomposites. *J. Nanomater.* **2014**, *2014*, 13.

62. Deepa, B.; Abraham, E.; Cordeiro, N.; Mozetic, M.; Mathew, A. P.; Oksman, K.; Faria, M.; Thomas, S.; Pothan, L. A. Utilization of various lignocellulosic biomass for the production of nanocellulose: A

comparative study. *Cellulose* **2015**, *22*, 1075–1090.

63. Jiang, F.; Hsieh, Y. L. Cellulose nanocrystal isolation from tomato peels and assembled nanofibers. *Carbohydr. Polym.* **2015**, *122*, 60–68.

64. Rhim, J. W.; Reddy, J. P.; Luo, X. Isolation of cellulose nanocrystals from onion skin and their utilization for the preparation of agar-based bio-nanocomposites films. *Cellulose* **2015**, *22*, 407–420.

65. Van Hai, L.; Son, H. N.; Seo, Y. B. Physical and biocomposite properties of nanocrystalline cellulose from wood, cotton linters, cattail, and red algae. *Cellulose* **2015**, *22*, 1789–1798.

66. Shahabi-Ghahafarrokhi, I.; Khodaiyan, F.; Mousavi, M.; Yousefi, H. Preparation and characterization of nanocellulose from beer industrial residues using acid hydrolysis/ultrasound. *Fibers Polym.* **2015**, *16*, 529–536.

67. Goh, K. Y.; Ching, Y. C.; Chuah, C. H.; Abdullah, L. C.; Liou, N. S. Individualization of microfibrillated celluloses from oil palm empty fruit bunch: Comparative studies between acid hydrolysis and ammonium persulfate oxidation. *Cellulose* **2016**, *23*, 379–390.

68. Velsquez-Cock, J.; Castro, C.; Ganan, P.; Osorio, M.; Putaux, J. L.; Serpa, A.; Zuluaga, R. Influence of the maturation time on the physico-chemical properties of nanocellulose and associated constituents isolated from pseudostems of banana plant c.v. Valery. *Ind. Crops Prod.* **2016**, *83*, 551–560.

69. Mueller, S.; Weder, C.; Foster, E. J. Isolation of cellulose nanocrystals from pseudostems of banana plants. *RSC Adv.* **2014**, *4*, 907–915.

70. Liu, C.; Li, B.; Du, H.; Lv, D.; Zhang, Y.; Yu, G.; Mu, X.; Peng, H. Properties of nanocellulose isolated from corncob residue using sulphuric acid, formic acid, oxidative and mechanical methods. *Carbohydr. Polym.* **2016**, *151*, 716–724.

71. Du-Yeong Kim; Byoung-Min Lee; Koo, D. H.; Kang, P.-H.; Jeun, J.-P. Preparation of nanocellulose from a kenaf core using E-beam irradiation and acid hydrolysis. *Cellulose* **2016**, *23*, 3039–3049.

72. Nascimento, D. M. do; Almeida, J. S.; Vale, M. do S.; Leitão, R. C.; Muniz, C. R.; Figueirêdo, M. C. B. de; Morais, J. P. S.; Morsyleide, de, F, R. A comprehensive approach for obtaining cellulose

nanocrystal from coconut fiber.Part I: Proposition of technological pathways. *Ind. Crops Prod.* **2016**, *93*, 66–75.

73. Mohaiyiddin, M. S.; Lin, O. H.; Owi, W. T.; Chan, C. H.; Chia, C. H.; Zakaria, S.; Villagracia, A. R.; Akil, H. M. Characterization of nanocellulose recovery from Elaeis guineensis frond for sustainable development. *Clean Technol. Environ. Policy* **2016**, *18*, 2503–2512.

74. Araki, J.; Wada, M.; Kuga, S.; Okano, T. Flow properties of microcrystalline cellulose suspension prepared by acid treatment of native cellulose. *Colloids Surfaces A Physicochem. Eng. Asp.* **1998**, *142*, 75–82.

75. Chang, P. R.; Jian, R.; Zheng, P.; Yu, J.; Ma, X. Preparation and properties of glycerol plasticized-starch (GPS)/cellulose nanoparticle (CN) composites. *Carbohydr. Polym.* **2010**, *79*, 301–305.

76. Faradilla, R. H. F.; Lee, G.; Rawal, A.; Hutomo, T.; Stenzel, M. H.; Arcot, J. Nanocellulose characteristics from the inner and outer layer of banana pseudo-stem prepared by TEMPO-mediated oxidation. *Cellulose* **2016**, *23*, 3023–3037.

77. Sakurada, I.; Nukushina, Y.; Ito, T. Experimental determination of the elastic modulus of crystalline regions in oriented polymers. *J. Polym. Sci.* **1962**, *57*, 651–660.

78. Nishino, T.; Takano, K.; Nakamae, K. Elastic modulus of the crystalline regions of cellulose polymorphs. *J. Polym. Sci. Part B. Polym. Phys.* **1995**, *33*, 1647–1651.

79. Tashiro, K.; Kobayashi, M. Theoretical evaluation of three-dimensional elastic constants of native and regenerated celluloses: Role of hydrogen bonds. *Polym.* **1991**, *32*, 1516–1526.

80. Marhofer, R. J.; Reiling, S.; Brickmannay, J. Computer simulations of crystal structures and elastic properties of cellulose. *Phys. Chem.* **1996**, *100*, 1350–1354.

81. Sturcova, A.; Davies, G. R.; Eichhorn, S. J. Elastic modulus and stress-transfer properties of tunicate cellulose whiskers. *Biomacromolecules* **2005**, *6*, 1055–1061.

82. Eichhorn, S. J.; Davies, G. R. Modelling the crystalline deformation of native and regenerated cellulose. *Cellulose* **2006**, *13*, 291–307.

83. Diddens, I.; Murphy, B.; Krisch, M.; Müller, M. Anisotropic elastic properties of cellulose measured using inelastic X-ray scattering. *Macromolecules* **2008**, *41*, 9755–9759.

84. Favier, V.; Canova, G. R.; Y, J. C.; Chanzy, H.; Dufresne, A.; Gauthier, C. Nanocomposite materials from latex and cellulose whiskers. *Polym. Adv. Technol.* **1995**, *6*, 351–355.

85. Helbert, W.; Cavaille, J. Y.; Dufresne, A. Thermoplastic nanocomposites filled with wheat straw cellulose whiskers. Part I: Processing and mechanical behavior. *Polym. Compos.* **1996**, *17*, 604–611.

86. Chazeau, L.; Cavaille, J. Y.; Canova, G.; Dendievel, R.; Boutherin, B. Viscoelastic properties of plasticized PVC reinforced with cellulose whiskers. *J. Appl. Polym. Sci.* **1999**, *71*, 1797–1808.

87. Anglès, M. N.; Dufresne, A. Plasticized starch/tunicin whiskers nanocomposites.1. Structural analysis. *Macromolecules* **2000**, *33*, 8344–8353.

88. Grunert, M.; Winter, W. T. Nanocomposites of cellulose acetatebutyrate reinforced with cellulose nanocrystals. *J. Polym. Environ.* **2002**, *10*, 27–30.

89. Azizi Samir, M. A. S.; Alloin, F.; Sanchez, J. Y.; Dufresne, A. Cellulose nanocrystals reinforced poly (oxyethylene). *Polym.* **2004**, *45*, 4149–4157.

90. Zimmermann, T.; Pöhler, E.; Geiger, T. Cellulose fibrils for polymer reinforcement. *Adv. Eng. Mater.* **2004**, *6*, 754–761.

91. Ljungberg, N.; Bonini, C.; Bortolussi, F.; Boisson, C.; Heux, L.; Cavaillé, J. Y. New nanocomposite materials reinforced with cellulose whiskers in atactic polypropylene: effect of surface and dispersion characteristics. *Biomacromolecules* **2005**, *6*, 2732–2739.

92. Bhatnagar, A.; Sain, M. Processing of cellulose nanofiber-reinforced composites. *J. Reinf. Plast. Compos.* **2005**, *24*, 1259–1267.

93. Bruce, D. M.; Hobson, R. N.; Farrent, J. W.; Hepworth, D. G. High-performance composites from low-cost plant primary cell walls. *Compos. Part A. Appl. Sci. Manuf.* **2005**, *36*, 1486–1493.

94. Wang, Y.; Cao, X.; Zhang, L. Effects of cellulose whiskers on

properties of soy protein thermoplastics. *Macromol. Biosci.* **2006**, *6*, 524–531.

95. Chakraborty, A.; Sain, M.; Kortschot, M. Cellulose microfibrils: A novel method of preparation using high shear refining and cryocrushing. *Holzforschung* **2005**, *59*, 102–107.

96. Wang, B.; Sain, M. Dispersion of soybean stock-based nanofiber in a plastic matrix. *Polym. Int.* **2007**, *56*, 538–546.

97. Wang, B.; Sain, M. Isolation of nanofibers from soybean source and their reinforcing capability on synthetic polymers. *Compos. Sci. Technol.* **2007**, *67*, 2521–2527.

98. Leitner, J.; Hinterstoisser, B.; Wastyn, M.; Keckes, J.; Gindl, W. Sugar beet cellulose nanofibril-reinforced composites. *Cellulose* **2007**, *14*, 419–425.

99. Petersson, L.; Kvien, I.; Oksman, K. Structure and thermal properties of poly (lactic acid)/cellulose whiskers nanocomposite materials. *Compos. Sci. Technol.* **2007**, *67*, 2535–2544.

100. Cao, X.; Dong, H.; Li, C. M. New nanocomposite materials reinforced with flax cellulose nanocrystals in waterborne polyurethane. *Biomacromolecules* **2007**, *8*, 899–904.

101. Li, Q.; Zhou, J.; Zhang, L. Structure and properties of the nanocomposite films of chitosan reinforced with cellulose whiskers. *J. Polym. Sci. Part B. Polym. Phys.* **2007**, *47*, 1069–1077.

102. Lu, J.; Wang, T.; Drzal, L. T. Preparation and properties of microfibrillated cellulose poly (vinyl alcohol) composite materials. *Compos. Part A. Appl. Sci. Manuf.* **2008**, *39*, 738–746.

103. Paralikar, S. A.; Simonsen, J.; Lombardi, J. Poly (vinyl alcohol)/cellulose nanocrystal barrier membranes. *J. Memb. Sci.* **2008**, *320*, 248–258.

104. Roohani, M.; Habibi, Y.; Belgacem, N. M.; Ebrahim, G.; Naghi, A.; Dufresne, A. Cellulose whiskers reinforced poly (vinyl alcohol) copolymers nanocomposites. *Eur. Polym. J.* **2008**, *44*, 2489–2498.

105. Lee, S. Y.; Mohan, D. J.; Kang, I. A.; Doh, G. H.; Lee, S.; Han, S. O. Nanocellulose reinforced PVA composite films: Effects of acid treatment and filler loading. *Fibers Polym.* **2009**, *10*, 77–82.

106. Qua, E. H.; Hornsby, P. R.; Sharma, H. S. S.; Lyons, G.; McCall, R. D. Preparation and characterization of poly (vinyl alcohol) nanocomposites made from cellulose nanofibers. *J. Appl. Polym. Sci.* **2009**, *113*, 2238–2247.

107. Cheng, Q.; Wang, S.; Rials, T. G. Poly (vinyl alcohol) nanocomposites reinforced with cellulose fibrils isolated by high intensity ultrasonication. *Compos. Part A* **2009**, *40*, 218–224.

108. Souza, S. F.; Leão, A. L.; Cai, J. H.; Wu, C.; Sain, M.; Cherian, B. M. Nanocellulose from curava fibers and their nanocomposites. *Mol. Cryst. Liq. Cryst.* **2010**, *522*, 42–52.

109. Peresin, M. S.; Habibi, Y.; Zoppe, J. O.; Pawlak, J. J.; Rojas, O. J. Nanofiber composites of poly (vinyl alcohol) and cellulose nanocrystals: Manufacture and characterization. *Biomacromolecules* **2010**, *11*, 674–681.

110. Kamphunthong, W.; Hornsby, P.; Sirisinha, K. Isolation of cellulose nanofibers from para rubberwood and their reinforcing effect in poly (vinyl alcohol) composites. *J. Appl. Polym. Sci.* **2012**, *125*, 1642–1651.

111. Zhang, W.; Yang, X.; Li, C.; Liang, M.; Lu, C.; Deng, Y. Mechanochemical activation of cellulose and its thermoplastic poly (vinyl alcohol) ecocomposites with enhanced physico-chemical properties. *Carbohydr. Polym.* **2011**, *83*, 257–263.

112. Frone, A. N.; Panaitescu, D. M.; Donescu, D.; Spataru, C. I.; Constantin Radovici, A.; Trusca, R.; Somoghi, R. Preparation and charecterization of PVA composites with cellulose nanofibers obtained by ultrasonication. *BioResources* **2011**, *6*, 487–512.

113. Bulota, M.; Jaaskelainen, A. S.; Paltakari, J.; Hughes, M. Properties of biocomposites: Influence of preparation method, testing environment and a comparison with theoretical models. *J. Mater. Sci.* **2011**, *46*, 3387–3398.

114. Cho, M.; Park, B. Tensile and thermal properties of nanocellulose-reinforced poly (vinyl alcohol) nanocomposites. *J. Ind. Eng. Chem.* **2011**, *17*, 36–40.

115. Uddin, A. J.; Araki, J.; Gotoh, Y. Toward " strong " green nanocomposites: poly (vinyl alcohol) reinforced with extremely

oriented cellulose whiskers. *Biomacromolecules* **2011**, *4*, 617–624.

116. Kaboorani, A.; Riedl, B.; Blanchet, P.; Fellin, M.; Hosseinaei, O.; Wang, S. Nanocrystalline cellulose (NCC): A renewable nano-material for poly (vinyl acetate) (PVAc) adhesive. *Eur. Polym. J.* **2012**, *48*, 1829–1837.

117. Martinez-Sanz, M.; Lopez-Rubio, A.; Lagaron, J. M. Nanocomposites of ethylene vinyl alcohol copolymer with thermally resistant cellulose nanowhiskers by melt compounding (I): Morphology and thermal properties. *J. Appl. Polym. Sci.* **2013**, *128*, 2666–2678.

118. Qiu, K.; Netravali, A. N. Fabrication and characterization of biodegradable composites based on microfibrillated cellulose and poly (vinyl alcohol). *Compos. Sci. Technol.* **2012**, *72*, 1588–1594.

119. Sharma, H. S. S.; Carmichael, E.; Muhamad, M.; McCall, D.; Andrews, F.; Lyons, G.; McRoberts, W. C.; Hornsbyc, P. R. Biorefining of perennial ryegrass for the production of nanofibrillated cellulose. *RSC Adv.* **2012**, *2*, 6424–6437.

120. Li, W.; Yue, J.; Liu, S. Preparation of nanocrystalline cellulose via ultrasound and its reinforcement capability for poly (vinyl alcohol) composites. *Ultrason. Sonochem.* **2012**, *19*, 479–485.

121. Liu, D.; Sun, X.; Tian, H.; Maiti, S.; Ma, Z. Effects of cellulose nanofibrils on the structure and properties on PVA nanocomposites. *Cellulose* **2013**, *20*, 2981–2989.

122. Li, W.; Zhao, X.; Huang, Z.; Liu, S. Nanocellulose fibrils isolated from BHKP using ultrasonication and their reinforcing properties in transparent poly (vinyl alcohol) films. *J. Polym. Res* **2013**, *20*, 210.

123. Alves, H.; Pires, W.; Neto, F.; Oliveira, N.; Pasquini, D. Extraction and characterization of cellulose nanocrystals from corncob for application as reinforcing agent in nanocomposites. *Ind. Crops Prod.* **2013**, *44*, 427–436.

124. Fortunati, E.; Puglia, D.; Luzi, F.; Santulli, C.; Kenny, J. M.; Torre, L. Binary PVA bio-nanocomposites containing cellulose nanocrystals extracted from different natural sources: Part I. *Carbohydr. Polym.* **2013**, *97*, 825–836.

125. Virtanen, S.; Vartianen, J.; Tammelin, T.; Vuoti, S. Modified nanofibrillated cellulose–poly (vinyl alcohol) films with improved

mechanical performance. *RSC Adv.* **2014**, *4*, 11343–11350.

126. Peng, J.; Ellingham, T.; Sabo, R.; Turng, L.-S.; Clemons, C. M. Short cellulose nanofibrils as reinforcement in poly (vinyl alcohol) fiber. *Cellulose* **2014**, *21*, 4287–4298.

127. Li, W.; Wu, Q.; Zhao, X.; Huang, Z.; Cao, J.; Li, J.; Liu, S. Enhanced thermal and mechanical properties of PVA composites formed with filamentous nanocellulose fibrils. *Carbohydr. Polym.* **2014**, *113*, 403–410.

128. Zhang, W.; He, X.; Li, C.; Lu, C.; Zhang, X.; Deng, Y. High performance poly (vinyl alcohol)/cellulose nanocrystals nanocomposites manufactured by injection molding. *Cellulose* **2014**, *21*, 485–494.

129. Kakroodi, A. R.; Panthapulakkal, S.; Sain, M.; Asiri, A. Cellulose nanofibers from the skin of beavertail cactus, Opuntia Basilaris, as reinforcements for poly (vinyl alcohol). *J. Appl. Polym. Sci.* **2015**, *132*, 1–7.

130. Voronova, M. I.; Surov, O. V; Guseinov, S. S.; Barannikov, V. P.; Zakharov, A. G. Thermal stability of poly (vinyl alcohol)/nanocrystalline cellulose composites. *Carbohydr. Polym.* **2015**, *130*, 440–447.

CHAPTER 3
MATERIALS AND METHODS

Abstract

The materials and experimental methods employed for the present study are given in this chapter. The establishment of chemical composition of sago seed shells, isolation of microcrystalline cellulose, cellulose nanocrystals and different instrumentation techniques used for the characterisation are highlighted. The characterisation technique used includes FT-IR spectroscopy, ATR-FTIR, X-ray diffraction, thermogravimetry, differential scanning calorimetry, particle size analysis, UV-Visible spectroscopy, scanning electron microscopy, transmission electron microscopy and atomic force microscopy. Moreover, the composite films were examined for mechanical properties, barrier properties and biodegradability.

3.1 MATERIALS

3.1.1 Sago seed shells

Sagos (*Cycas circinalis*) are known to be an Indian-endemic, restricted to the Western Ghats in the states of Kerala, Karnataka, Tamil Nadu and the south of Maharashtra. Sago seed shells were collected locally and dried in sunlight. The air dried sago seed shells were powdered mechanically and used for analysis. The images of sago (*Cycas circinalys*), air dried sago seed shells and powdered sago seed shells are shown in **Figure 3.1**

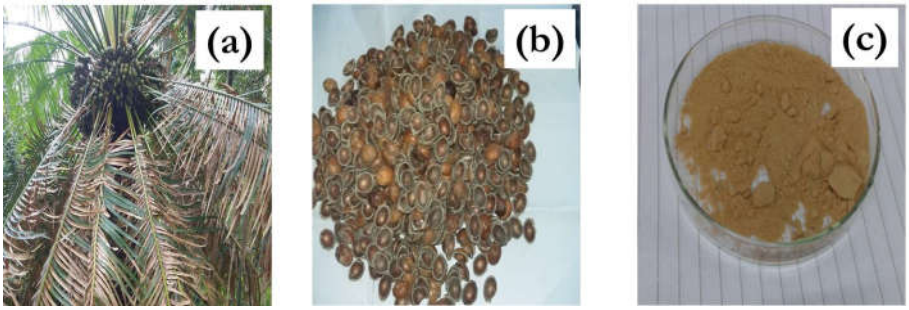

Figure 3.1 Images of (a) sago (*Cycas circinalys*), (b) air dried sago seed shells and (c) powdered sago seed shells.

3.1.2 Poly (vinyl alcohol) (PVA)

Poly (vinyl alcohol) with molecular weight in the range of 60000-125000, fully hydrolysed having the degree of hydrolysis 98-100% was purchased from HIMEDIA

3.1.3 Chemicals

Chemicals like toluene, ethanol, glacial acetic acid, sodium hydroxide, hydrochloric acid and sulphuric acid used were obtained from Merck India and sodium chlorite 80% from Loba chem, India.

3.1.4 Dialysis membrane

Dialysis membranes used have molecular weight cut off 12000-14000 Da and obtained from HIMEDIA

3.2 METHODS

3.2.1 Determination of composition of sago seed shells

The powdered and 53 μm sieved samples were dried in hot air oven maintained at 100-105 ^{0}C for 3-4 h till constant weight was obtained. ASTM methods were employed to establish the composition of sago seed shells. Since lignocellulosic materials are generally composed of extractives, klason lignin, holocellulose, α-cellulose and ash content, analyses were carried out for above components. Extractives were determined by ASTM D1107-96, klason lignin established by ASTM D1106-96, holocellulose was isolated by method described by Wise *et al* 1946 [1], α-cellulose determined as per ASTM D 1103-60, hemicellulose by difference between holocellulose and α-cellulose and ash content by T 211 om 02.

3.2.2 Isolation of microcrystalline cellulose (MCC)

α-Cellulose has been converted into MCC by following methods. Schematic representation of analysis and isolation of MCC are shown in **Scheme 3.1. Figure 3.2** shows the images during this process. The isolated MCC has off-white colour.

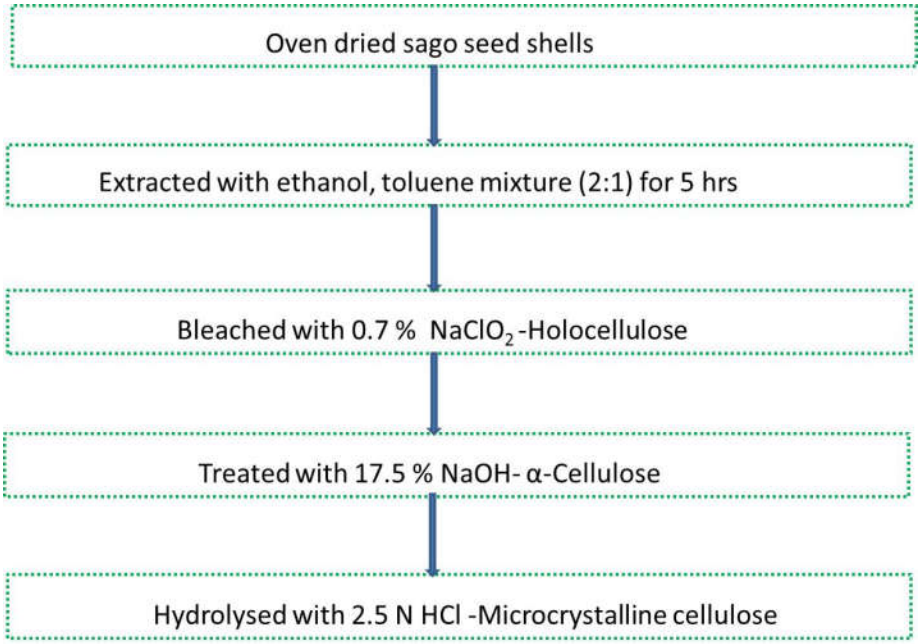

Scheme 3.1 Schematic representation of analysis and isolation of MCC.

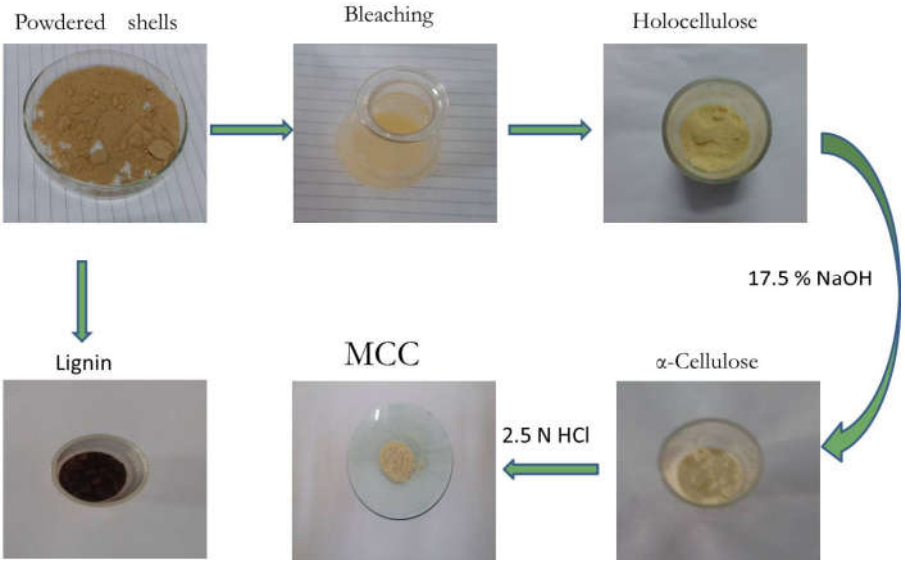

Figure 3.2 Images of different components during analysis and that of MCC.

3.2.3 Fabrication of MCC reinforced PVA composites

The fabrication of composite film is represented in **Scheme 3.2**. Solution casting technique is the most common method used for the preparation of film due to its easiness [2]. PVA solution was prepared by dissolving 5 g in 80 mL of distilled water at 90 ^{0}C for 1h. PVA-MCC suspension was prepared by adding 1/2/3/ weight % of MCC which was isolated from sago seed shell. The suspension is then dispersed by ultrasonic treatment, by keeping in ice bath for 1 h at 30% amplitude using SONICS Vibra Cell. The solution was then gently poured into a glass plate with controlled levelling of approximately 0.1-0.2 thickness, taking care not to entrap any bubbles in the solution. The plate was kept for 12 h in an air oven maintained at 80 ^{0}C, then at room temperature for 12 h for conditioning. The prepared film was labelled as 5PVA-1MCC, 5PVA-2MCC, 5PVA-3MCC, which contains 1, 2 and 3 weight % of MCC respectively.

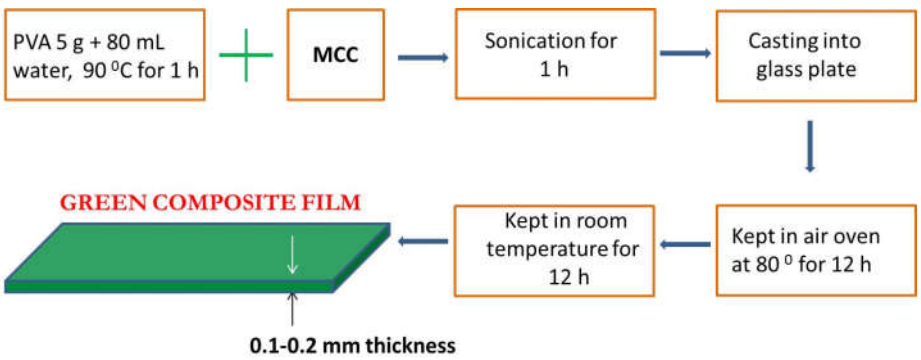

Scheme 3.2 Flow chart of green composite film fabrication.

3.2.4 Isolation of cellulose nanocrystals from sago seed shells

The method of isolation of cellulose nanocrystals are shown in **Scheme 3.3.** CNCs suspension was prepared from already isolated α-cellulose, which was obtained by sieving through 53 µm mesh [3].

Hydrolysis was carried out with 64% (w/w) sulphuric acid (9 mL: 1g) at 45 ^{0}C for 45 min with vigorous stirring. Immediately followed by the acid hydrolysis, the suspension was diluted to tenfold with deionised water to quench the reaction. The suspension was centrifuged at 4,500 rpm for 10 min to concentrate the cellulose crystals and to remove the excess of aqueous acid. The resultant precipitate was rinsed, centrifuged, and dialyzed against deionised water until constant neutral pH was achieved. The suspension was sonicated by keeping in ice bath repeatedly using SONICS Vibra Cell at 30% amplitude for 30 minutes and resulting suspension was freeze-dried.

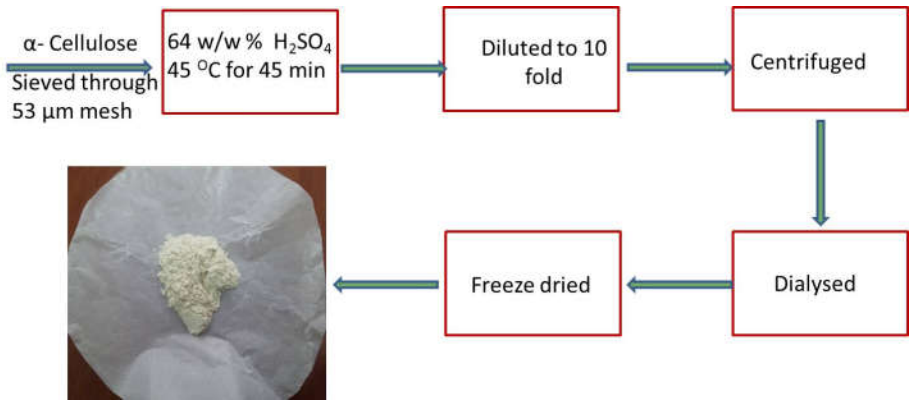

Scheme 3.3 Flow chart of the isolation of cellulose nanocrystals.

3.2.5 Fabrication of bio-nanocomposites of PVA reinforced with cellulose nanocrystals.

Fabrication method is same as shown in **Scheme 3.2** except instead of MCC, cellulose nanocrystals are used. PVA solution was prepared by dissolving 5 g in 80 mL of distilled water at 90 ^{0}C for 1h. PVA-CNC suspension was prepared by adding 0.5/0.75/1 weight % of CNCs relative to the PVA weight and then dispersed by ultrasonic treatment using SONICS Vibra Cell by keeping in ice bath for 1 h at 30% amplitude. The solution was then carefully poured into a glass plate with controlled levelling of

approximately 0.1-0.2 mm thickness, taking care not to entrap any bubbles in the solution. The plate was kept for 12 h in an air oven maintained at 80 ^{0}C, then at room temperature for 12 h for conditioning. The prepared film was labelled as 5PVA-0.5CNC, 5PVA-0.75CNC, 5PVA-1CNC, which contains 0.5, 0.75 and 1 wt.% of CNCs respectively.

3.2.6 Fabrication of bio-nanocomposite of PVA reinforced with cellulose nanocrystals for barrier membrane applications

Fabrication method is same as shown in **Scheme 3.2** instead of MCC cellulose nanocrystals were used and in addition to that, half the volume (~ 25mL) of the total solution was used for fabrication. Solution of PVA was prepared by dissolving (5 g in 70 mL) of distilled water at 90 ^{0}C for 1h. PVA-CNC suspension was prepared by adding 0.5/0.75/1 weight % (relative to the PVA mass) of isolated cellulose nanocrystals (CNCs) and then dispersed by ultrasonic treatment for 1 h at 30% amplitude using SONICS Vibra Cell in an ice bath. 25 mL of this solution was then carefully poured into a Teflon plate with controlled levelling of approximately 0.1-0.2 mm thickness, taking care not to entrap any bubbles in the solution. The plate was kept for 12 h in an air oven maintained at 80 ^{0}C, then at room temperature for 12 h for conditioning. The prepared films were labelled as 5PVA-0.5CNC, 5PVA-0.75CNC, 5PVA-1CNC, which contains 0.5, 0.75 and 1 wt.% of CNC respectively. Different barrier membranes fabricated are shown in **Figure 3.3**

Figure 3.3 Images of (a) 5PVA film, (b) 5PVA-0.5CNC (c) 5PVA-0.75CNC and (d) 5PVA-1CNC.

3.3 CHARACTERIZATION

3.3.1 FTIR

Infrared region of the electromagnetic spectrum is utilised in infrared spectroscopy to identify functional group present in the material, comprising of near, mid, and far-infrared regions. The fundamental vibration and vibrational rotational spectra of molecule are found in mid-infrared region having 4000-400 cm^{-1}. In modern infrared spectrometers or spectrophotometers, the optical pathway produces interferogram a complex wave like pattern, containing all the frequencies which make up infrared spectrum. Mathematical operation, Fourier transform can separate individual frequencies and produce spectrum identical to that of dispersive spectrometer [4]. FTIR spectra was used to identify the changes taking place during the treatment or by the chemical reaction, by monitoring functional and other characteristic groups present in the sample. The FTIR spectra were recorded by mixing the IR transparent salt KBr and pressing into a pellet.

FTIR spectra were recorded in the range of 4000-400 cm^{-1} with JASCO FTIR-4100 spectrometer using KBr pellet.

3.3.2 Attenuated total reflectance-FTIR (ATR-FTIR)

ATR is a sampling technique which employs IR beam, directed towards a crystal having relatively higher refractive index usually >2. When IR beams hits, it gets reflected from the internal surface of the crystal producing an evanescent wave orthogonal to the sample, which is in intimate contact with the ATR crystal. Some of the energy of evanescent wave is absorbed by the sample and reflected radiation is returned to the detector. Materials like soft polymers, rubbers, soft powders, pastes, gels, surface coatings etc., can be analysed by ATR-FTIR [5]. Therefore ATR is widely

used as a FTIR sampling technique. ATR allows qualitative or quantitative analysis of samples with little or no sample preparation which greatly speed up sample analysis. Since ATR-FTIR is characterised by thin sample path length or penetration of the IR beam into the sample, which is against the traditional FTIR sampling by transmission method.

ATR-FTIR spectrum of composites were taken by an attenuated total reflectance FT-IR spectrometer JASCO FTIR-4700 in the range of 400-4000 cm^{-1}.

3.3.3 X-ray diffraction

X-ray diffraction is a non-destructive technique that gives information regarding chemical composition, crystal structure, atomic spacing and properties of organic and inorganic materials. Since crystalline substances can act as three dimensional diffraction gratings for X-rays, because the wavelengths of X-rays are similar to the spacing of planes in a crystal lattice. The principle involves the constructive interference of monochromatic X-rays from crystal. The X-rays are generated in cathode ray tube, monochromatic radiation is produced by filtration followed by collimation and directed towards the sample. The interaction between the incident rays and the sample takes place producing constructive interference, when diffracted rays obey Bragg's Law $n\lambda=2d \sin\theta$, where n=1, 2, 3… (usually taken as 1), λ=wavelength (1.5418 Å for copper), d=interatomic spacing in angstroms and θ=diffraction angle in degrees.

This law relates the wavelength of X-ray used and the diffraction angle and the lattice spacing in sample, so that crystal structure of solids can be identified. By scanning the sample through 2θ angles the diffracted X-rays are detected. When the sample rotates in the path of the collimated X-ray

beam by an angle θ, while the detector is placed on an arm to collect the diffracted X-rays and the arm rotates at an angle of 2θ [6]. For powdered sample all possible diffraction directions of the lattice can be attained due to the random orientation. For polymers periodicity in molecular structure arising due to periodicity in repeat unit, repeat distance associated with periodicity in crystal. Large amount of information are obtained from diffraction patterns. Understanding and elucidation of crystalline, drawn or oriented polymers, degree of crystallinity, that is relative amount of crystalline and amorphous regions and crystallite size [7].

The X-ray diffraction of the materials was carried out by using RIGAKU MINIFLEX-600 diffractometer with Cu Kα (λ=1.54 A^0). The samples were scanned at 2θ range of 10 to 60^0 at a step size of 0.02^0.

3.3.4 UV-Visible Spectra

The transparency of the composites films were measured using Jasco-V 550 UV-VIS spectrophotometer in the range 200-900 nm.

3.3.5 Thermal analysis

3.3.5.1 Thermogravimetry (TG)

Thermal analysis involves monitoring the behaviour of materials as a function of temperature. Weight changes of the materials, when it is heated or cooled at controlled rate are measured as a function of temperature. In TG, thermograms are obtained by plotting weight loss against temperature and in the case of differential thermogram (DTG) weight change with respect to change in temperature are plotted against temperature. TG is used for the characterisation of wide variety of materials including inorganic compounds, organic compounds, minerals, polymers etc. Thermogravimetric curves are

specific for a given materials due to unique sequence of physico-chemical reactions taking place over specific temperature ranges and at given heating rate.

Thermal properties of polymeric materials are studied by thermogravimetry. Thermogravimetric data indicates a number thermal breakdown, weight loss of the material in each stage, etc. Both TG and DTG give information about the nature and extent of degradation of the material due to several transformations like decomposition, oxidation, dehydration, depolymerisation, removal of volatile compounds etc. TG gives information like, polymer decomposition temperatures, thermal stability, extent of cure of cross linked polymers, effect of additives, oxidative stability, ash, filler, moisture, residual solvent, plasticizer contents of polymers, rate of decomposition, activation energy etc [8].

TG was carried out using TA Q50 instrument. The decomposition was studied from room temperature to 650 ^{0}C with a heating rate of 10 ^{0}C per minute, under nitrogen atmosphere.

3.3.5.2 Differential scanning calorimetry (DSC)

DSC is another important thermal analysis technique, involves the measurement of energy required to establish a nearly zero temperature difference between a substance and an inert reference material, recorded as function of temperature or time, when the two specimens are subjected identical temperature in an environment heated or cooled at a controlled rate. In DSC the differential power in milliwatts required to maintain the sample and reference at the same temperature is plotted against the temperature [9]

DSC gives information regarding the glass transition temperature, melting temperature, crystallization temperature, heat capacity, percentage

crystallinity etc. Since these parameters are very important for the characterisation of polymers and composites, DSC is considered as a very important tool for the characterisation of polymers and composites. DSC gives quantitative, qualitative information and exothermic or endothermic process during physical and chemical changes. The difference in heat energy required to maintain the sample and reference nearly at identical temperature are given as the heat changes associated with process.

DSC analyses were performed using Perkin Elmer 4000 under nitrogen atmosphere by keeping the flow rate of 20 mL/min, between 30 ^{0}C and 300 ^{0}C and at a scanning rate of 10 ^{0}C/min. The glass transition was taken at the onset of the glass transition endotherm (T_g) melting temperature (T_m) as the peak point at melting endotherm and ΔH_f obtained from the area under the melting endotherms.

3.3.6 Morphological studies

3.3.6.1 Scanning electron microscopy (SEM)

Morphology involves the study of structure of objects using microscope. Microscope may vary in their ability of resolution, magnification and contrast mechanisms. Optical microscopy uses visible light as a source for illumination, lenses to magnify the objects, and resolution of only 0.2 micrometres. Electron microscopy is an important tool because it allows the observation and characterisation in nm to micro meter scale. It can give information regarding topology, morphology, composition and crystallographic information.

Polymer composite morphology can give information regarding the size, shape of fillers, additives and their distribution. Since the properties of composites depends upon the uniform distribution of filler particle, their size,

shape and agglomeration. It can also give information regarding surface features of natural and synthetic polymers, fracture and failure mechanism of composites under tear, tension and abrasion [7].

The surface morphology was studied using JEOL Model JSM - 6390LV SEM in different magnifications (X100, X1500, X2500, and X5000). SEM micrographs were taken at voltage of 10, 15 & 20 kV.

3.3.6.2 Transmission electron microscopy (TEM)

TEM utilises three different interactions, transmitted beam, diffracted beam and inelastically scattered electrons, when an electron beam is irradiated with sample. The thick sample will appear as dark because they have few transmitted unscattered electrons, while thin areas will have more transmitted electrons and will appear as lighter.

TEM observations were performed using JEOL model JEM 2100. Very diluted aqueous suspension was sonicated in a water bath sonicator, and then a drop of the solution was deposited on carbon coated copper grid, which was dried and used for imaging.

3.3.6.3 Atomic force microscopy (AFM)

It is the one of the scanning probe microscopic techniques used. Here physical probe is used, that roaster scan across the surface and the tip surface forces are measured. It gives information regarding the interatomic repulsive force and van der Walls forces, leading to surface information.

AFM was taken on WI Tec Alpha 300RA (Germany) in non-contact mode having the tip force constant 2.8 N/m. Drops of dilute aqueous suspensions deposited on glass and left to dry at room temperature prior to analysis and composite samples were observed directly.

3.3.7 Particle size distribution and zeta potential (Z P)

Dynamic light scattering (DLS) is used for determining the size of particles in colloidal suspensions [10]. The DLS utilizes time variation of scattered light from suspended particles under brownian motion to measure hydrodynamic size distribution, using photon correlation spectroscopy [11].

Zeta potential is the main factor influencing repulsion between particles which measures the stability of particles in water. Z P is defined as the mobility of a particle per electric field unit and is measured by applying an electric field in a homogeneous aqueous suspension using the Helmholtz–Smoluchowski equation [12]. Dynamic light scattering is used to study the mobility of the aqueous suspension of particles under electric field undergoing electrophoresis and converted to zeta potential. Dilute aqueous suspension of the sample were used to measure the particle size by monitoring the scattered light intensity at an angle 90^0, by measuring the diffusion of particles moving under Brownian motion and converting this to size and size distribution. The zeta potential was calculated by measuring the electrophoretic mobility of the suspension and converting the mobility in to potential. It uses laser doppler microelectrophoresis and electric field to the dispersion of particles, which then move with a velocity related to their zeta potential.

The particle size distribution and zeta (ζ) potential of the nanocellulose colloids were analysed using HORIBA, Zeta Sizer Nano Series with water as the dispersant at room temperature (25 ^{0}C).

3.3.8 Mechanical properties

Since the final use of any product involves some mechanical loading, the mechanical properties of polymers and composites are very important.

Information like tensile, flexural, compression and shear will guide us to optimise the formulations, processes and quality control. Most important test carried out to know the strength is tensile test, done on a universal testing machine. Tensile tests relate the ability of the polymer or composites to withstand the pulling force and the limit which the material can be stretched before breaking. The specimens were placed vertically in the grips of the universal testing machine having the gauge length kept at 40 mm. As the test starts, when the grip pulls out, the specimen elongates, the load value (F) is recorded when the specimen get broken. Tensile properties like tensile strength, elongation at break and Young's modulus can be obtained. The dumbbell shaped standard specimens are usually used for tensile strength measurements.

Tensile strength: It is the force measured by the load cell at the time of break divided by the original cross sectional area of the sample.

Elongation at break: It is measured in terms of initial length (L_0) and final length (L_1) at break.

Elongation at break (%) = $(L_1-L_0)x100/ L_0$

The measurements were carried out at a crosshead speed of 10 mm/min having the grip separation of 40 mm using SHIMADZU (AGX-PLUS-10kN), performed with ISO-37-Type-2 (80X12.5X4 mm) specimen. Tensile strength measurements were performed at room temperature for at least five samples from each composite film and the thickness of the films was measured using a digital micrometre 'Mitutoyo', Japan at 5 random positions.

3.3.9 Barrier properties

3.3.9.1 Water vapour transmission rate (WVTR)

WVTR of the films was measured according to ASTM E 96-95 method with slight modifications. Circular cups with inner diameter 35 mm and height 45 mm were chosen. Distilled water (25 mL) was taken in each cup and sealed perfectly with films. The distance between water level and the film was 20 mm and placed in desiccator containing anhydrous calcium chloride at 25 ^{0}C. The amount of water vapours transferred through the films was measured as the mass loss of the cup at a time interval of 1 h. WVTR in $gh^{-1}m^{-2}$ is obtained by plotting the weight loss against time and dividing the slope of the graph with the area of the film in m^2. The experiment was repeated three times and average of values were taken [13,14].

3.3.9.2 Moisture uptake (MU)

Circular samples having diameter 1.94 cm were cut from the film and used for studies. Initially, the samples were dried in a vacuum oven maintained at 60 ^{0}C for about 24 h, cooled in a desiccator and immediately weighted.

Vacuum oven dried samples having the initial weight (M_o), were placed in a desiccator conditioned to 98% relative humidity with a saturated copper sulphate solution. At time intervals (t), the sample weight (M_t) was determined until an equilibrium value (M_∞) was reached. The sample thickness was measured using digital micrometre 'Mitutoyo" Japan at 5 different places and average of three samples from each composite film were tested [15].The MU was calculated using the **Equation 3.1**

$$MU\ (\%) = (M_t – M_0)\ x100/M_0 \text{ ----------} \mathbf{3.1}$$

M_t is the weight of the sample kept at 98% relative humidity at time‘t’ and M_0 is the initial weight of the sample.

3.3.9.3 Gas barrier

The oxygen transmission rate of the film was measured using the method ISO15105-1.

3.3.10 Biodegradation by soil burial test

The biodegradability of composite films was evaluated by soil burial experiment. Biodegradation, bio-recycling and composting are different ways employed for eliminating polymeric wastes. Direct and indirect methods are used for monitoring biodegradability of plastics and composites. The indoor soil burial experiment was done in a series of plastic trays containing garden soil. Dumb bell shaped [ISO-37-Type-2 (80X12.5X4 mm)] samples were used for biodegradation study, which was previously dried at 70 ^{0}C for 24 h. Weighed and buried in garden soil for two months. Water was sprayed to retain the moisture at regular time intervals. After two months, the samples were withdrawn washed with distilled water and dried at 70 ^{0}C in an oven until constant weight was obtained [16–19]. The degradation in soil was also monitored by measuring tensile strength after soil burial and by morphological examination through SEM [20].

REFERENCES

1. Wise, L. E.; Murphy, M.; Adieco, A. D. A chlorite holocellulose, its fractionation and bearing on summative wood analysis and studies on the hemicelluloses. *Pap. Trace J.* **1946**, *122*, 35–42.

2. Li, W.; Yue, J.; Liu, S. Preparation of nanocrystalline cellulose via ultrasound and its reinforcement capability for poly (vinyl alcohol) composites. *Ultrason. Sonochem.* **2012**, *19*, 479–485.

3. Naduparambath, S.; Purushothaman, E. Sago seed shell: Determination of the composition and isolation of microcrystalline cellulose (MCC). *Cellulose* **2016**, *23*, 1803–1812.

4. Pavia, D. L.; Lampman, G. M.; Kriz, G. S. *Introduction to spectroscopy*; Second edition; Saunders golden sunburst series, 1996.

5. Chatwal, G. R.; Sham K Anand *Insrumental method of analysis*; Eighth edition; Himalaya publishing house, 2003.

6. Kaur, H. *Instrumental method of analysis*; First edition; Pragati Prakashan, 2012.

7. Ghosh, P. *Polymer science and technology plastics, rubber, blends and composites*; mcGraw hill education (India) Private limited, 2014.

8. Wunderlich, B. *Thermal analysis of polymeric materials*; Springer, Berlin, 2005.

9. Willard, H. H.; Merrit, L. L.; John A Dean; Stella, F. A. *Instrumental method of analysis*; cbs Publishers and Distributers, 1986.

10. Berne, B. J.; Pecora, R. *Dynamic light scattering with applications to chemistry, biology and physics*; Wiley Interscience, New York, 1976.

11. Xu, R. Shear plane and hydrodynamic diameter of microspheres in suspension. *Langmiur* **1998**, *7463*, 2593–2597.

12. H. E. Ries. Microelectrophoresis measurement on polymeric flocculants alone and in excess model colloids. *Nature* **1970**, *226*, 72–73.

13. Rahman, P. M.; Mujeeb, V. M. A.; Muraleedharan, K.; Thomas, S. K. Chitosan/nano ZnO composite films: Enhanced mechanical, antimicrobial and dielectric properties. *Arab. J. Chem.* **2016**.

14. Saxena, A.; Ragauskas, A. J. Water transmission barrier properties of biodegradable films based on cellulosic whiskers and xylan. *Carbohydr. Polym.* **2009**, *78*, 357–360.

15. Rodriguez, N. L. G. de; Thielemans, W.; Dufresne, A. Sisal cellulose whiskers reinforced polyvinyl acetate nanocomposites. *Cellulose* **2006**, *13*, 261–270.

16. Lani, N, S.; Nagadi, N.; Johari, A.; Jusoh, M. Isolation, characterization, and application of nanocellulose from oil palm empty fruit bunch fiber as nanocomposites. *J. Nanomater.* **2014**, *2014*, 13.

17. Bras, J.; Hassan, M. L.; Bruzesse, C.; Hassan, E. A.; El-wakil, N. A.; Dufresne, A. Mechanical, barrier, and biodegradability properties of bagasse cellulose whiskers reinforced natural rubber nanocomposites. *Ind. Crops Prod.* **2010**, *32*, 627–633.

18. Ismail, H.; Zaaba, N. F. Effect of unmodified and modified sago starch on properties of (sago starch)/silica/PVA plastic films. *J. Vinyl Addit. Technol.* **2014**, *20*, 185–192.

19. Azahari, N. A.; Othman, N.; Ismail, H. Biodegradation studies of poly (vinyl alcohol)/corn starch blend films in solid and solution media. *J. Phys. Sci.* **2011**, *22*, 15–31.

20. Muniandy, K.; Ismail, H.; Othman, N. Biodegradation, morphological, and FTIR study of rattan powder- filled natural rubber composites as function of filler loading and a silane coupling agent. *BioResources* **2012**, *7*, 957–971.

CHAPTER 4

SAGO SEED SHELL: DETERMINATION OF COMPOSITION AND ISOLATION OF MICROCRYSTALLINE CELLULOSE

Abstract

This chapter presents the determination of composition and isolation of microcrystalline cellulose from sago seed shells (Cycas circinalis). Sago seed shells are agricultural wastes which are discarded after taking the pith. The composition of sago seed shells has been determined by using standard methods. Parameters like extractives (ASTM D1107-96), Klason lignin (ASTM D1106-96), holocellulose (Wise et al. 1946), a-cellulose (ASTM D 1103-60), hemicellulose (by difference), and ash content (T 211 om 02) were determined. The components were characterized using FTIR, TG, XRD, SEM, TEM and AFM. a-Cellulose has been converted into microcrystalline cellulose (MCC) by acid hydrolysis. MCC was also characterized by using FTIR, TG, XRD, SEM, TEM and AFM.

Part of this chapter has been published in Cellulose (2016) 23:1803–1812

4.1 INTRODUCTION

Lignocellulosic materials have been investigated and exploited for decades as raw materials for a number of applications like paper and pulp, energy, ethanol, as additives in optical and pharmaceutical industries, reinforcement in polymer composites etc [1,2]. The compositional analysis of lignocellulosic feed stocks like corn stover, sugar cane, tobacco stalks, wheat straw, other agricultural and forest residues are important for their utilisation in a number of fields [3]. The convenience of these materials lies in the fact that, they are obtained easily from natural waste. Hemicellulose, cellulose and lignin are the three main components of biomass and they in general cover respectively 20–40, 40–60, and 10– 25 wt.% [4].

Among this, cellulose is a versatile biopolymer, which is biodegradable and renewable, used in a wide variety of industries [5]. It is a linear polymer consisting of β-(1→4) glucopyranose units. During biosynthesis they are self-assembled into microfibrils and are then packed to macrofibrils containing amorphous and crystalline regions [6]. It is characterised by hydrophilicity, low density, reinforcing ability, amenable for modification. In addition to these, it has environmental advantages and has attracted many scientists to develop cellulose based composites [7]. Cellulose can be hydrolysed using mineral acids like HCI and H_2SO_4, so that the amorphous regions are removed. Based on the extent of removal of amorphous regions and on dimension, microcrystalline cellulose and nanocelluloses can be produced.

Hemicellulose is composed of different types of cycled saccharides such as xylose, mannose, glucose etc. It is has highly branched random structure with mainly amorphous character. Lignins are amorphous polymers

formed by phenyl propane units, mainly consisting of aromatic units such as guaiacyl, syringyl and phenylpropane [8].

Microcrystalline cellulose (MCC) is a white, odourless, fine crystalline powder, used in a wide variety of industries like cosmetics, food and pharmaceuticals as suspension stabiliser, water retainer and as reinforcement in tablets etc. Based on the origin the properties like crystallinity, moisture content, surface area, porous structure, particle size and molecular weight of MCC are found to vary [9]. MCC can be added as reinforcing filler in polymer matrix to give biocomposites. Moreover, it is one of the precursors for obtaining nanocellulose.

Eventhough, wood and cotton are the principal sources for the commercial production of MCC, other sources, like news print waste, water hyacinth [10], sugar beet pulp, corn cob, groundnut shell, Indian bamboo and luffa cylindrica, rice hulls, wheat and rice straws have also been studied [11].

Paralikar and Bhatawdekar in 1988 isolated MCC from bagasse pulp after bleaching with sodium chlorite followed by acid hydrolysis for 15 min with 2N HC1 at boiling temperature. The weight loss during hydrolysis, moisture regain, pH and ash content were in good agreement with the standard [12]. Gaonear and Kulkarni 1989 isolated MCC from coconut shells. The results showed that properties like moisture, pH, starch content, cellulose content, and ash content are comparable to commercial MCC [10].

Uesu *et al*.2000 isolated MCC from soybean husk after isolating cellulose. The results showed that the prepared sample has similar crystallinity and lower particle size than the commercial MCC [13]. Bochek *et al*.2003 isolated MCC using acid hydrolysis from short flax fiber, flax straw and cotton linter. The results showed that the kinetics of flax cellulose

hydrolysis is influenced by fats, pectins, and lignins contained in the fibers [14].

El-Sakhawy and Hassan 2007 used pulp from agricultural residues like bagasse, rice straw, and cotton stalks for the isolation of MCC. Hydrolysis was carried out using hydrochloric and sulphuric acids. The acids used were found to affect particle size, thermal stability, tensile strength, and cohesiveness of the tablets made from the different MCC samples [9]. Jahan *et al*.2011 isolated cellulose from jute fibres based on formic acid/peroxyformic acid process. Cellulose on further hydrolysis gave MCC [15].

Haafiz *et al*.2013 isolated MCC from oil palm empty fruit bunch. AFM analysis showed the presence of spherical features. X-ray diffraction revealed the cellulose-I polymorph with 87% crystallinity [16]. Achor *et al.* 2014 isolated α-cellulose from the back of the fruit of *Lageriana siceraria* (water gourd) and subjected to modification by controlled acid micronisation to produce MCC using 2.5N HCl. MCC displayed superior swelling and hydration capacities as compared to Avicel PH101, which is a commercial MCC used for comparison [17].

Sago (*Cycas circinalis*) is known to be an Indian-endemic, restricted to the Western Ghats, in the states of Kerala, Karnataka, Tamil Nadu and the south of Maharashtra. Research attention has been mainly focussed on the edible part of the seed and no systematic investigation has been carried out on the shells of sago seeds which are usually discarded as agricultural waste. Eventhough, good number of sources have been used for the isolation of MCC, only very few reports are available for their isolation from seed shells. Therefore, the present chapter deals with the determination of composition and the efforts to isolate the much useful MCC from sago seed shells, since

seed shells are usually composed of lignin, hemicellulose, cellulose, extractives and other minor components.

4.2 RESULTS AND DISCUSSION

4.2.1 Determination of composition of sago seed shells

The sago seed shells were collected locally and dried in air for 2-3 days. The air- dried sago seed shells were powdered and sieved through 53 µm mesh. Powdered and sieved sample was oven dried in hot air oven maintained at 100-105 ^{0}C for 3-4 hours till constant weight was obtained. The following analysis was carried out on oven dry sample. Extractives (ASTM D1107-96), klason lignin (ASTM D1106-96), holocellulose [18], α-cellulose (ASTM D 1103-60), hemi cellulose (by difference) and ash content (T 211 om 02)

4.2.2 Bleaching (Holocellulose)

The oven dry sample was extracted in Soxhlet apparatus with ethanol-toluene mixture (2:1) for five hours. The extracted residue was oven dried 100-105 ^{0}C for 3-4 hours till constant weight was obtained (ASTM D1107-96). The residue (1 g) was treated with 0.7 % $NaClO_2$ (20 mL) in a water bath kept at 80 ^{0}C, maintaining the pH at 5 by stirring with acetic acid, for 5 hours. The residue was filtered, washed several times with distilled water till the washings become neutral, and finally oven dried at 100-105 ^{0}C for 3-4 hours till constant weight was obtained [18]. This process was carried out in order to delignify and to obtain holocellulose.

4.2.3 Isolation of microcrystalline cellulose (MCC)

Preparation of microcrystalline cellulose was carried out by using the method adopted by Ohwoavworhua *et al* with a slight modification [19]. In a

typical procedure holocellulose obtained after bleaching from oven dry sample (2 g) was treated with 17.5% NaOH (25 mL), making three additions for about 45 minutes .The solution was kept for 1 hour and added sufficient quantity of distilled water to make the concentration of NaOH 8.3%. The solution was filtered washed with distilled water and with 10% acetic acid. The residue was again washed several times with distilled water till the washings were neutral and oven dried by maintaining the temperature at 100-105 ^{0}C for 3-4 hours till constant weight was obtained (ASTM D 1103-60).

α-Cellulose (1g) obtained was hydrolysed with 2.5 N HCl (17 mL) into a glass vessel at the boiling temperature for 15 minutes. The hot acid mixture was poured in to 50 mL cold water followed by vigorous stirring and allowed to stand overnight. The MCC obtained was filtered, washed with distilled water till it became neutral and dried in hot air oven at 60 ^{0}C for half an hour [17].

Weight percentage of different components isolated from sago seed shells were determined and are listed in **Table 4.1**

Table 4.1 Weight % (w/w) of different components isolated from sago seed shells.

Components	Weight %
Extractives	8.2±1
Klason lignin	23.6±0.8
Holocellulose	59.0±1.2
α-Cellulose	36.5±1
Hemicellulose	22.5±1
Ash content	9.2±0.2

The analysis shows that it has reasonably good lignin content and high cellulose, when compared with corn cob, peanut shell, rice straw and sorghum leaf and stalk [20]. **Table 4.2** gives a comparative study of sago seed shells with other biomass [20].

Table 4.2 Cellulose content and % composition of different biomass.

Agricultural Wastes	Components (% w/w)				
	Lignin	Holocellulose	Hemicellulose	Cellulose	Others
Bagasse	20	67	23	44	13
Corn cob	12.8	76.6	42.5	34.1	10.6
Peanut shell	35.2	34.2	12.1	22.1	30.6
Rice hull	12.9	58.7	9.6	49.1	28.4
Rice straw	7	59	26	33	34
Sugar cane leaf and stalk	13	69	29	40	18
Sorghum leaf and stalk	11	61	30	31	28
Sago seed shell	**23.6**	**59**	**22.5**	**36.5**	**17.4**

Moreover, corn cob, peanut shell, rice straw, etc have already been evaluated for the isolation of MCC. Therefore, sago seed shells can be used as a potential source for the extraction of cellulose and MCC.

4.2.4 FTIR analysis

Figure 4.1 shows the FTIR spectrum of lignin, otherwise called klason lignin, which is composed of phenyl propane derivatives and has a complex three dimensional structure. It is found together with polysaccharide in the biomass. It has perfect amorphous structure and acts as glue between cellulose fibre, by virtue of the interaction or linkage between the cellulose

and matrix. The spectrum obtained shows typical phenyl propane (lignin skeleton) vibrations due to methyl and methylene groups and aromatic ring. The most significant bands in lignin spectrum are due to structural subunits like guiacyl propane, syringyl propane and parahydroxyphenyl propane.

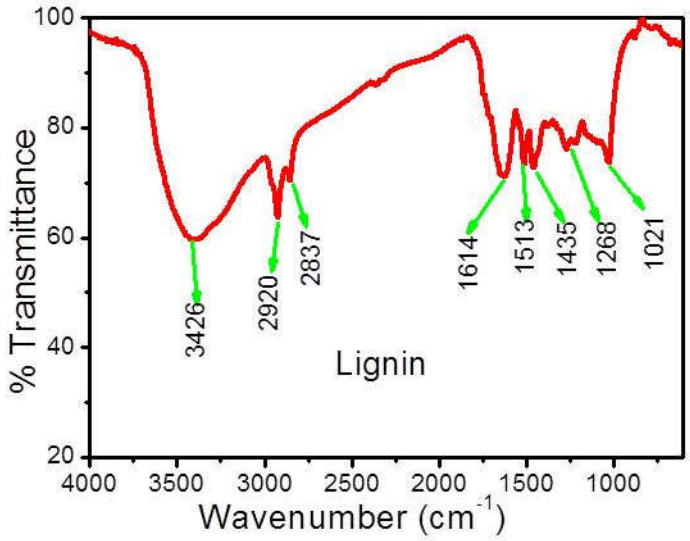

Figure 4.1 FTIR spectrum of lignin.

The frequency at 3426 cm^{-1} is due to O-H stretching, 2920 cm^{-1} and 2837 cm^{-1} are due to C-H stretching in methyl and methylene groups. 1614 and 1513 cm^{-1} are due to C=C stretching of aromatic ring in lignin [3]. The stretching frequency at 1435 cm^{-1} is due to $O\text{-}CH_3$ vibrations and 1268 cm^{-1} is due to C-O stretching of aryl groups [4]. The frequency at 1021cm^{-1} has to be attributed to C-O stretching in primary alcohols [3].

Figure 4.2 shows the FTIR spectrum of holocellulose. Cellulose together with hemicellulose is holocellulose. Holocellulose acts as the compatibiliser between cellulose and lignin. It forms an amorphous matrix

surrounding cellulose and it is softer than cellulose. Hemicellulose is composed of xylose, mannose, glucose, galactose, arabinose and uronic acids.

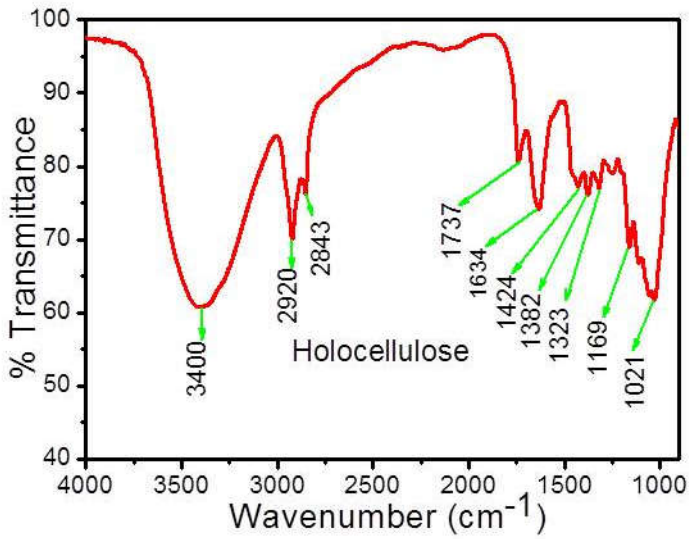

Figure 4.2 FTIR spectrum of holocellulose.

The frequency at 3400 cm^{-1} is due to O-H stretching. Frequencies at 2920 cm^{-1} and 2843 cm^{-1} are due to C-H stretching in methyl and methylene groups and 1737 cm^{-1} is the carbonyl stretching in conjugated carboxylic groups (carbonyl stretching of the acetyl and uronic ester groups of hemicelluloses or the ester linkage of carboxylic groups of ferulic and *p*-coumaric acids of hemicelluloses). 1634 cm^{-1} may be due to absorbed water and 1424 cm^{-1} corresponds to the C–O stretch and CH or OH bending in hemicelluloses. The bands at 1382 and 1169 cm^{-1} are attributed to C–H deformation and C–O–C vibration in hemicelluloses respectively [21]. The frequency at 1323 cm^{-1} is due to OH bending and 1021 cm^{-1} is due to C-O-H bending which are typical of xylans [22]. By comparing the FTIR of **Figure 4.1** and **Figure 4.2**, it can be concluded that the stretching frequency at 1614

and 1516 cm^{-1} which are assigned to aromatic skeleton and the characteristic feature of lignin is absent in **Figure 4.2.** Moreover, frequency at 1737 cm^{-1} present in **Figure 4.2** indicates the carbonyl group, which is absent in the **Figure 4.1**.

Figure 4.3 (a) shows the FTIR spectrum of α-cellulose, the broad band at 3419 cm^{-1} is due to O-H stretching having strong inter- and intra-molecular hydrogen bonding. Frequencies at 2921 cm^{-1}, 2846 cm^{-1} are due to C-H stretching in methyl and methylene groups. Frequency at 1643 cm^{-1} is due to absorbed water. Frequencies at 1437 cm^{-1}, 1383 $cm^{-1,}$ and 1318 cm^{-1} are due to the bending of CH, CH_2, OH respectively which are typical for polysaccharides and 1036 cm^{-1} is due to C-O stretching.

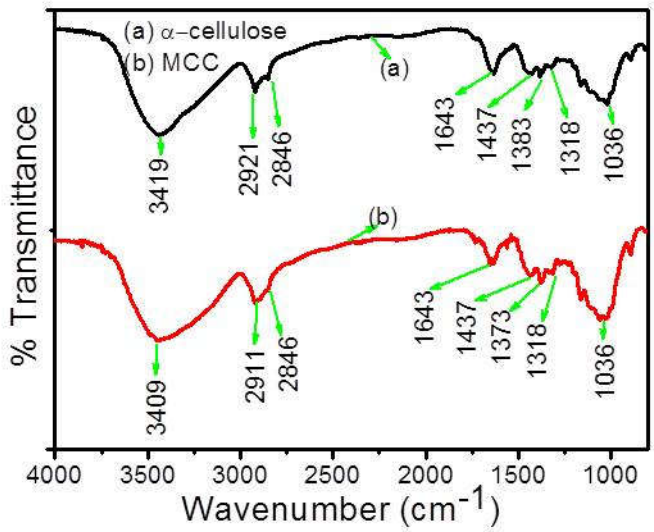

Figure 4.3 FTIR Spectra of (a) α-cellulose and (b) MCC.

Figure 4.3 (b) shows the FTIR spectrum of isolated MCC. The FTIR spectrum reveals that α-cellulose and MCC show almost similar absorption frequencies at 2911, 2846, 1437, 1373, 1318 and 1036 cm^{-1}. The O-H

stretching frequency in α-cellulose is found at 3419 cm^{-1} and for MCC, it is at 3409 cm^{-1}. The decrease in vibrational frequency and band broadening is attributed to the extent of hydrogen bonding.

4.2.5 Thermogravimetry (TG)

Figures 4.4 (a)-(d) show the TG of sago seed shell, holocellulose, α-cellulose and MCC respectively. Each shows starting decomposition around 100 ^{0}C due to evaporation of water. From **Figure 4.4** (a) wide range 230-600 ^{0}C for sago shells are attributed to decomposition of lignin, holocellulose and other components present in the seed shell.

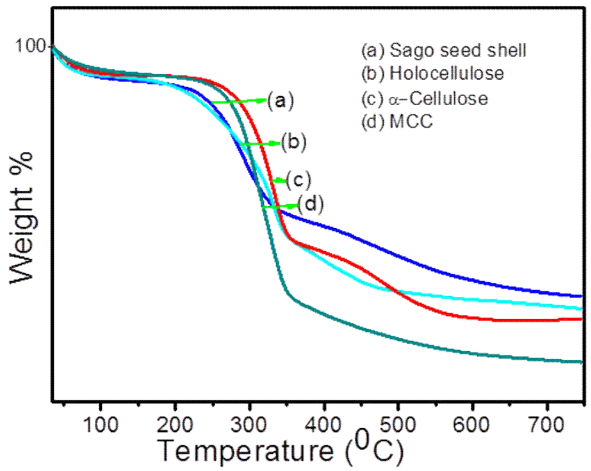

Figure 4.4 TG curves of (a) sago seed shell, (b) holocellulose, (c) α-cellulose and (d) MCC.

For holocellulose from **Figure 4.4** (b), the main decomposition is in the range 200-340 ^{0}C [23,24]. From the DTG curve **Figure 4.5** (b) that of holocellulose, which has shoulder around 250 ^{0}C, is due to hemicellulose and the peak at 340 ^{0}C is assigned to cellulose, indicating the presence crystalline, amorphous nature and also to the heterogeneity in structure [25]. From **Figure 4.4** (c) & (d) α-cellulose and MCC have almost the same

decomposition temperatures in the range 250-344 ^{0}C, which is due to degradation processes of cellulose such as decarboxylation, depolymeristion and decomposition of glycosyl units. The decomposition temperature of α-cellulose and MCC is found to be higher than holocellulose, moreover there is no shoulder around 250 ^{0}C indicating the removal of hemicellulose portions. This can be clearly identified from their DTG curves **Figure 4.5** (c) and (d). The second stage decomposition of α-cellulose from **Figure 4.4** (c), is in the range 344-512 ^{0}C, however from **Figure 4.4** (d) for MCC this is absent. These can be clearly observed from their DTG curves **Figure 4.5** (c) and (d) also. The pattern of thermogram for MCC [**Figure 4.4**(d)] is well defined, indicating well-ordered structure due to efficient removal of amorphous regions, which is further supported by XRD analysis. The TG results show that the thermal stability of the MCC is significantly lower than the shell powder; this is because more heat stable non-cellulosic materials in the shell powder have been removed during treatment [26]. TG results of different components isolated are presented in **Table 4.3**

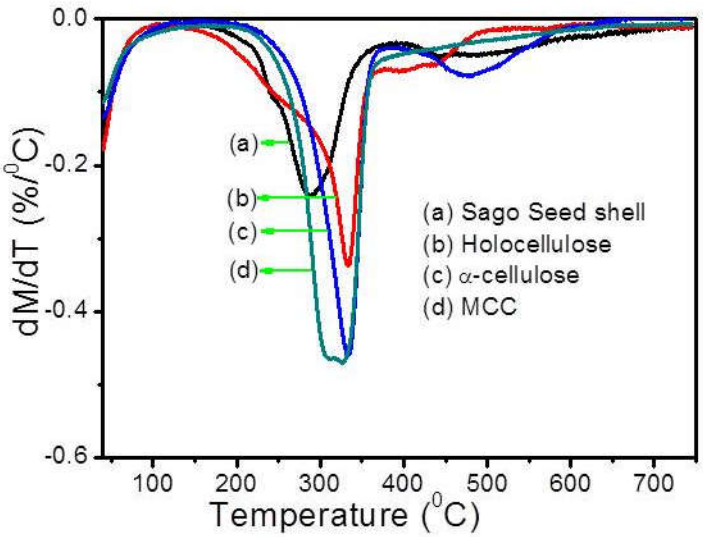

Figure 4.5 DTG curves of (a) sago seed shell, (b) holocellulose, (c) α-cellulose and (d) MCC

Table 4.3 TG results of sago seed shells, holocellulose, α-cellulose and MCC. Onset temperature (T_{on}), degradation temperature on maximum weight-loss rate (T_{max}) in ^0C

Components	Decomposition Temperature	
	T_{on} (^0C)	T_{max} (^0C)
Sago seed shells	230	600
Holocellulose	200	340
α-Cellulose	250	344
MCC	250	344

4.2.6 XRD analysis

Figures 4.6 (a-c) show XRD pattern of sago seed shell, α-cellulose and MCC. It has been well established that cellulose contains both crystalline and amorphous regions. From **Figure 4.6** (a) the X-ray pattern of the sago seed shells, the peaks are not defined, but in **Figure 4.6** (b), that of isolated α-cellulose the peaks are defined and can be observable at $2\theta=21.2^0$, 34.6^0 and shoulder in the 2θ range of $14–17^0$, which represent typical cellulose I structure [27]. The degree of crystallinity is determined by using the **Equation 4.1**, and is found to be 44%. The crystallinity index is high for cellulose due to the removal of lignin, hemicellulose which existed as amorphous regions that reorient cellulose chains [1].

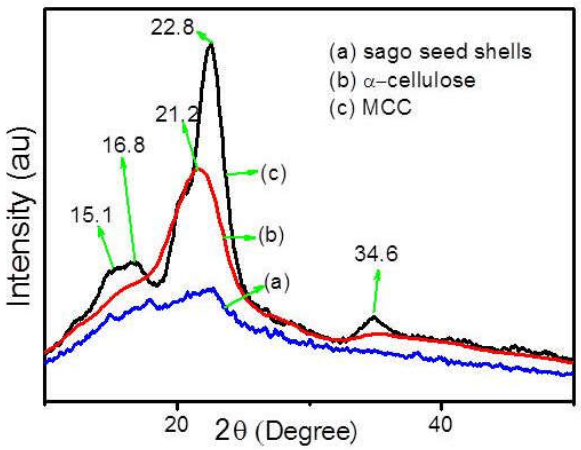

Figure 4.6 XRD patterns of (a) sago seed shell, (b) α-cellulose and (c) MCC.

Figure 4.6 (c) shows the X-ray pattern of MCC, which has the pattern similar to that of α- cellulose, but the peaks are more defined and intensified, with a sharp peak at 2θ=15.1, 16.8, 22.8, and 34.6^0 corresponding to the $(1\bar{1}0)$, (110), (200), and (004) crystallographic planes [28]. The X-ray diffraction pattern of MCC shows possibility of small amount of cellulose II also [28]. The degree of crystallinity is found to be increased from 44 to 67%, exhibiting higher crystallinity due to the efficient removal of the amorphous parts by the cleavage of glycosidic linkages releasing crystallites. The degree of crystallinity is presented in **Table 4.4**. When there is efficient removal of amorphous region, the rigidity increases which is further supported by thermal analysis. Using more crystalline cellulose materials like MCC or nanocellulose, the mechanical property of composites will increase.

Degree of crystallinity (DC) = $(I_{200} - I_{am})$ x100/(I_{200}) ---------- **4.1** [29].

Where I_{200} is the intensity of 2 0 0 peak at $2\theta=22.8^0$ and I_{am} is the minimum intensity at the amorphous region at $2\theta = 18^0$

Table 4.4 Degree of crystallinity (DC) of sago seed shells, α-cellulose and MCC

Components	D C (%)
Sago seed shells	-----
α-Cellulose	44
MCC	67

4.2.7 SEM analysis

SEM analysis was carried out to study the morphology and textural properties of different components extracted. **Figures 4.7** (a)-(c) reveal the morphological change occurred during the isolation process.

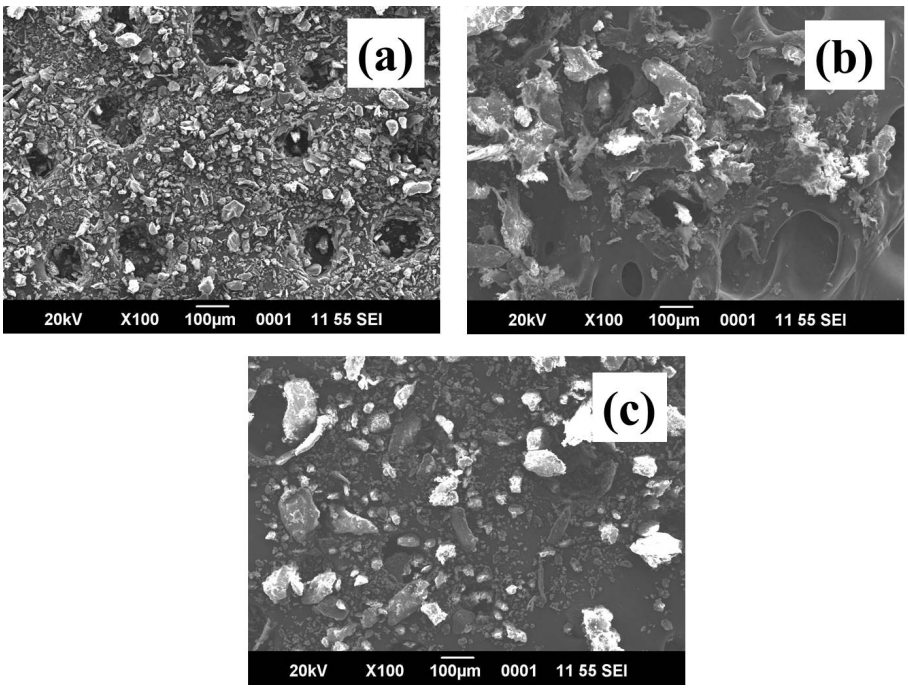

Figures 4.7 SEM images of (a) sago seed shell, (b) α-cellulose and (c) MCC.

From **Figure 4.7** (a) it can be observed that there is randomly oriented distribution of morphologies in the structures of seed shells, due to lignin, hemicellulose and other components present. Hemicellulose acts as a compatibiliser between celluloses and lignin. Lignin which acts as a binder is gradually removed to help the isolation of MCC. The isolated MCC consists of a mixture of aggregated and non-aggregated fibres, showed an aggregated structure composed of small fibres with coalesced boundaries. It has morphology similar to that of commercial MCC [30].

4.2.8 TEM analysis

The TEM image of isolated MCC is shown in **Figure 4.8**.

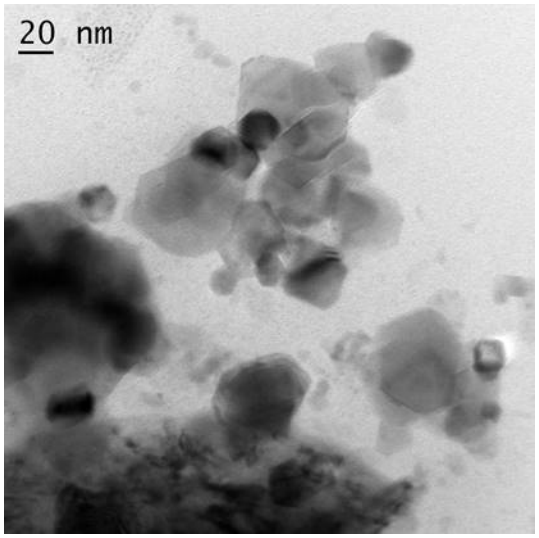

Figure 4.8 TEM images of MCC.

TEM image clearly shows that small MCC particles are agglomerated to form large particles in the micron scale having random orientations along with some non-agglomerated structures [31]. TEM results corroborate with the surface morphology obtained by SEM.

4.2.9 AFM analysis

The surface morphology has also been investigated by AFM. In AFM two modes are used to record data during scanning, the height image and the other 3D image. **Figure 4.9** (a) shows the AFM height image of isolated MCC. The height image displays topographical details by tracking the surface with the probe and the 3D image gives the contrast between soft and hard polymer segment.

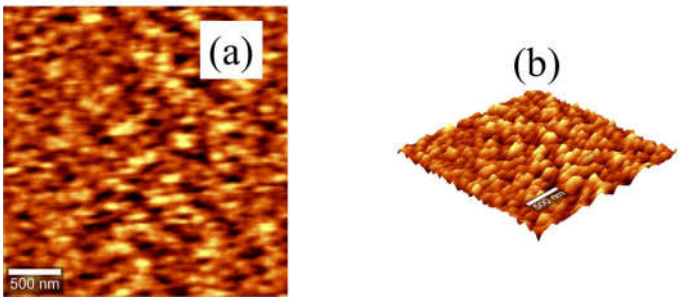

Figure 4.9 AFM images of MCC (a) height view and (b) 3D view

The results of two-dimensional AFM image **Figure 4.9** (a) shows larger extent of agglomeration or aggregated structure. The height image contains mostly brighter regions indicating crystalline regions and some dark regions implying amorphous regions. **Figure 4.9** (b) shows the 3D image, reveals that the isolated MCC consists of spherical particles, with non-uniform and rough surfaces [16]. Both TEM and AFM results reveal the microstructural behavior of isolated MCC.

4.3 CONCLUSION

The composition of sago seed shells has been established by standard methods of determination and has been found to be extractives, klason lignin, holocellulose, α-cellulose, hemi cellulose (by difference) and ash content. It has reasonably good lignin content and high cellulose, therefore sago seed shells can be used as a potential source for the extraction of cellulose. FTIR spectra show the presence of lignin, holocellulose and α-cellulose. TG of holocellulose shows lower onset degradation temperature than α-cellulose and reveals the presence of holocellulose and α-cellulose. α-Cellulose isolated has been converted into MCC. α-Cellulose and MCC exhibited similar FTIR spectra, but –OH stretching frequency was found to be slightly

less for MCC. TG shows similar decomposition temperatures for MCC and α-cellulose, moreover MCC showed a well-defined curve. XRD pattern of α-cellulose exhibited cellulose I structure, but small amount of cellulose II was also present in MCC and the degree of crystllinity was found to be increased due to efficient removal of amorphous regions. TG and XRD results support each other. SEM analysis of MCC reveals the presence of aggregated and non-aggregated fibers, further supported by TEM. AFM analysis of MCC shows the presence of spherical shapes with non-uniform and rough surfaces.

REFERENCES

1. Li, R.; Fei, J.; Cai, Y.; Li, Y.; Feng, J.; Yao, J. Cellulose whiskers extracted from mulberry: A novel biomass production. *Carbohydr. Polym.* **2009**, *76*, 94–99.

2. John, M. J.; Thomas, S. Biofibres and biocomposites. *Carbohydr. Polym.* **2008**, *71*, 343–364.

3. Kline, L. M.; Hayes, D. G.; Womac, A. R.; Labbé, N. Simplified determination of lignin content in hard and soft woods via UV-spectrophotometric analysis of biomass dissolved in ionic liquids. *BioResources* **2010**, *5*, 1366–1383.

4. Yang, H.; Yan, R.; Chen, H.; Lee, D. H.; Zheng, C. Characteristics of hemicellulose, cellulose and lignin pyrolysis. *Fuel* **2007**, *86*, 1781–1788.

5. Klemm, D.; Heublein, B.; Fink, H. P.; Bohn, A. Cellulose: Fascinating biopolymer and sustainable raw material. *Angew. Chemie - Int. Ed.* **2005**, *44*, 3358–3393.

6. Nishiyama, Y. Structure and properties of the cellulose microfibril. *J. Wood Sci.* **2009**, *55*, 241–249.

7. Eichhorn, S. J.; Dufresne, A.; Aranguren, M.; Marcovich, N. E.; Capadona, J. R.; Rowan, S. J.; Weder, C.; Thielemans, W.; Roman, M.; Renneckar, S.; Gindl, W.; Veigel, S.; Keckes, J.; Yano, H.; Abe, K.; Nogi, M.; Nakagaito, A. N.; Mangalam, A.; Simonsen, J.; Benight, A. S.; Bismarck, A.; Berglund, L. A.; Peijs, T. Review: Current international research into cellulose nanofibres and nanocomposites. *J. Mater. Sci.* **2010**, *45*, 1–33.

8. Morán, J. I.; Alvarez, V. A.; Cyras, V. P.; Vázquez, A. Extraction of cellulose and preparation of nanocellulose from sisal fibers. *Cellulose* **2008**, *15*, 149–159.

9. El-Sakhawy, M.; Hassan, M. L. Physical and mechanical properties of microcrystalline cellulose prepared from agricultural residues. *Carbohydr. Polym.* **2007**, *67*, 1–10.

10. Goankar; Kulkarni. Microcrystalline cellulsoe from cocunut shells. *Acta Polym.* **1989**, *40*, 292–293.

11. Adel, A. M.; El-wahab, Z. H. A.; Ibrahim, A. A.; Al-shemy, M. T.

Characterization of microcrystalline cellulose prepared from lignocellulosic materials. Part II: Physicochemical properties. *Carbohydr. Polym.* **2011**, *83*, 676–687.

12. Paralikar, K. M.; Bhatawdekar, S. P. Microcrystalline cellulose from bagasse pulp. *Biol. Wastes* **1988**, *24*, 75–77.

13. Uesu, N. Y.; Go, E. A.; Adelina Winkler, H. Microcrystalline cellulose from soybean husk: Effects of solvent treatments on its properties as acetylsalicylic acid carrier. *Int. J. Pharm.* **2000**, *206*, 85–96.

14. Bochek, A. M.; Shevchuk, I. L.; Lavrent, V. N. Fabrication of microcrystalline and powdered cellulose from short flax fiber and flax straw. *Russ. J. Appl. Chem.* **2003**, *76*, 1679–1682.

15. Jahan, M. S.; Saeed, A.; He, Z.; Yonghao, N. Jute as raw material for the preparation of microcrystalline cellulose. *Cellulose* **2011**, *18*, 451–459.

16. Haafiz, M. K. M.; Eichhorn, S. J.; Hassan, A.; Jawaid, M. Isolation and characterization of microcrystalline cellulose from oil palm biomass residue. *Carbohydr. Polym.* **2013**, *93*, 628–634.

17. Achor, M.; Oyeniyi, Y, J.; Yahaya, A. Extraction and characterization of microcrystalline cellulose obtained from the back of the fruit of Lageriana siceraria (water gourd). *J. Appl. Pharm. Sci.* **2014**, *4*, 57–60.

18. Wise, L. E.; Murphy, M.; Adieco, A. D. A chlorite holocellulose, its fractionation and bearing on summative wood analysis and studies on the hemicelluloses. *Pap. Trace J.* **1946**, *122*, 35–42.

19. Ohwoavworha, F. O.; Kunle, O. O.; Ofoefule, S. I. Extraction and characterisation of microcrystalline cellulose derived from Luffa cylindrica plant. *African J. Pharm. Res. Dev.* **2004**, *1*, 1–6.

20. Boonmee, A. Hydrolysis of various thai agricultural biomasses using the crude enzyme from aspergillus aculeatus iizuka FR60 isolated from soil. *Brazilian J. Microbiol.* **2012**, *43*, 456–466.

21. Sun, R.; Fang, J. M.; Goodwin, A.; Lawther, J. M.; Bolton, A. J. Isolation and characterization of polysaccharides from abaca fiber. *J. Agric. Food Chem.* **1998**, *46*, 2817–2822.

22. Fang, J. M.; Sun, R. C.; Tomkinson, J. Isolation and characterization of hemicelluloses and cellulose from rye straw by alkaline peroxide extraction. *Cellulose* **2000**, *7*, 87–107.

23. Joseph, P. V.; Joseph, K.; Thomas, S.; Pillai, C. K. S.; Prasad, V. S.; Groeninckx, G.; Sarkissova, M. The thermal and crystallisation studies of short sisal fibre reinforced polypropylene composites. *Compos. Part A. Appl. Sci. Manuf.* **2003**, *34*, 253–266.

24. Poletto, M.; L., H.; Júnior, O.; Zattera, A. J. Native cellulose: Structure, characterization and thermal properties. *Material* **2014**, *7*, 6105–6119.

25. Sebio-Pun, T.; Naya, S.; Lopez-Beceiro, J.; Tarrı´o-Saavedra, J.; Artiaga, R. Thermogravimetric analysis of wood, holocellulose, and lignin from five wood species. *J .Therm. Anal . Calorim.* **2012**, *109*, 1163–1167.

26. Carrier, M.; Loppinet-serani, A.; Denux, D.; Lasnier, J.; Cansell, F. H.-P. F.; Aymonier, C. Thermogravimetric analysis as a new method to determine the lignocellulosic composition of biomass. *Biomass and Bioenergy* **2011**, *35*, 298–307.

27. Bondeson, D.; Mathew, A.; Oksman, K. Optimization of the isolation of nanocrystals from microcrystalline cellulose by acid hydrolysis. *Cellulose* **2006**, *13*, 171–180.

28. Sèbe, G.; Ham-Pichavant, F.; Ibarboure, E.; Koffi, A. L. C. Supramolecular structure characterization of cellulose II nanowhiskers produced by acid hydrolysis of cellulose I substrates. *Biomacromolecules* **2011**, *13*, 570–578.

29. Segal, L.; Creely, J. J.; Martin, A. E.; Conrad, C. M. An empirical method for estimating the degree of crystallinity of native cellulose using the X-ray diffraction. *Text. Res. J.* **1959**, *29*, 786–794.

30. Kumar, V.; Reus-medina, M. D. L.; Yang, D. Preparation, characterization, and tabletting properties of a new cellulose-based pharmaceutical aid. *Int. J. Pharm.* **2002**, *235*, 129–140.

31. Haafiz, M. K. M.; Hassan, A.; Zakaria, Z.; Inuwa, I. M. Isolation and characterization of cellulose nanowhiskers from oil palm biomass microcrystalline cellulose. *Carbohydr. Polym.* **2014**, *103*, 119–125.

CHAPTER 5
DEVELOPMENT OF GREEN COMPOSITES OF POLY (VINYL ALCOHOL) REINFORCED WITH MCC DERIVED FROM SAGO SEED SHELLS

Abstract

This chapter presents the development of green composites of poly (vinyl alcohol) (PVA) reinforced with microcrystalline cellulose (MCC) isolated from sago seed shells. Composites were prepared by adding 1, 2 and 3 weight % of MCC, which were characterised using FTIR, ATR-FTIR, XRD, DSC, TG, UV-VIS, SEM, AFM and mechanical testing. Particle size distribution of used MCC was analysed by DLS. The results obtained from FTIR, ATR-FTIR, XRD and DSC substantiates each other. TG results reveal the increased thermal stability compared to the PVA film. The SEM analysis shows the uniform distribution for lower loading, which is further supported by AFM. UV-Visible spectra reveal the good transparency of prepared films. Mechanical testing was also performed; the results reveal that 1 weight % of MCC in PVA gained moderate tensile strength.

Part of this chapter has been published in Journal Polymer Composites-2017. "Development of Green Composites of Poly (Vinyl Alcohol) Reinforced with Microcrystalline Cellulose Derived from Sago Seed Shells" DOI 10.1002/pc.

5.1 INTRODUCTION

Biomass as feedstock for the production of high performance materials enables a possible application to generate value-added products from agro waste. Traditionally, many lignocellulosic materials were used as household fuels, sometimes burnt *in situ* in the fields as a means of disposal. In addition to this for the production of paper pulp, ethanol, charcoal etc., has also been tried as fillers/reinforcements in polymers [1]. Polymers from renewable resources have attracted considerable attention over the last two decades due to environmental concerns. Wide range of naturally occurring polymers like cellulose, starch etc., are actively being used in many applications. Eventhough, biopolymers are highly bio degradable; they are inherited with moisture sensitivity, brittleness, low mechanical strength, high sensitivity to atmosphere etc.

Biocomposites can be prepared by incorporating inorganic filler into the biopolymer matrix or biopolymer and natural fibres into synthetic polymer. The most widely known and used natural-organic fillers are wood flour and fibres [2]. Renewability, biodegradability and sustainability make them good choice. Natural fibres from bast, leaf or hard fibres, seed, fruit, wood, cereal straw, and other grass fibres are being used in composites [3]. Not only natural fibres but biopolymers like cellulose and starch that are extracted from biomass resources are also being used in the development of biocomposites.

Attention is now focussed on the development of green composites, which are green in all respects, in which the reinforcement and matrix are biodegradable. Green composites may be used effectively in many applications such as mass-produced consumer products with short life cycles or products intended for one-time or short-term use before disposal. PVA is

highly recognized as a biodegradable polymer, readily consumed by microorganisms and enzymes when exposed to natural environment [4,5]. Due to biodegradability, water-solubility, gas barrier properties, biocompatibility, good thermal stability, availability, flexibility, transparency, toughness and cost, PVA find use in packaging, medical, and energy-absorption applications. Commercial PVA is available both in highly hydrolysed grades and partially hydrolysed ones. The degree of hydrolysis or the content of acetate groups in PVA affects its chemical properties, solubility and crystallisability [6]. It is one of the rare polymers even with its carbon-carbon single bond, is fully biodegradable, because of the presence of hydroxyl groups on the alternating carbon. It is strongly hydrophilic, soluble in water and thus promotes its biodegradation.

Since PVA is highly polar, can be prepared in water solutions and in solution it forms numerous positive interactions through hydroxyl groups, it is well suited for being mixed with natural polymers like cellulose and starch, due to the possible formation of hydrogen bonds [7]. One of the most important commercial products obtained from cellulose is MCC, used mainly in pharmaceuticals. Apart from its conventional use, MCC is used as potential reinforcement in polymers. Thus, the growing interest in eco-friendly materials for a number of applications has motivated the use of these biopolymers, where synthetic polymers or mineral fillers are traditionally used [8].

MCC being hydrophilic can be added as filler in PVA to produce green composites. Nishiot and Manley in 1988 studied blend of cellulose with PVA from mixed solutions containing N,N-Dimethylacetamide and Lithium chloride, by coagulation in a nonsolvent. The results from WAXD and DSC showed that the crystallinity of PVA decreased with increasing cellulose

content. Above 60 wt.% cellulose content, interaction through hydrogen bonding was revealed by considerable miscibility in the amorphous regions [9]

Park *et al*.2001 studied blend hydrogels containing PVA and methyl cellulose (MC), by crosslinking with glutaraldehyde in an aqueous solution in the presence of HCl. DSC showed depression in melting and crystallisation temperature of PVA with increase in MC content. DMA results exhibited higher miscibility than non-crosslinked blends [10]. Cinelli *et al*.in 2003 studied blends of PVA and corn fibre (CF) obtained from wet milling process for fuel ethanol production. CF and PVA were processed in variable amounts, containing glycerol, pentaerythrytol as plasticizer and corn starch. Increase in Young's modulus was observed using pentaerythrytol in larger amount than glycerol. Moreover, the addition of starch moderately reduced the tensile properties of composites [11]. The same authors also studied the blend films of PVA and orange fibres with corn starch, using hexamethoxymethylmelamine as cross linking agent. Modest decrease in decomposition temperature was observed when PVA and orange fibre are blended together. The water permeability properties and biodegradability of the hybrid films in compost environment have given promising results and cross linking agent affected the extent of degradation [12].

El-Zaher and Osiris 2005 studied the doping of hydroxypropyl cellulose (HPC) in different weight percentages, using PVA as the matrix. DSC and XRD showed the changes in crystallinity [13]. The effect of commercial MCC as reinforcement in PVA was studied by Chakraborty *et al.* in 2006. Composites showed increase in tensile strength than neat PVA [14]. The effect of HPC in PVA was also studied by Osiris and Manal in 2012. The XRD showed broadening and sharpening of peaks and the blends exhibited improvement in thermal stability [15].

Attia and El-kader in 2013 prepared blends containing PVA and 2-hydroxy ethyl cellulose (2HEC) in different compositions. Infrared spectra revealed the compatibility between PVA and 2HEC through the formation of hydrogen bond, moreover single glass transition temperature for blends was obtained [16]. MCC isolated from waste cotton fabric was used as reinforcement for melt-processed PVA with water and formamide as plasticizer by Sun *et al*.2014. The results revealed that crystallization of PVA has been confined and melting temperature decreased due to possible interaction through hydrogen bonding and MCC-PVA composites exhibited improvement in modulus and tensile strength [17].

Not only PVA, other matrices like poly (lactic acid) [18], polyurethane [19], nylon [20], PVC [21], modified PP [22] and PP by using modified MCC [23] have also been studied.

However, only scanty reports have appeared in the literature using MCC alone. Therefore, the main objective of the present work is to study the properties of different MCC- PVA composites, in which MCC has been isolated from sago seed shell to develop green composites of PVA reinforced with MCC.

5.2 RESULTS AND DISCUSSION

5.2.1 Fabrication of green composite film

The isolated MCC was used for the fabrication of green composites of PVA reinforced with MCC. MCC isolated was powdered, sieved through 90 μm mesh and used for fabrication. The detailed method of fabrication has already been given in **Chapter 3.2.3**. Different green composites fabricated are listed in **Table 5.1**

Table 5.1 Green composites of MCC and PVA.

Wt. of PVA (g)	Wt. % of MCC relative to PVA (g)	Composite films
5	0	5PVA
5	1	5PVA-1MCC
5	2	5PVA-2MCC
5	3	5PVA-3MCC

5.2.2 Dynamic light scattering (DLS)

The size distribution of the used MCC is shown in **Figure 5.1**. The size distribution of particles in suspension, emulsions, colloids, polymer etc., are determined using dynamic light scattering.

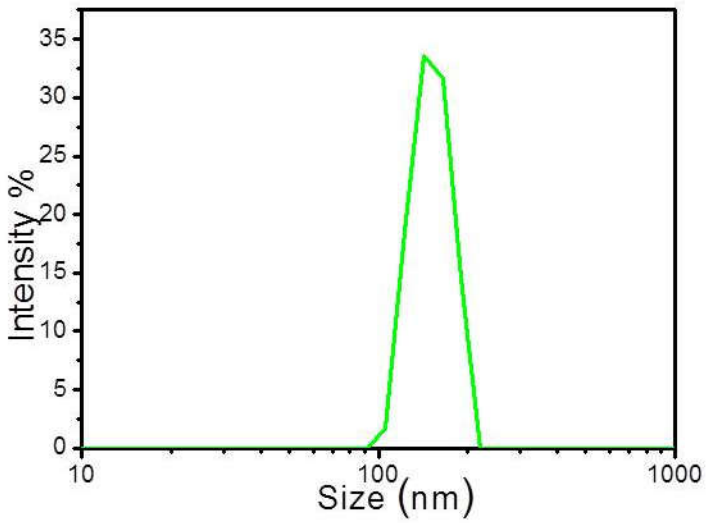

Figure 5.1 DLS curve of MCC.

The water suspended MCC sample was diluted, sonicated and analysed by the DLS particle size analyser. The data reveals that MCC used

for composite has particle size > 100 nm, with an average size of 151 nm (S D 22)

5.2.3 FTIR and ATR-FTIR analyses

Figure 5.2 (a) shows the FTIR spectra of the PVA, (b) and (c) show ATR-FTIR spectra of composites 5PVA-1MCC and 5PVA-3MCC respectively. From **Figure 5.2** (a) the frequency at 3408 cm^{-1} is due to the stretching vibration of its side hydroxyl groups, 2925 cm^{-1} is due to CH_2 group stretching vibrations, 1712 cm^{-1} is due to C=O from residual acetate group or oxidation during manufacturing process present in the PVA [13,24]. Frequency at 1437 cm^{-1} is attributed to O-H or C-H bending, or CH_2 deformations. Frequency at 1093 cm^{-1} is due to C-O stretching vibrations and 844 cm^{-1} is due to skeletal and CH_2 rocking, they are characteristic of neat PVA [13,25,26].

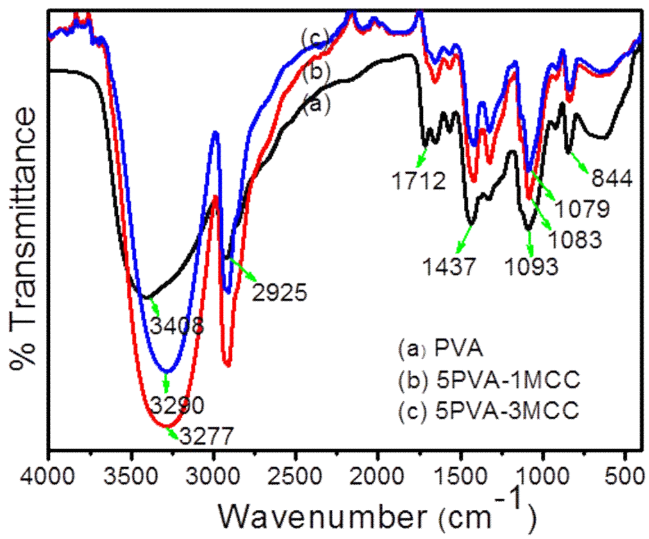

Figure 5.2 (a) FTIR spectra of PVA, (b) ATR-FTIR spectra of 5PVA-1MCC and (c) ATR-FTIR spectra 5PVA-3MCC

Comparison of the **Figures 5.2** (a) and (b), stretching frequency at 3408 cm^{-1} of neat PVA get shifted to 3290 cm^{-1} for PVA-1MCC, indicating the disruption of hydrogen bond existed in PVA film and possibility of formation of new hydrogen bond between OH groups of PVA and MCC due to sonication [27]. In composite films the possibility of hydrogen bonds are mainly between the glucose ring ether oxygen and hydroxyl groups in PVA, while other hydrogen bonds are also formed between secondary OH at either the C-2 or C-3 position and -OH of the PVA [28]. Some possible interactions between PVA and MCC are represented in **Scheme 5.1.** For PVA-3MCC from **Figure 5.2** (c), the O-H stretching frequencies get further shifted to 3277 cm^{-1}. The frequency of C=O stretch at 1712 cm^{-1} has almost vanished indicating interaction between MCC and PVA not only arises from O–H group but also from C–O group of pure PVA [29]. The frequency at 1093 cm^{-1} has been used as an assessment tool of PVA structure because it is a semi crystalline synthetic polymer able to form some domains depending on several process parameters. It was also noticed that the absorption frequency at 1093 cm^{-1} slightly shifts toward the lower frequency of 1083 cm^{-1} for 5PVA-1MCC and 1079 cm^{-1} for 5PVA-3MCC, suggesting changes in the crystalline domains of PVA. The results are further supported by XRD and DSC.

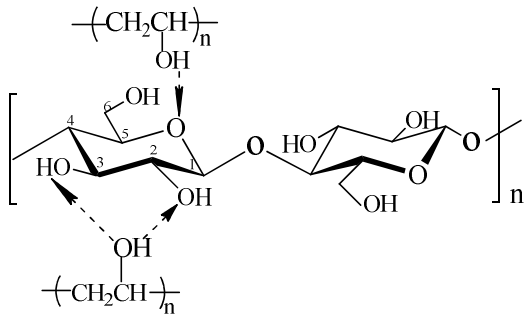

Scheme 5.1 Interaction between PVA and MCC.

5.2.4 XRD analysis

Figure 5.3 shows the XRD patterns of 5PVA film and 5PVA-MCC composites. It was found that the XRD pattern **Figure 5.3** (a) of 5PVA film contains a peak at $2\theta=19.4^0$, corresponding to the characteristic semi crystalline nature of pure PVA [27,30].

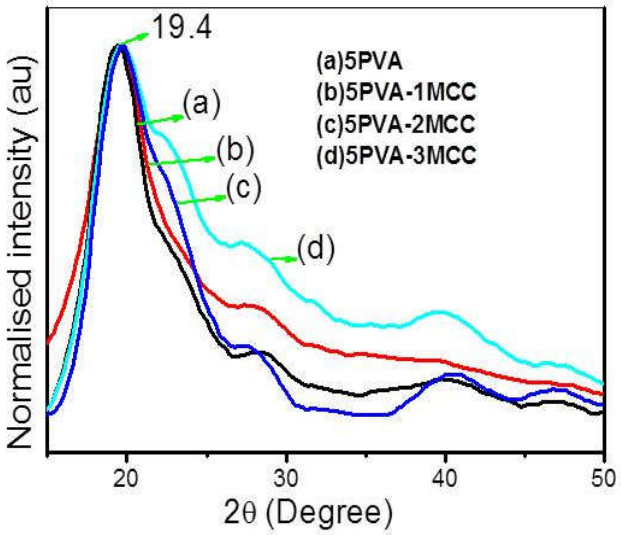

Figure 5.3 XRD patterns of (a) 5PVA film, (b) 5PVA-1MCC, (c) 5PVA-2MCC and (d) 5PVA-3MCC

From **Figure 5.3** (b-d)**,** the peak at 19.4 does not make any shift but an increase in peak broadening of pure PVA observed when MCC is incorporated [31]. This result could be due to the disruption of the PVA crystallinity with the incorporation of MCC, imparting amorphous nature to the PVA-MCC composites. The decrease in crystallinity of the solution cast film is probably due to decreased intra-molecular hydrogen bonding, and increased inter-molecular hydrogen bonding with MCC [32]. Moreover, crystllinity of each polymer is affected by the presence of others [33].

5.2.5 Differential scanning calorimetry (DSC)

Figure 5.4 shows the DSC curves obtained for 5PVA film and 5PVA-MCC composites. PVA is one of the partially crystalline polymers exhibiting both glass transition temperature (T_g) and melting isotherm (T_m) establishing that crystalline and amorphous phases in different amounts can co-exist. PVA shows T_m in the range 180-240 ^{0}C and T_g between 58–85 ^{0}C, depending on the degree of hydrolysis, degree of polymerisation and other factors [34,35]. Since MCC is having some crystallinity, does not show any T_g, and it degrades prior to melting. As a result, the DSC thermogram mainly represents the PVA behaviour. It has strong physical inter-chain and intra-chain interactions such as hydrogen bonding in its structure.

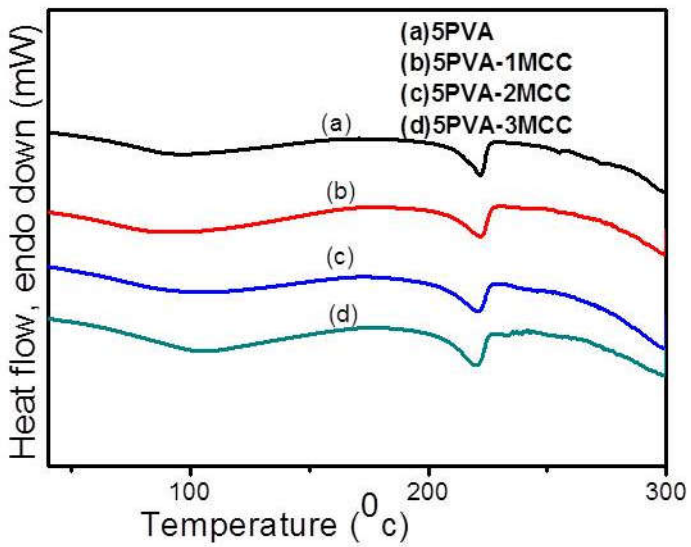

Figure 5.4 DSC curves of (a) 5PVA film, (b) 5PVA-1MCC, (c) 5PVA-2MCC and (d) 5PVA-3MCC.

Figure 5.4 (a) reveals that 5PVA film displays the glass transition temperature at 74 ^{0}C and a sharp endothermic curve at 222 ^{0}C. From **Figures**

5.4 (b-d), for composites with different amounts of MCC content the glass transition temperatures (T_g) are shifted to higher temperatures, 80 ^{0}C for 5PVA-1MCC, 83 ^{0}C for 5PVA-2MCC and 84 ^{0}C for 5PVA-3MCC respectively. Since T_g is related to the flexibility of polymeric segments, the result may be related to the limitation of restricted segmental motions of PVA chains, which were confined by MCC because of the interactions through hydrogen bonding, leading to increased glass transition temperature [13,36]. The endothermic peak of PVA-MCC composites corresponding to melting are slightly shifted to lower values as the MCC content is increased, the melting temperatures are found to be 221, 220, and 219 ^{0}C for 5PVA-1MCC, 5PVA-2MCC and 5PVA-3MCC respectively. The difference in the shape and area of the melting endotherms are attributed to the different degrees of crystallinity found in the composites. The slight depression of the melting temperature and the peak broadening indicate that the ordered association of the PVA molecules is decreased by the presence of MCC [10,37]. Moreover, sonication process helps to break down some of the strong hydrogen bonding interactions which is prevalent in MCC and to establish new hydrogen bonds with PVA matrix. The results obtained are presented in **Table 5.2**.

Table 5.2 DSC results of 5PVA and 5PVA-MCC composites

Polymer/ composite	Glass transition temperature (T_g) (^{0}C)	Melting temperature (T_m) (^{0}C)
5PVA	74	222
5PVA-1MCC	80	221
5PVA-2MCC	83	220
5PVA-3MCC	84	219

5.2.6 Thermogravimetry (TG)

TG was used to study the thermal performance of 5PVA film and PVA-MCC composite films. TG [**Figure 5.5** (a-d)] and DTG [**Figure 5.6** (a-d)] curves show the presence of three stage degradation pattern. All the samples show an initial weight loss in a temperature range 60 to 140 ^{0}C resulting from the loss of moisture in PVA due to evaporation of physically weak and chemically strong bound water. After moisture desorption, two main decomposition stages were observed for both 5PVA film and 5PVA-MCC composites, which suggests the co-existence of more than one degradation process. From **Figure 5.5** (a) for neat 5PVA, the second stage degradation transition occurs at 250-335 ^{0}C is due to the structural degradation of PVA, involving dehydration reactions or removal of ester linkages to form volatile products. The second and third degradation steps are consistent with the generally accepted mechanism for the degradation of PVA [37].

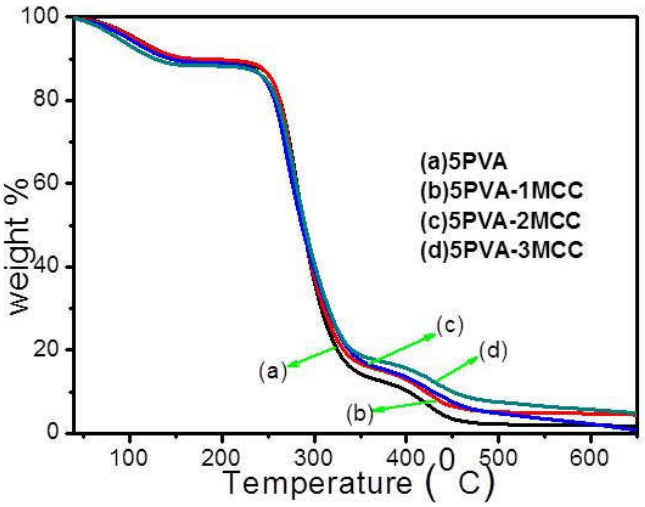

Figure 5.5 TG curves of (a) 5PVA film, (b) 5PVA-1MCC, (c) 5PVA-2MCC and (d) 5PVA-3MCC.

From **Figure 5.5** (b-d), the second stage degradation temperatures for composite films are in the range of 259-344, 252-341, and 250-332 ^{0}C for 5PVA-1MCC, 5PVA-2MCC, and 5PVA-3MCC respectively. The formation of additional hydrogen bonds between PVA and MCC, improves the decomposition temperature (T_{on}) in the second stage decomposition of composites. This demonstrates that in general, MCC can improve the thermal stability of the composites [17,38]. But 5PVA-2MCC and 5PVA-3MCC have shown slightly low T_{on} due to the reduced interfacial adhesion, which is further supported by tensile strength measurements.

Figure 5.6 (a-d) shows the DTG curve of 5PVA and 5PVA-MCC composites. DTG_{max}, which is the peak point in dM/dT, reveals that 5PVA and 5PVA-1MCC has almost similar peak point. But for 5PVA-2MCC and 5PVA-3MCC the DTG_{max} is found to be less, due to reduced interfacial adhesion between PVA and MCC. The third stage decomposition for 5PVA and for composites was found to be almost the same, which can be well understood from the DTG curves [39]. The results obtained are also presented in **Table 5. 3**

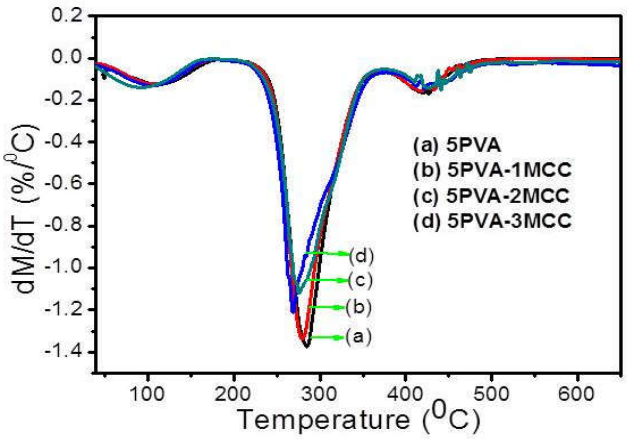

Figure 5.6 DTG curves of (a) 5 PVA film, (b) 5PVA-1MCC, (c) 5PVA-2MCC and (d) 5PVA-3MCC.

Table 5.3 TG and DTG results of 5PVA film and 5PVA-MCC composites.

Polymer/ composite	Second stage decomposition			Third stage decomposition	
	T_{on} (^{0}C)	T_{max} (^{0}C)	DTG_{max} (^{0}C)	T_{on} (^{0}C)	T_{max} (^{0}C)
5PVA	250	335	284	400	450
5PVA-1MCC	259	344	282	400	450
5PVA-2MCC	252	341	278	400	455
5PVA-3MCC	250	332	275	405	455

5.2.7 UV-Visible spectra

The light transmittance (Tr) of the composite films was studied by recording the UV-Visible spectra from 200 to 900 nm, which are shown in **Figure 5.7**. The films obviously showed higher Tr values at the range of visible light (400–800 nm) than the ultraviolet light (200–400 nm). The Tr values of 5PVA film is 68-78% at the wavelength from 400 to 800 nm, indicating their good transparency.

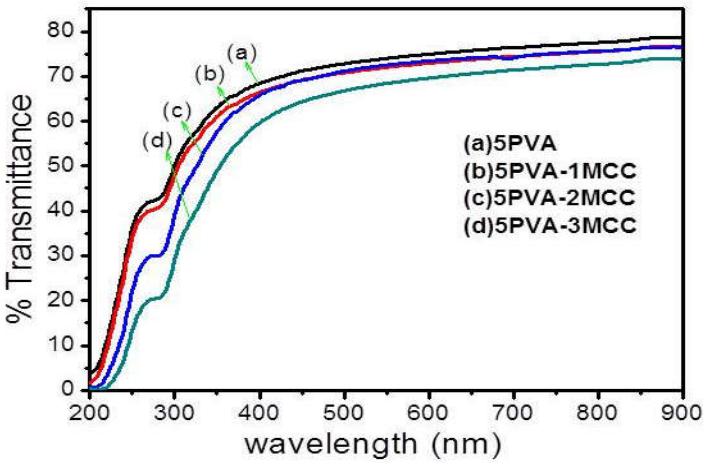

Figure 5.7 UV-Visible spectra of (a) 5PVA film, (b) 5PVA-1MCC, (c) 5PVA-2MCC and (d) 5PVA-3MCC.

From **Figure 5.7** (b-d) for composites as MCC content increases a slight reduction in the transparency of PVA-MCC composites film was observed, due to the incorporation of bigger MCC particles. However, 5PVA-1MCC and 5PVA-2MCC show almost similar transmittance values in the visible range. No red or blue shift of these bands indicated that any charge transfer or chemical change in the composites during the addition of MCC [40]. Eventhough, all the composite films demonstrated high transparency in the whole visible region they are slightly lower than that of glass, which is about 80%.

5.2.8 SEM analysis

The surface morphological character of the prepared pure 5PVA film and 5PVA-1MCC composites were investigated by SEM analysis and the images are shown in **Figure 5.8**.

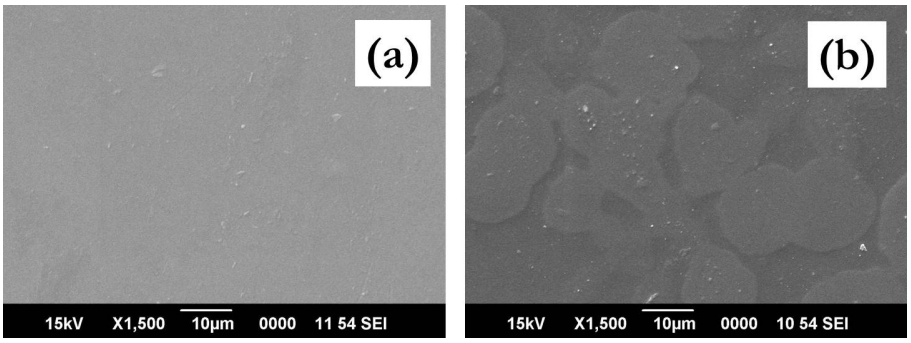

Figure 5.8 SEM images of (a) 5 PVA film and (b) 5PVA-1MCC composites.

From F**igure 5.8** (a) homogenous structure with smooth surface is observed for PVA film. **Figure 5.8** (b) the SEM of 5PVA-1MCC shows almost uniform distribution of spherical shaped particle and also with some irregular shapes. This distribution is further supported by AFM analysis.

5.2.9 AFM analysis

Figures 5.9 shows the AFM height images (a) 5PVA film, (b) 5PVA-1MCC, (c) 5PVA-3MCC composites.

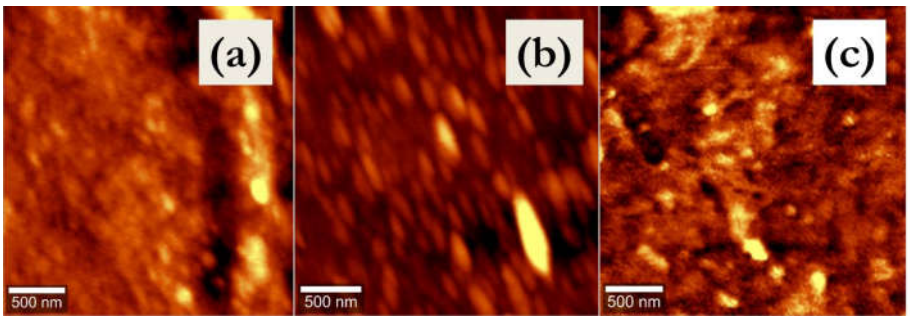

Figure 5.9 AFM height view images of (a) 5PVA film (b) 5PVA-1MCC and (c) 5PVA-3MCC composites

Figure 5.9 (a), the AFM height image of 5PVA film contains bright region and dark regions, corresponding to crystalline and amorphous regions in the polymer matrix. Surface morphological change during the incorporation of MCC into the PVA matrix can be clearly shown by **Figures 5.9** (b) and (c), the AFM height image of 5PVA-1MCC and 5PVA-3MCC respectively.

Figure 5.10 (a), AFM 3D images of 5PVA film reveals smooth surface with light coloured regions corresponding to higher apparent topography that is crystalline regions and dark coloured corresponding to amorphous regions. The films exhibiting both of these indicated its semi crystalline nature, which may arise from the random distribution of polymeric chains in an amorphous matrix [41].

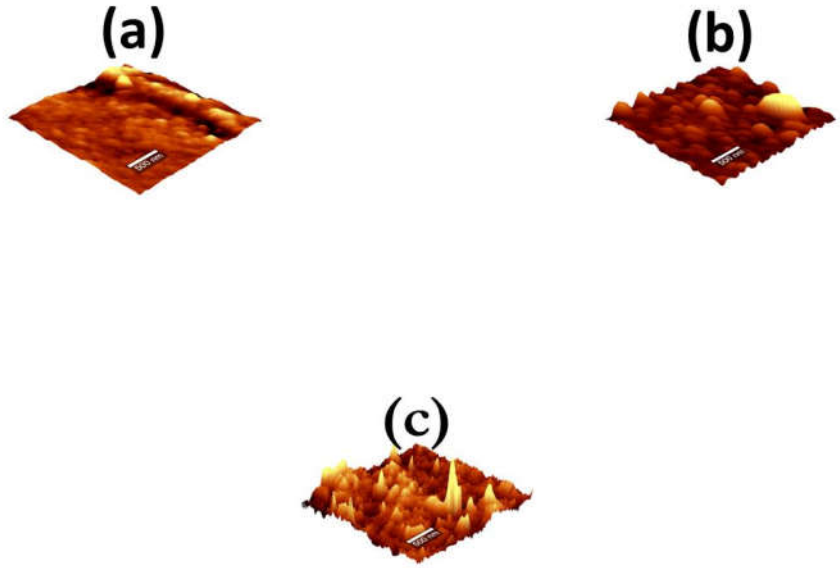

Figure 5.10 AFM 3D images of (a) 5PVA film, (b) 5PVA-1MCC and (c) 5PVA-3MCC

It can also be observed from **Figure 5.10** (b), AFM 3D image of 5PVA-1MCC that, there is considerable morphological change during the incorporation of MCC into PVA matrix. Uniform distribution of almost spherically shaped MCC and the dark regions shows the more amorphous nature of PVA matrix due to the incorporation of MCC. The SEM images [**Figure 5.8** (b)] also add testimony to these findings. The pronounced surface morphological change can be observed at higher loading leading to agglomeration. Agglomerations of particles were observed for 5PVA-3MCC from **Figure 5.10** (c), the AFM 3D image of 5PVA-3MCC. The highly agglomerated nature of 5PVA-3MCC is further supported by its reduced tensile strength values.

5.2.10 Mechanical properties

5.2.10.1 Tensile strength

The mechanical behaviour of 5PVA film and 5PVA- MCC composites were evaluated, the tensile strength values are graphically represented in **Figure 5.11**. It is well known that the mechanical properties of composites depend largely on individual components and on their interfacial adhesion.

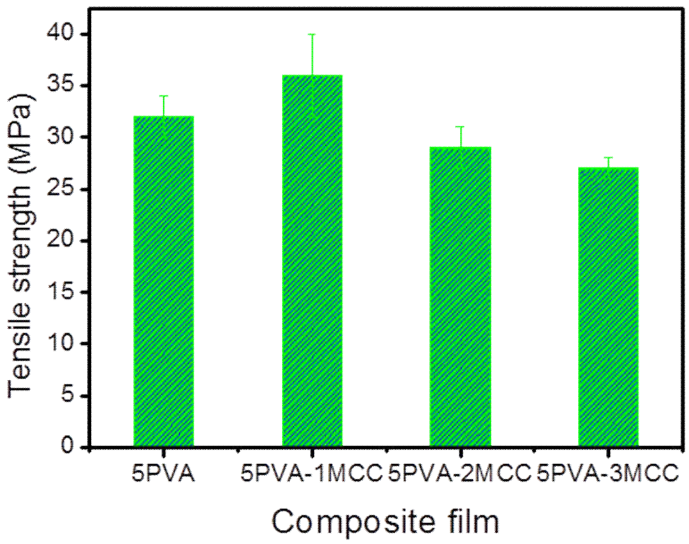

Figure 5.11.Tensile strength of 5PVA and 5PVA-MCC composites.

An increase in tensile strength observed for 5PVA-1MCC, indicating reinforcing effect due to uniform distribution of MCC in the polymer matrix. The uniform distribution and agglomeration has already been substantiated by SEM and AFM analysis [**Figure 5.8** (b) and **5.10** (b)]. Good interfacial interaction and stress transfer between MCC and polymer matrices are essential for good mechanical properties of composites [42]. These results

further confirm the presence of strong interfacial interaction and good dispersion between MCC and PVA [14,17]. Eventhough, there is only 12.5% increase in tensile strength by the reinforcement of MCC, much higher enhancement can be expected with more crystalline cellulose materials like nanocellulose. At higher MCC concentration filler- filler interaction predominates leading to lower tensile strength.

5.2.10.2 Elongation at break

The elongation at break of the composites are presented in **Figure 5.12** the values are found to be increased as the filler content increases and attains almost steady value at higher filler loading [17].

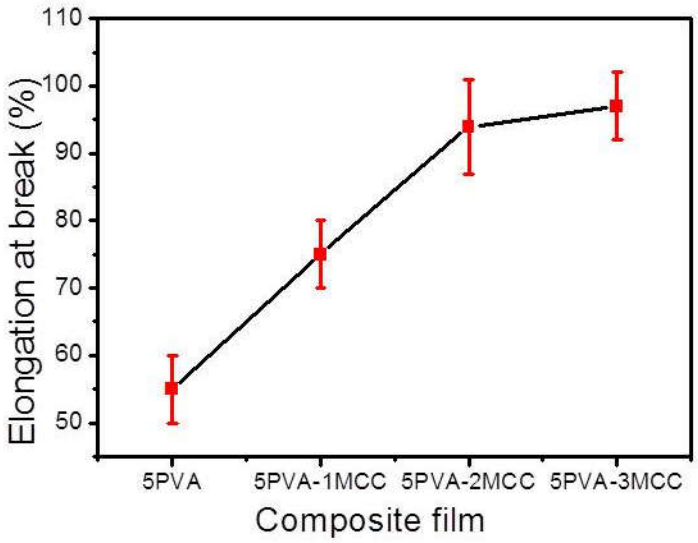

Figure 5.12 Elongation at break of 5PVA and 5PVA-MCC composites.

4.3 CONCLUSION

Reinforcing PVA with biopolymers like MCC provides interesting route for the preparation of green composites. Green composites of PVA with

MCC isolated from sago seed shells have been developed and optimised for better properties. DLS measurements show that the particle size of used MCC is >100 nm. The FTIR and ATR-FTIR spectra reveal the incorporation of MCC into the polymer matrix through hydrogen bonding. XRD patterns show broadening of peaks at different MCC concentrations. DSC reveals increase in the glass transition temperature and lowering in melting temperature for PVA-MCC composites. The results obtained from ATR-FTIR, XRD and DSC substantiates each other. TG results show increased thermal stability for 5PVA-1MCC at second stage decomposition compared to PVA film and the composites shown almost same stability at third stage. SEM analysis shows the uniform distribution for lower loading, which is further supported by AFM. UV-Visible spectra reveal good transparency of prepared films and marginal reduction in the transparency of PVA-MCC composites films, as MCC content increases. The tensile strength of 5PVA-1MCC increased slightly due to uniform distribution and decreased for composites at higher loading due to possible agglomeration. TG and tensile strength show that MCC as reinforcement in PVA can improve thermal and mechanical strength at low concentration.

REFERENCES

1. Satyanarayana, K. G.; Arizaga, G. G. C.; Wypych, F. Biodegradable composites based on lignocellulosic fibers-An overview. *Prog. Polym. Sci.* **2009**, *34*, 982–1021.

2. La Mantia, F. P.; Morreale, M. Green composites: A brief review. *Compos. Part A* **2011**, *42*, 579–588.

3. John, M. J.; Thomas, S. Biofibres and biocomposites. *Carbohydr. Polym.* **2008**, *71*, 343–364.

4. Chiellini, E.; Corti, A.; Solaro, R. Biodegradation of poly (vinyl alcohol) based blown films under different environmental conditions. *Polym. Degrad. Stab.* **1999**, *64*, 305–312.

5. Spiridon, I.; Popescu, M. C.; Bodaralu, R.; Vasile, C. Enzymatic degradation of some nanocomposites of poly (vinyl alcohol) with starch. *Polym. Degrad. Stab.* **2008**, *93*, 1884–1890.

6. Peppas, N, A. *Hydrogels in medicine and pharmacy 2*; CRC Press, Florida, 1986.

7. Song, T.; Tanpichai, S.; Oksman, K. Cross-linked poly (vinyl alcohol) (PVA) foams reinforced with cellulose nanocrystals (CNCs). *Cellulose* **2016**, *23*, 1925–1938.

8. Alves, H.; Pires, W.; Neto, F.; Oliveira, N.; Pasquini, D. Extraction and characterization of cellulose nanocrystals from corncob for application as reinforcing agent in nanocomposites. *Ind. Crops Prod.* **2013**, *44*, 427–436.

9. Nishiot, Y.; Manley, R. S. J. Cellulose/poly (vinyl alcohol) blends prepared from solutions in N,N-Dimethylacetamide-Lithium Chloride. *Macromolecules* **1988**, *21*, 1270–1277.

10. Park, J. S.; Park, J. W.; Ruckenstein, E. Thermal and dynamic mechanical analysis of PVA/MC blend hydrogels. *Polym.* **2001**, *42*, 4271–4280.

11. Cinelli, P.; Lawton, J. W.; Gordon, S. H.; Imam, S. H.; Chiellini, E. Injection molded hybrid composites based on corn fibers and poly (vinyl alcohol). *Macromol. Symp.* **2003**, *197*, 115–124.

12. Cinelli, P.; Chiellini, E.; Gordon, S. H.; Imam, S. H. Characteristics and degradation of hybrid composite films prepared from PVA, starch and lignocellulosics. *Macromol. Symp.* **2003**, *197*, 143–155.

13. El-Zaher, N. A.; Osiris, W. G. Thermal and structural properties of poly (vinyl alcohol) doped with hydroxypropyl cellulose. *J. Appl. Polym. Sci.* **2005**, *96*, 1914–1923.

14. Chakraborty, A.; Sain, M. Reinforcing potential of wood pulp-derived microfibres in a PVA matrix. *Holzforschung* **2006**, *60*, 53–58.

15. Guirguis, O. W.; Moselhey, M. T. H. Thermal and structural studies of poly (vinyl alcohol) and hydroxypropyl cellulose blends. *Nat. Sci.* **2012**, *4*, 57–67.

16. Attia, G.; El-kader, M. F. H. A. Structural, optical and thermal characterization of PVA/2HEC polyblend films. *Int. J. Electrochem. Sci.* **2013**, *8*, 5672–5687.

17. Sun, X.; Lu, C.; Liu, Y.; Zhang, W.; Zhang, X. Melt-processed poly (vinyl alcohol) composites filled with microcrystalline cellulose from waste cotton fabrics. *Carbohydr. Polym.* **2014**, *101*, 642–649.

18. Mathew, A. P.; Oksman, K.; Sain, M. Mechanical properties of biodegradable composites from poly lactic acid (PLA) and microcrystalline cellulose (MCC). *J. Appl. Polym. Sci.* **2005**, *97*, 2014–2025.

19. Hatakeyama, H.; Kato, N.; Nanbo, T.; Hatakeyama, T. Water absorbent polyurethane composites derived from molasses and lignin filled with microcrystalline cellulose. *J.Mater.Sci.* **2012**, *47*, 7254–7261.

20. Kiziltas, A.; Gardner, D. J.; Han, Y.; Yang, H. Dynamic mechanical behavior and thermal properties of microcrystalline cellulose (MCC)-filled nylon 6 composites. *Thermochim. Acta* **2011**, *519*, 38–43.

21. Chuayjuljit, S.; Su-Uthai, S.; Charuchinda, S. Poly (vinyl chloride) film filled with microcrystalline cellulose prepared from cotton fabric waste: Properties and biodegradability study. *Waste Manag. Res.* **2010**, *28*, 109–117.

22. Xiuju, Z.; Juncai, S.; Huajun, Y.; Zidan, L.; Shaozao, T. Mechanical properties, morphology, thermal performance, crystallization behavior, and kinetics of PP/microcrystal cellulose composites

compatibilized by two different compatibilizers. *J.Thermoplast. Compos.* **2011**, *24*, 735–754.

23. Thummanukitcharoen; Limpanart; Srikulkit. Preparation of organosilane treated microcrystalline (SiMCC) and SiMCC/polypropylene composites. *J. Met. Mater. Miner.* **2012**, *22*.

24. Ibrahim, A. S.; Attia, G.; Abo-Ellil, M. S.; Abd El-Kader, F. H. Electrical studies on PVA-PE copolymer. *J. Appl. Polym. Sci.* **1997**, *63*, 343–348.

25. Chhatri, A.; Bajpai, J.; Bajpai, A. K.; Sandhu, S. S.; Jain, N.; Biswas, J. Cryogenic fabrication of savlon loaded macroporous blends of alginate and poly (vinyl alcohol) (PVA). swelling, deswelling and antibacterial behaviors. *Carbohydr. Polym.* **2011**, *83*, 876–882.

26. Lee, H. W.; Karim, M. R.; Park, J. H.; Ghim, H. Do; Choi, J. H.; Kim, K.; Deng, Y.; Yeum, J. H. Poly (vinyl alcohol)/chitosan oligosaccharide blend submicrometer fibers prepared from aqueous solutions by the electrospinning method. *J. Appl. Polym. Sci.* **2009**, *111*, 132–140.

27. Liu, Y.; Liu, D.; Sui, G. Effects of cellulose nanowhiskers on the properties of poly (vinyl alcohol)/graphene nanoplatelets nanocomposites. *Polym. Compos.* **2015**.

28. Sawatari, C.; Kondo, T. Interchain hydrogen bonds in blend films of poly (vinyl alcohol) and its derivatives with poly (ethylene oxide). *Macromolecules* **1999**, *32*, 1949–1955.

29. Hema, M.; Selvasekerapandian, S.; Sakunthala, A.; Arunkumar, D.; Nithya, H. Structural, vibrational and electrical characterization of PVA-NH4Br polymer electrolyte system. *Phys. B* **2008**, *403*, 2740–2747.

30. Ricciardi, R.; Finizia, A.; Rosa, C.; Lauprêtre, F. X-ray diffraction analysis of poly (vinyl alcohol) hydrogels, obtained by freezing and thawing techniques. *Macromolecules* **2004**, *37*, 1921–1927.

31. Chen, J.; Li, Y.; Zhang, Y.; Zhu, Y. Preparation and characterization of graphene oxide reinforced PVA film with boric acid as crosslinker. *J. Appl. Polym. Sci.* **2015**, *132*, 1–8.

32. Jayasekara, R.; Harding, I.; Bowater, I.; Christie, G. B. Y.; Lonergan, G. T. Preparation, surface modification and characterisation of

solution cast starch PVA blended films. *Polym. Test.* **2004**, *23*, 17–27.

33. Ahad, N.; Saion, E.; Gharibshahi, E. Structural, thermal, and electrical properties of PVA-sodium salicylate solid composite polymer electrolyte. *J. Nanomater.* **2012**, *2012*, 94.

34. Wiria, F. E.; Chua, C. K.; Leong, K. F.; Quah, Z. Y.; Chandrasekaran, M.; Lee, M. W. Improved biocomposite development of poly (vinyl alcohol) and hydroxyapatite for tissue engineering scaffold fabrication using selective laser sintering. *J. Mater. Sci. Mater. Med.* **2008**, *19*, 989–996.

35. Tang, X.; Alavi, S. Recent advances in starch, poly (vinyl alcohol) based polymer blends, nanocomposites and their biodegradability. *Carbohydr. Polym.* **2011**, *85*, 7–16.

36. Liu, D.; Sun, X.; Tian, H.; Maiti, S.; Ma, Z. Effects of cellulose nanofibrils on the structure and properties on PVA nanocomposites. *Cellulose* **2013**, *20*, 2981–2989.

37. Qiu, K.; Netravali, A. N. Fabrication and characterization of biodegradable composites based on microfibrillated cellulose and poly (vinyl alcohol). *Compos. Sci. Technol.* **2012**, *72*, 1588–1594.

38. Lee, S. Y.; Mohan, D. J.; Kang, I. A.; Doh, G. H.; Lee, S.; Han, S. O. Nanocellulose reinforced PVA composite films: Effects of acid treatment and filler loading. *Fibers Polym.* **2009**, *10*, 77–82.

39. Lu, J.; Wang, T.; Drzal, L. T. Preparation and properties of microfibrillated cellulose poly (vinyl alcohol) composite materials. *Compos. Part A. Appl. Sci. Manuf.* **2008**, *39*, 738–746.

40. Chen, Y.; Cao, X.; Chang, P. R.; Huneault, M. A. Comparative study on the films of poly (vinyl alcohol)/pea starch nanocrystals and poly (vinyl alcohol)/native pea starch. *Carbohydr. Polym.* **2008**, *73*, 8–17.

41. Sreeja, S.; Sreedhanya, S.; Smijesh, N.; Philip, R.; Muneera, C. I. Organic dye impregnated poly (vinyl alcohol) nanocomposite as an efficient optical limiter: Structure, morphology and photophysical properties. *J. Mater. Chem. C* **2013**, *1*, 3851.

42. Sonia, A.; Dasan, K. P.; Jayachandran, J. Thermal characteristics of ethylene-co-vinyl acetate/cellulose microfibers composites. *Polym. Compos.* **2013**, *34*, 616–625.

CHAPTER 6
ISOLATION OF CELLULOSE NANOCRYSTALS FROM SAGO SEED SHELLS

Abstract

This chapter presents the isolation of cellulose nanocrystals (CNCs) from Sago seed shells (Cycas circinalis) by acid hydrolysis. The isolated CNCs were characterized by FTIR, XRD, SEM, TEM, AFM, DLS, Zeta (ζ) potential and TG. FTIR spectrum of CNCs shows similar frequencies as that of α-cellulose. XRD diffraction pattern shows co-existence of cellulose I and cellulose II. SEM image shows the reduction in size during acid hydrolysis. TEM image shows that the isolated CNCs contained networked structures and almost spherical shaped particles having 10-15 nm in size. AFM clearly reveals that isolated CNCs have nano dimensions and this is also supported by DLS. TG describes the lower thermal stability of CNCs compared with that of α-cellulose.

Part of this chapter has been published in Carbohydrate Polymers. "Isolation and characterisation of cellulose nanocrystals from sago seed shells", 2017; DOI. 10.1016/j.carbpol. 2017.09.088."

6.1 INTRODUCTION

Growing global environmental concerns and new environmental regulations have forced the search for new materials that are environmentally benign. Lignocellulosic materials apart from being used in traditional applications are also employed for the isolation of cellulose nanomaterials. The nanometre sized single fibre of cellulose is commonly referred to as cellulose nanocrystals (CNCs), whiskers, nanowhiskers, microfibrillated cellulose (MFC), microfibril aggregates or nanofibers. CNCs and nanofibrillated celluloses (NFCs) constitute the two main families of nanocellulose, which are different in morphology. CNCs are extracted from fibres after the complete dissolution of non-crystalline fractions, while the nanofibrillated cellulose results from the application of high shearing forces of disintegration leading to a high degree of fibrillation, which yields highly interconnected fibrils [1]. The aspect ratio distinguishes NFC and MFC from CNCs. CNCs has a very low aspect ratio (10–100) while NFC and MFC have a high aspect ratio of >1000. NFC and MFC retain both the crystalline and amorphous regions, and have the shape and structure of spaghetti [2]. The ordered regions are cellulose chain packages that are stabilized by a strong and complex network of hydrogen bonds that resemble nanocrystalline rods [3].

Cellulose nanomaterials are important nano scale materials with desirable physicochemical properties like one of the strongest natural material with high tensile strength, high Young's modulus, high aspect ratio, large surface area and other favourable electrical and optical properties. Accessibility to modifications by sulphonation, oxidation, cationisation, grafting etc made cellulose nanomaterials in diverse applications [4]. An important feature of cellulose materials is their hydrophilicity, which makes

them suitable for combination with hydrophilic polymers but generally incompatible with hydrophobic matrices. Various chemical modification methods have been explored for combining cellulose with hydrophobic polymers. Furthermore, nanocellulose is classified in the category of non-toxic material [5].

Cellulose consists of polydispersed linear polymer of poly β-(1, 4)-D-glucose with a syndiotactic configuration. The complex structure of biomass derived cellulose is such that the structure can be analysed on different levels, such as structural, morphological, supramolecular consisting of macrofibrils, fibres, pores, microfibrils, crystalline, amorphous regions and finally the molecular level, consisting of glucan chains and hydrogen bonds [2]. The critical constituent responsible for natural fibre strength and stiffness is cellulose microfibrils. These microfibrils have a width ranging from 5 to 30 nm, are highly crystalline materials formed by the aggregation of long thread like bundles of molecules stabilized laterally by hydrogen bonds between hydroxyl groups and oxygens of adjacent molecules [6].

Potential applications of cellulose nanomaterials include barrier films, antimicrobial films, transparent films, flexible displays, reinforcing fillers for polymers, biomedical implants, pharmaceuticals, drug delivery, fibres and textiles, templates for electronic components, separation membranes, batteries, supercapacitors, electroactive polymers etc [7].

Various top down methods have been adopted for the preparation of cellulose nanomaterials. These include steam explosion treatment [6], high pressure homogenization [8], ultrasonic technique [9], acid/alkaline-hydrolysis [10,11] and enzyme-assisted hydrolysis [12] as well as the combined methods. When acid hydrolysis is used to obtain the nanocellulose, the stability and the dimensions of nanocelluloses are dependent not only on

the acid species, acid concentration, time, temperature of hydrolysis reaction, but also on the different origins of cellulose [13]. Bondenson *et al*.2006 optimised the conditions to obtain nanocellulsoe [14]. After that, a number of sources have been explored including, ramie, MCC, industrial bio-residue, grass fiber, rice husk, whatman filter paper, bacterial cellulose, cotton (cotton wool), industrial bio-residue (sludge), eucalyptus kraft pulp, rice straw, soy hulls, mengkuang leaves, sugarcane bagasse, algae, mulberry, sesame husk, sisal fibres, bamboo, colored cotton, tunicate, coconut husk, curaua fibres etc [15].

Cellulose nanocrystals with rod, sphere and network morphologies were isolated by Lu and Hsieh in 2010 by acid hydrolysis from cotton cellulose followed by freeze drying. Freeze drying significantly improved specific surface than original cellulose [16]. The same authors in 2012 isolated cellulose from chardonnay grape skins and on subsequent acid hydrolysis CNCs were obtained. They are mostly spherical nanoparticles with diameters ranging from 10 to 100 nm and a mean diameter of 48.1±14.6 nm by TEM. AFM analysis showed that the spherical nanoparticles consist of a nano-rod core surrounded by tiny cellulose fragments as shell [17].

Recently, nanocellulose was isolated from oil palm frond ((OPF), *Elaeis guineensis frond*) by Mohaiyiddin *et al*. in 2016 using chemical treatments including alkaline, bleaching and acid hydrolysis processes. Particle size analyser showed that OPF nanocellulose specimens were smaller in size, compared to sigma nanocellulose done for comparison. However, other analysis confirmed the formation of nanocellulose. FESEM analysis showed that nanocelluloses have needle like shaped structures having diameter in the range 50–70 nm [18]. Bleached corncob residue (CCR), a lignocellulosic waste was used by Liu *et al.* in 2016 to isolate nanocellulose

using four different methods such as sulphuric acid hydrolysis, formic acid (FA) hydrolysis, 2,2,6,6-tetramethylpiperidine-1-oxyl (TEMPO)-mediated oxidation, and pulp refining. Longer cellulose nanocrystals were obtained by FA hydrolysis than by sulphuric acid, and showed high crystallinity and thermal stability. The cellulose nanofibrils with fine and individualized structures were obtained by TEMPO mediated oxidation. The intensive pulp refining led to the formation of cellulose nanofibers having longest length and thickest diameter [19].

Kim *et al*.2016 isolated cellulose from kenaf core using chemical treatment. Subsequently nanocellulose was produced using electron beam irradiation followed by acid hydrolysis. The results showed decrease in cellulose molecular weight, polydispersity, decomposition temperature and crystallinity when the electron beam irradiation was increased. Moreover, the yield of nanocellulose decreased when the absorbed dose and acid hydrolysis time increased while the size distribution became narrower [20].

Eventhough, large number of sources have been used for the isolation of CNCs, only a very little work has been reported on the isolation of CNCs from seed shells. Therefore the main objective of the present chapter is the isolation and characterisation of CNCs from sago seed shells.

6.2 RESULTS AND DISCUSSION

6.2.1 Isolation of cellulose nanocrystals (CNCs)

α-Cellulose isolated was powdered, sieved through 53 μm mesh and used for the isolation of CNCs. Acid hydrolysis with sulphuric acid is the common procedure employed for the isolation of cellulose nanocrystals**.** The detailed method of isolation has already been given in **Chapter 3.2.4.** A

probable mechanism of acid hydrolysis of cellulose involves the following steps, as presented in **Scheme 6.1** [15]**.**

i) The H^+ ion generated by the sulphuric acid protonates the oxygen of glycosides to form conjugated acid.

ii) Breaking of C–O bonds along with removal of conjugated acid into cyclic carbocation.

iii) On the addition of water the proton and free sugar get liberated.

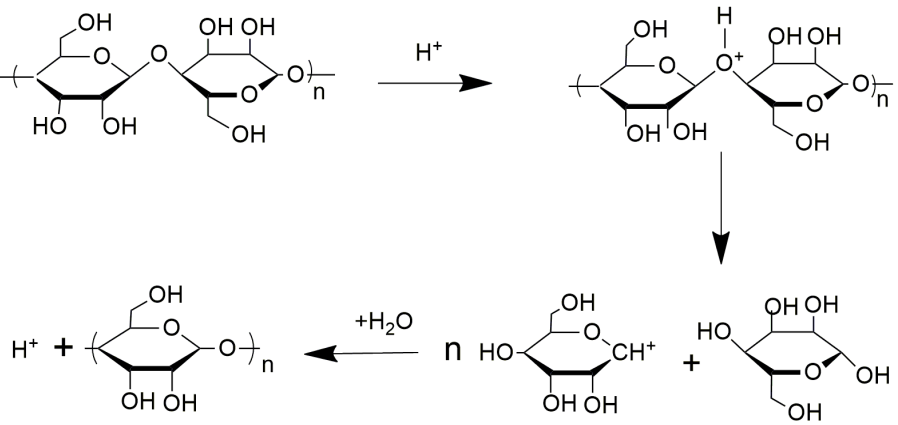

Scheme 6.1 Probable mechanism of acid hydrolysis of cellulose [15]

6.2.2 FTIR analysis.

Figure 6.1 shows the FT-IR spectra of α-cellulose and CNCs. FTIR spectroscopy has been extensively used to obtain information during various chemical treatments. From **Figure 6.1**(a), a strong band appeared at 3,443 cm^{-1}, which is related to the stretching vibration of O–H groups having strong inter- and intra-molecular hydrogen bonding. Stretching frequency at 2,904 cm^{-1} is due to the symmetric C–H vibrations and 1,642 cm^{-1} originated

from the absorbed water. Frequencies at 1434, 1379 and 1317 cm^{-1} are due to the bending of CH, CH_2 and OH respectively, which are typical for polysaccharides and 1164 cm^{-1} is due to asymmetric vibrations (C–O–C). The frequency at 897 cm^{-1} indicated the typical structure of cellulose (due to β-glycosidic linkages of glucose ring of cellulose) [21,22].

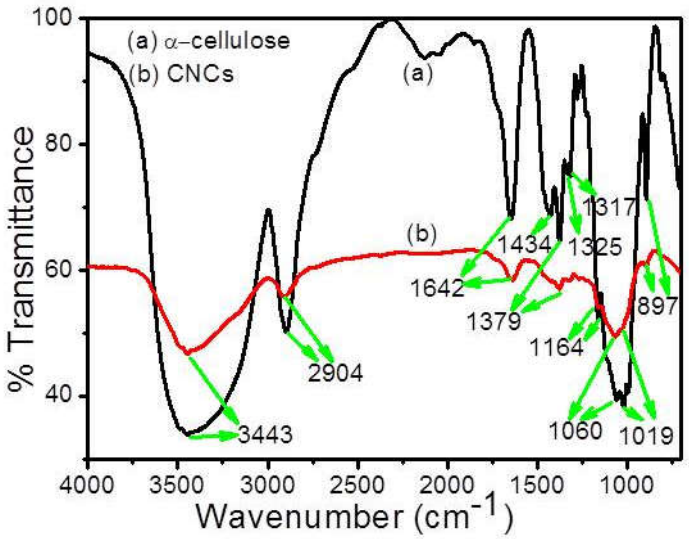

Figure 6.1 FTIR spectra of (a) α-cellulose and (b) CNCs.

Frequency at 1325 cm^{-1} is attributed to S ring (CH_2 rocking at C_6 in cellulose). After acid hydrolysis, the frequency at 1325 cm^{-1} was almost eliminated in CNCs and this may be due to the developed hydrogen bonding network in crystalline structure of CNCs and decreased the rocking movement of CH_2 [23]. The characteristic frequencies of cellulose were evident at 1019, 1060 cm^{-1} which corresponded to C-O-C stretching and 897 cm^{-1} due to C-H rocking vibrations that are present in both α-cellulose and CNCs [13,24,25]. Compared with α-cellulose, CNCs from [**Figure 6.1** (b)] have no obvious difference [26]. As a result of hydrolysis, cellulose chain

scission occurs in different extents, leading to different amounts of free O–H groups being present. This effect can be appreciated from changes in the broadening of the hydroxyl peak [27], which may be due to the disruption of intra- and inter-molecular hydrogen bonding.

6.2.3 XRD analysis

Figure 6.2 (a) exhibits the XRD pattern obtained for α-cellulose and (b) that of CNCs. The crystallinity of cellulose and nanocellulose is an important factor for determining its thermal and mechanical properties [26]. It has been proposed that the crystallite size is a matter of importance to describe the crystal structure of cellulose [28]. X-ray diffraction pattern of CNCs [**Figure 6.2** (b)] displays a well-defined mixture of polymorphs of cellulose I and cellulose II. The presence of cellulose II can be observed by characteristic peaks at 2θ=12 (110), 20 (210) and 22 (200) [29,30] and cellulose I, by the presence of peaks at 2θ=14.5 ($1\bar{1}0$), 17.5 (110), 22 (200), and 34.6 (004) [23,31]. The appearance of doublet after chemical treatments, as shown in **Figure 6.2** (b), indicates the transformation of native cellulose from cellulose I to cellulose II [32]. In our previous study (Chapter **4.2.6**) of isolation of microcrystalline cellulose from sago seed shells, the possibility of existence of cellulose II was predicted and is now well pronounced and clearly observable in CNCs [33].

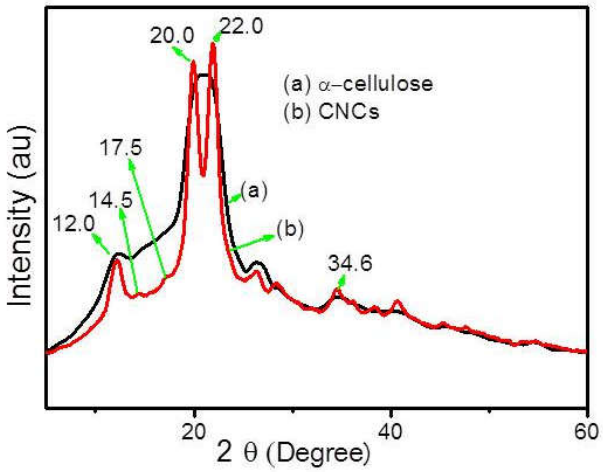

Figure 6.2 XRD patterns of (a) α-cellulose and (b) CNCs.

Eventhough, cellulose exist as several polymorphs as I, II, III and IV, cellulose I is the crystalline cellulose which is produced from the natural source. It is metastable and can be thermodynamically converted to cellulose II or III [34]. The most stable structure of cellulose is cellulose II, can be obtained by solubilisation and recrystallization. This can be explained by the formation of a new Na-cellulose I lattice through the alkaline pre-treatment before the acid hydrolysis reaction. In the lattice structure -OH groups of the cellulose are replaced by ONa groups, expanding the molecular dimensions. Rinsing with water will remove the linked Na ions and leads to the most stable crystalline structure, which is cellulose II [32,35]. By increasing the alkaline concentration, the intermolecular bonds are progressively weakened by swelling and penetration of sodium hydrates inside the cellulose fibre matrix. This leads to the realignment and complete recrystallization of cellulose fibres to break the already existing intermolecular chain links to produce new crystalline lattice structures [30]. It was reported that the crystalline transformation in natural fibres happens with an alkali

concentration of up to 32% [36]. The 17.5% w/v NaOH solution used for isolation of α-cellulose may convert cellulose I into cellulose II, but pronounced and clearly visible only in CNCs [33,37]. Moreover, cellulose II is associated to the re-precipitation of cellulose I after hydrolysis with 64% sulphuric acid solution, which can be a solvent for cellulose II and is more susceptible to hydrolysis than native cellulose [38]. The major distinction between these two forms of cellulose lies in the layout of their atoms, cellulose II has an antiparallel packing, whereas the chains in cellulose I run in a parallel direction.

The degree of crystallinity was calculated by using **Equation 4.1**, where I_{200} is the maximum intensity of the principal peak (200) lattice diffraction at $2\theta=22^0$ for cellulose I, and $2\theta=20^0$ for cellulose II, and I_{am} is the intensity of diffraction attributed to amorphous cellulose at $2\theta=18^0$ for cellulose I, and at $2\theta=16^0$ for cellulose II [39–41].

The degree of crystallinity index calculated was found to be 72% for cellulose II. Crystallinity in the range of 70-90% have been reported by other researchers for nanocrystals isolated from different sources by acid hydrolysis [25,31,42]. Crystallinity index of Cellulose I was found to be 69%, increased slightly, because acid treatment of 45 min duration not only removed the amorphous regions of cellulose but partly destroyed the crystalline ones. A similar observation due to the effect of hydrolysis on time was observed in a previous study [43,44]. It is to be noted that, the degree of crystallinity of microcrystalline cellulose and α-cellulose from our previous work (**Table 4.4**) are 67% and 44% respectively [33]. The crystallite size was determined from X-ray diffractograms by applying Scherrer's **Equation 6.1**

$$D_{hkl} = K\lambda / \beta_{1/2} \cos\theta \text{ ---------- } \mathbf{6.1}$$

where D_{hkl} is the crystallite dimension in the direction normal to the hkl lattice planes, K is the correction factor and usually taken to be 0.9, λ is the radiation wavelength, θ is the diffraction angle and $\beta_{1/2}$ is the peak width at half maximum intensity measured at the doublet peak.

Scherrer's equation is restricted to samples of high crystallinity and without any broadening of peaks and applied to cellulose I, the value obtained was 9.4 nm. Cellulose crystallinity is of prime importance as this is a key factor to determine the reinforcing capability and mechanical strength of cellulose to be utilized in composite applications. The highly crystalline fibres are expected to be more effective in providing higher reinforcement for composite materials owing to the increased stiffness and rigidity, achieving a higher Young's modulus [45].

6.2.4 SEM analysis.

Figure 6.3 (a-c) shows the SEM images of sago seed shells, α-cellulose and CNCs respectively. Morphology of sago seed shells, α-cellulose and CNCs were analysed by SEM images. Morphological examination of the CNCs is essential because the source of cellulose and hydrolysis technique have profound influence on the dimension and properties of nanocellulose. Drying process of CNCs suspension is important for its storage, transportation and generation of various desired structures [46].

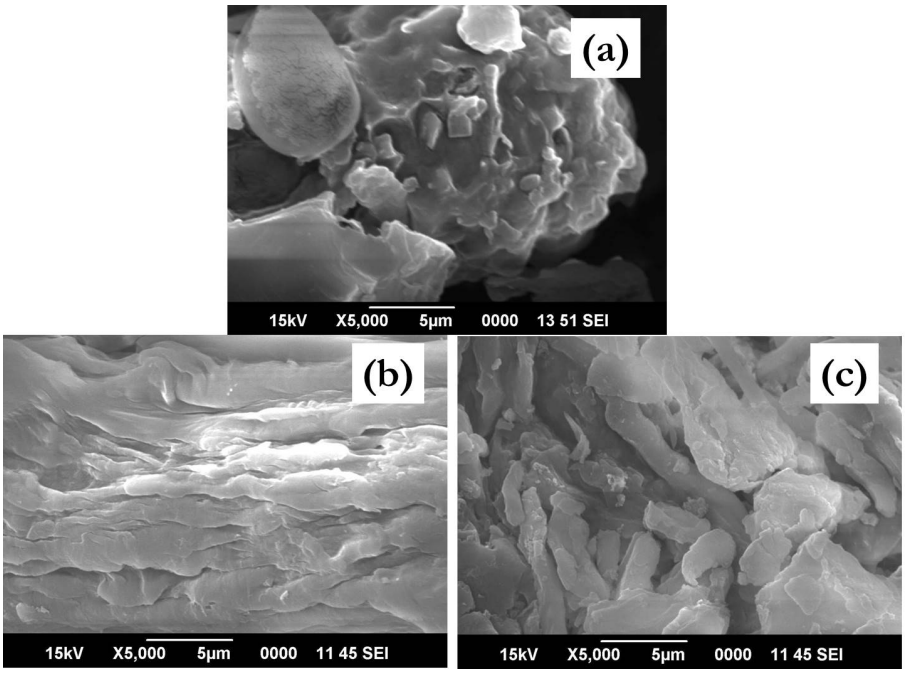

Figure 6.3 SEM images of (a) sago seed shells, (b) α-cellulose and (c) CNCs.

Figure 6.3 (a) SEM images of sago seed shells show highly agglomerated and rough surface due to the presence of lignin, hemicellulose, extractives etc. From **Figure 6.3** (b) SEM image of α-cellulose, shows self-assembled structures like stacked flakes due to strong interfibrillar attraction via hydrogen bonding among the surface hydroxyl groups. From **Figure 6.3** (c) SEM images of isolated CNCs, it can be clearly observed that freeze dried sample shows reduction in size after acid hydrolysis due to the successful removal of amorphous regions [25]. This fact is further confirmed by TEM and AFM. Considerable particle size reduction, coupled with a loss of fibrous character occurs, indicating the surface etching and erosion nature of the hydrolysis process [27]. Aggregation of nanocelluloses can be observed in **Figure 6.3** (c), which is a common phenomenon reported by many authors

[47,48]. However, the real structures of nanocellulose cannot be clearly understood by SEM images.

6.2.4 TEM analysis.

Figures 6.4 (a) and (b) show the TEM images of isolated CNCs. The dimensions of nanocellulose depend strongly on the processing techniques and hydrolysis conditions. In general, stronger acidity, longer reaction time and higher temperature might yield shorter CNCs [49].

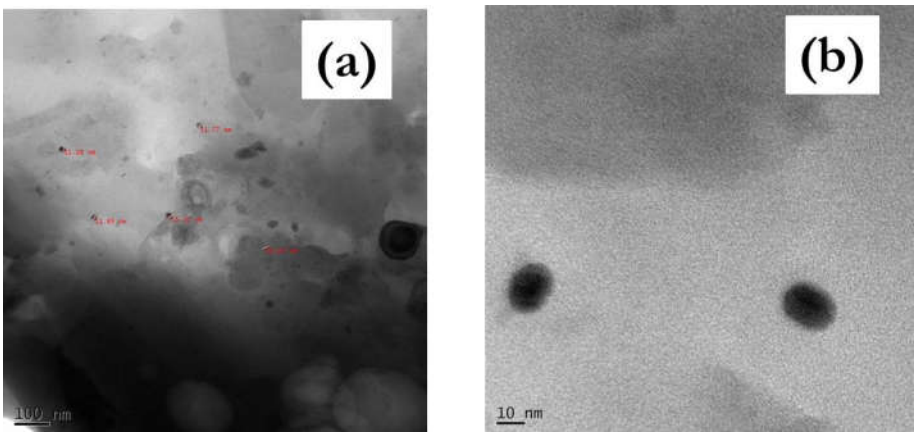

Figures 6.4 (a) and (b) TEM image of CNCs.

Figure 6.4 (a) and (b) clearly show that TEM image consist of network like structure along with spherical shaped particles, having size 10-15 nm [**Figure 6.4 (b)]** [16,50,51]. The ultrasonic treatment might play an important role in forming the spherical CNC [52]. Spherical nanocellulose is formed due to self-assembly of short cellulose rods via interfacial hydrogen bonds. The strong hydrogen bonding among cellulose nanocrystals overcomes the repulsion of surface negative charges, leading to the formation of self-assembled porous networks [53]. It is possible that the network structured cellulose nanocrystals embedded in the abundant spherical

cellulose nanocrystals in the freeze-drying process. Another probable explanation is that the network structured cellulose may be formed by the over-irradiation of electron beams during TEM observation [16].

6.2.5 AFM analysis.

The surface morphology of isolated CNCs was also obtained by AFM analysis. In AFM two modes are used to record data during scanning, one for the height image and the other for 3D image.

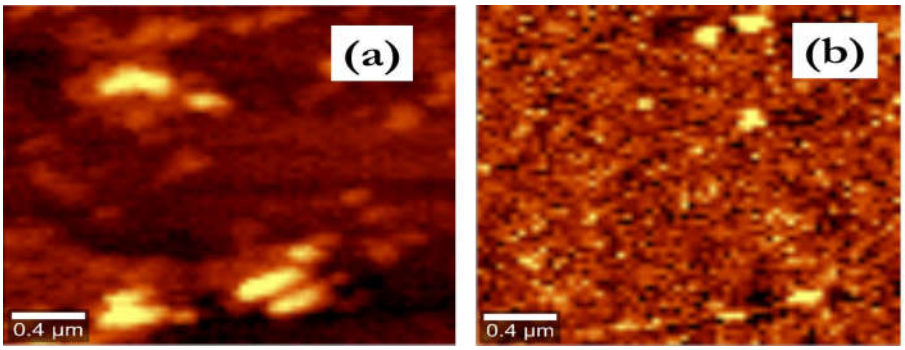

Figure 6.5 AFM height images of (a) α-cellulose and (b) CNCs.

Figures 6.5 (a) and (b) show the AFM height image of α-cellulose and isolated CNCs respectively. The height image displays topographical details by tracking the surface with the probe and the 3D image gives the contrast between soft and hard polymer segment. The bright regions represent the crystalline areas while the dark areas stand for the amorphous portions in the direction of the fiber axis in the cellulose structure [54].

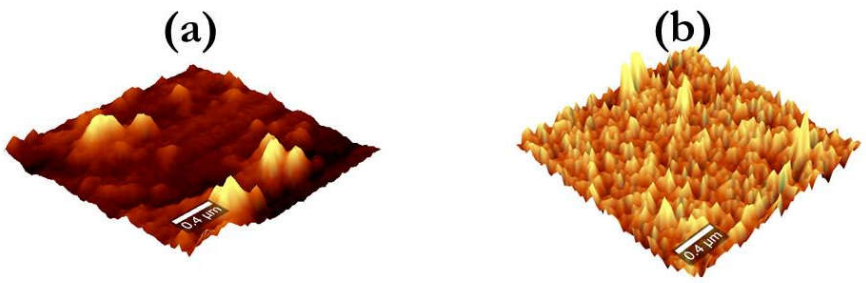

Figure 6.6 AFM 3 D images of (a) α-cellulose and (b) CNCs

From **Figure 6.6** (a), it can be clearly observed that the α-cellulose has size above 100 nm and moreover, the AFM image contains both brighter regions and dark regions indicating crystalline and amorphous nature of cellulose. From **Figure 6.6** (b) that of CNCs, contains only bright images indicating its fully crystalline nature. Moreover, CNCs contain almost spherical and other shaped structures having approximately less than 50 nm size. The dimensions of nanocellulose depend strongly on the processing techniques and the prepared samples exhibited distinct features. Sulphuric acid hydrolysis usually could cleave the amorphous region of microfibrils transversely, resulting in diameter reduction of fibres from micron to nanometers [55]. The approximate diameters for most of the nanocellulose fibres obtained from different sources like banana rachis, sisal, kapok, pineapple leaf and coir, were found to be between 10–60, 20–80, 20–70, 50–150 and 40–90 nm respectively and the calculated width of the nanocellulose particles is larger than the actual value due to the severe tip broadening effect in AFM measurements. The tip broadening effect is less pronounced in the rod-shaped cellulose nanofibrils compared to the spherical shaped nanoparticles. Therefore, the calculated width of the nanocellulose samples mentioned above may be approximately 10% more than the actual value [25]. Aggregation and overlapping of individual cellulose nanofibrils make it

difficult the accurate determination of size and aspect ratio of the nanocellulose. The AFM picture also indicates very high surface area of the nanocellulose which is useful for enhanced polymer nanocellulose interaction during composite manufacturing. The AFM results were used to support the TEM results. The value found for the crystallite size through the Scherrer's equation is nearest the value found by TEM.

6.2.6 Dynamic Light Scattering (DLS)

Figure 6.7 shows the particles size distribution plot of isolated CNCs. The DLS technique has been employed to find the statistical distribution of the particles present. CNCs were suspended in water and analysed for particle size by the DLS.

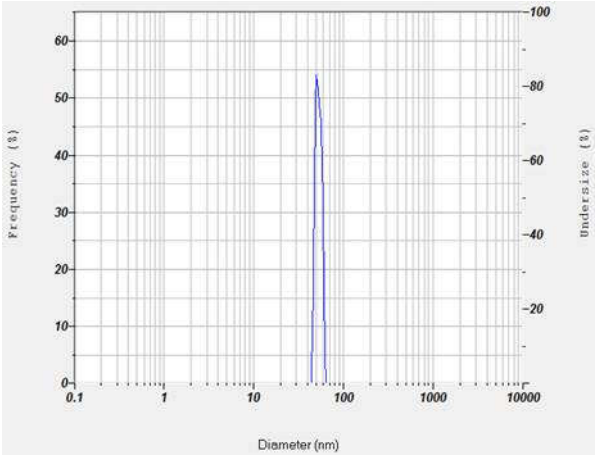

Figure 6.7 DLS curve of CNCs.

Figure 6.7 indicates that the CNCs contain majority of the particles lying in the nano range. Moreover, a narrow size distribution of the particles is seen. The minimum particle size is found to be 45.7 nm which accounts for 10%, then a gradual and steady increase in the size of the particles which

reaches a peak at 50.1 nm accounting for about 50% and 90% of particle has the size 55.6 nm, having a mean value of 50.4 ±3.1 [18].

6.2.7 Zeta (ζ) potential measurements

Figure 6.8 shows the zeta (ζ) potential curve of isolated CNCs. Stability of the nanocellulose in suspension was determined by the zeta potential measurement. The presence of negative charge developed by grafting of sulphate groups due to sulphuric acid hydrolysis induces the formation of a negative electrostatic layer covering the nanocrystals and promotes their dispersion in water. Agglomeration of nanocellulose will occur if the zeta potential value is within the range of -15 to 15 mV [56]. Within this range, the nanocellulose particles do not have enough charge to repulse each other, hence forming agglomeration. Stable suspension of nanocellulose should have a zeta potential value of less than -30 mV and greater than 30 mV [18] or higher than 25 mV [57]. Moreover small zeta potential value suggests weak electrostatic repulsive forces among CNCs [58].

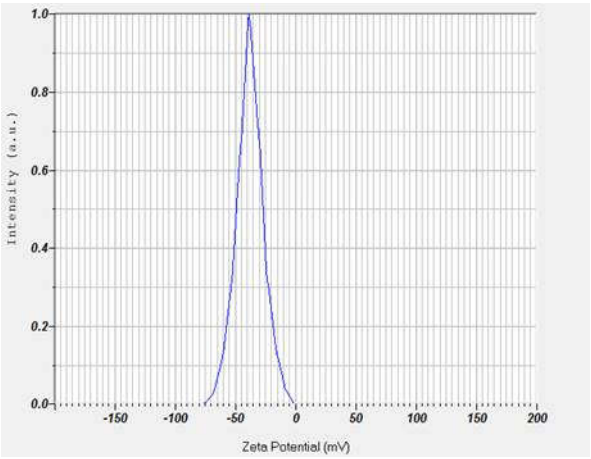

Figure 6.8 Zeta potential of CNCs.

The CNCs isolated shown a negative zeta potential value of -37.8. Higher negative value may be due to sulphate groups introduced by sulphuric hydrolysis that are attached to the CNCs chain which create repulsive forces to repel each other. Negative zeta potential below -30, demonstrates their ability to remain stable in solution [59], the value is close to stable suspension but not too high. The performance of the nanocellulose as reinforcing agent is also associated with surface charge (zeta potential). Nano sized particles should have high zeta potential, so that the colloidal suspension can resist aggregation, to increase its degree of dispersion in the composite.

6.2.8 Thermogravimetry (TG)

Figure 6.9 shows the TG curve of α-cellulose and CNCs. Each shows initial weight loss between 50 and 80 ^{0}C due to evaporation of water. α-Cellulose undergoes degradation processes with the production of flammable volatiles, which are released through dehydration, hydrolysis, oxidation, decarboxylation and transglycosylation [60]. For α-cellulose, drastic loss or first stage at the range 250–345 ^{0}C, followed by slow or second stage weight losses up to 512 ^{0}C was observed. For CNCs, the vast majority of weight loss occurred in the range of 225–464 ^{0}C [13,20]. It is known that as the molecular weight distribution increases, the onset temperature reduces and the degradation range increases [54,61].

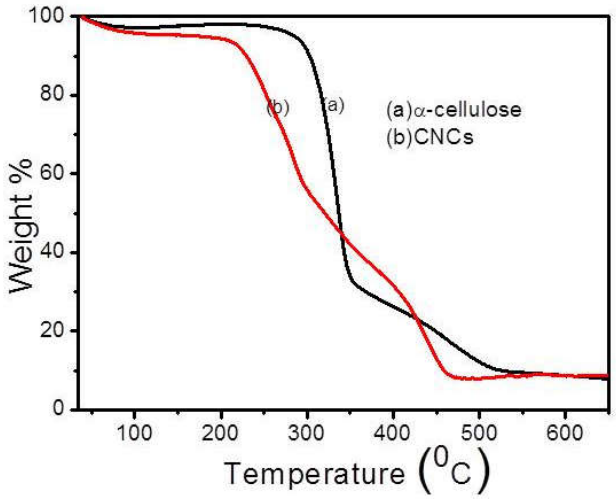

Figure 6.9 TG curves of (a) α-cellulose and (b) CNCs.

CNCs exhibited the low onset decomposition temperature of 225 ^{0}C and obvious differences in the degradation behaviours. Compared to α-cellulose, degradation occurred within a wider temperature range and showed well-separated pyrolysis processes. The high surface areas of CNCs play an important role in diminishing their thermal stability due to the increased exposure of surface area to heat. Moreover, the lower decomposition temperatures also indicate faster heat transfer in CNCs. The CNCs have been reported to function as efficient pathways for phonons. It can be observed that early decomposition temperature is the consequence of the hydrolysis process, which results in a massive reduction of the molecular weight. It was also believed that sulphuric acid hydrolysis not only removes the noncrystalline segment, but could also potentially dissolve some crystalline segments, making it more susceptible to degradation in response to increase in temperature [54]. It is widely accepted that the negative charged sulphate groups introduced on the outer surface of the cellulose crystals resulted in decrease in the thermal stability [62]. It has been reported that the activation

energies of the degradation of cellulose nanocrystals were significantly lowered by introducing sulphate groups *via* sulphuric acid hydrolysis [63]. Moreover, two different decomposition stages can also be explained by the presence of highly sulphated amorphous domains and unsulphated crystalline domains. The highly sulphated regions were more susceptible to degradation at lower temperature, whereas the higher temperature decomposition corresponded to the breakdown of unsulphated crystals [47]. But both α-cellulose and CNCs from **Figure 6.9** have shown almost same char at 650 ^{0}C [37].

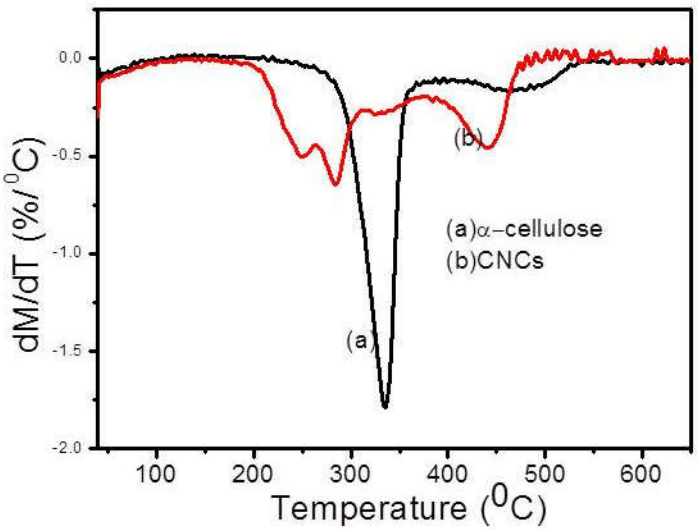

Figure 6.10 DTG curves of (a) α-cellulose and (b) CNCs

Furthermore based on the DTG **Figure 6.10** the thermal decomposition peaks of the maximum weight loss appeared at 350, 465 ^{0}C for α-cellulose and 249, 282^0, 442 ^{0}C for CNCs respectively. The three well defined peak degradation temperatures for CNCs also confirm their different degradation pathways. The results obtained are presented in **Table 6.1**

Table 6.1 TG and DTG results of α-cellulose and CNCs.

Name of components	First stage decomposition			Second stage decomposition		
	T_{on} (^{0}C)	T_{max} (^{0}C)	DTG (^{0}C)	T_{on} (^{0}C)	T_{max} (^{0}C)	DTG (^{0}C)
α-cellulose	250	345	350	345	512	465
CNCs	225	464	249, 282,	----	----	442

4.3 CONCLUSION.

Cellulose nanocrystals (CNCs) have been isolated from sago seed shells by acid hydrolysis. FTIR spectra reveal similar frequencies as that of α-cellulose, moreover due to hydrolysis different amounts of free O–H groups caused changes in broadening of the hydroxyl peak. XRD pattern shows the co-existence of cellulose I and cellulose II with crystallinity index of 72% for cellulose II, 69% for cellulose I having crystallite size of 9.4 nm for cellulose I. The presence of cellulose II observed at 2θ =12 (110), 20 (210) and 22 (200) and cellulose I at 2θ =14.5 ($1\bar{1}0$1), 17.5(110) 22 (200), and 34.6 (004). SEM analysis shows considerable reduction in size and changes in surface morphology occurred during the isolation of CNCs from α-cellulose. TEM analysis shows that the isolated CNCs contain networked structures and almost spherical shaped particles having 10-15 nm in size. AFM analysis also supports nanometer size of isolated CNCs and moreover, the AFM contains almost spherical and other shaped CNCs with approximately 50 nm size. DLS measurements give the average particle size of 50.4±3.1 nm and zeta potential of -37.8 mV. Since CNCs are having high surface, the increased exposure of surface to heat along with fast heat transfer make CNCs thermally less stable than α-cellulose and thus having different degradation pathways.

REFERENCES

1. Kalia, S.; Boufi, S.; Celli, A.; Kango, S. Nanofibrillated cellulose: Surface modification and potential applications. *Colloid Polym. Sci.* **2014**, *292*, 5–31.

2. Osong, S. H.; Norgren, S.; Engstrand, P. Processing of wood-based microfibrillated cellulose and nanofibrillated cellulose, and applications relating to papermaking: A review. *Cellulose* **2016**, *23*, 93–123.

3. Habibi, Y.; Lucia, L. A.; Rojas, O. J. Cellulose nanocrystals: Chemistry, self-assembly, and applications. *Chem. Rev.* **2010**, *110*, 3479–3500.

4. Lam, E.; Male, K. B.; Chong, J. H.; Leung, A. C. W.; Luong, J. H. T. Applications of functionalized and nanoparticle-modified nanocrystalline cellulose. *Trends Biotechnol.* **2012**, *30*, 283–290.

5. Vartiainen, J.; Pöhler, T.; Sirola, K.; Pylkkänen, L.; Alenius, H.; Hokkinen, J.; Tapper, U.; Lahtinen, P.; Kapanen, A.; Putkisto, K.; Hiekkataipale, P.; Eronen, P.; Ruokolainen, J.; Laukkanen, A. Health and environmental safety aspects of friction grinding and spray drying of microfibrillated cellulose. *Cellulose* **2011**, *18*, 775–786.

6. Deepa, B.; Abraham, E.; Cherian, B. M.; Bismarck, A.; Blaker, J. J.; Pothan, L. A.; Leao, A. L.; de Souza, S. F.; Kottaisamy, M. Structure, morphology and thermal characteristics of banana nano fibers obtained by steam explosion. *Bioresour. Technol.* **2011**, *102*, 1988–1997.

7. Moon, R. J.; Martini, A.; Nairn; Simonsen, J.; Jeff, Y. Cellulose nanomaterials review: Structure, properties and nanocomposites. *Chem. Soc. Rev.* **2011**, *40*, 3941–3994.

8. Li, J.; Wei, X.; Wang, Q.; Chen, J.; Chang, G.; Kong, L.; Su, J.; Liu, Y. Homogeneous isolation of nanocellulose from sugarcane bagasse by high pressure homogenization. *Carbohydr. Polym.* **2012**, *90*, 1609–1613.

9. Li, W.; Yue, J.; Liu, S. Preparation of nanocrystalline cellulose via ultrasound and its reinforcement capability for poly (vinyl alcohol) composites. *Ultrason. Sonochem.* **2012**, *19*, 479–485.

10. Johar, N.; Ahmad, I.; Dufresne, A. Extraction, preparation and characterization of cellulose fibres and nanocrystals from rice husk. *Ind. Crops Prod.* **2012**, *37*, 93–99.

11. Zaman, M.; Xiao, H.; Chibante, F.; Ni, Y. Synthesis and characterization of cationically modified nanocrystalline cellulose. *Carbohydr. Polym.* **2012**, *89*, 163–170.

12. Henriksson, M.; Henriksson, G.; Berglund, L. A.; Lindström, T. An environmentally friendly method for enzyme-assisted preparation of microfibrillated cellulose (MFC) nanofibers. *Eur. Polym. J.* **2007**, *43*, 3434–3441.

13. Li, R.; Fei, J.; Cai, Y.; Li, Y.; Feng, J.; Yao, J. Cellulose whiskers extracted from mulberry: A novel biomass production. *Carbohydr. Polym.* **2009**, *76*, 94–99.

14. Bondeson, D.; Mathew, A.; Oksman, K. Optimization of the isolation of nanocrystals from microcrystalline cellulose by acid hydrolysis. *Cellulose* **2006**, *13*, 171–180.

15. Jonoobi, M.; Oladi, R.; Davoudpour, Y.; Oksman, K.; Dufresne, A.; Hamzeh, Y.; Davoodi, R. Different preparation methods and properties of nanostructured cellulose from various natural resources and residues: A review. *Cellulose* **2015**, *22*, 935–969.

16. Lu, P.; Hsieh, Y. L. Preparation and properties of cellulose nanocrystals: Rods, spheres, and network. *Carbohydr. Polym.* **2010**, *82*, 329–336.

17. Lu, P.; Hsieh, Y. Lo Cellulose isolation and core-shell nanostructures of cellulose nanocrystals from chardonnay grape skins. *Carbohydr. Polym.* **2012**, *87*, 2546–2553.

18. Mohaiyiddin, M. S.; Lin, O. H.; Owi, W. T.; Chan, C. H.; Chia, C. H.; Zakaria, S.; Villagracia, A. R.; Akil, H. M. Characterization of nanocellulose recovery from Elaeis guineensis frond for sustainable development. *Clean Technol. Environ. Policy* **2016**, *18*, 2503–2512.

19. Liu, C.; Li, B.; Du, H.; Lv, D.; Zhang, Y.; Yu, G.; Mu, X.; Peng, H. Properties of nanocellulose isolated from corncob residue using sulphuric acid, formic acid, oxidative and mechanical methods. *Carbohydr. Polym.* **2016**, *151*, 716–724.

20. Du-Yeong Kim; Byoung-Min Lee; Koo, D. H.; Kang, P.-H.; Jeun, J.-P. Preparation of nanocellulose from a kenaf core using E-beam irradiation and acid hydrolysis. *Cellulose* **2016**, *23*, 3039–3049.

21. Nascimento, D. M. do; Almeida, J. S.; Vale, M. do S.; Leitão, R. C.; Muniz, C. R.; Figueirêdo, M. C. B. de; Morais, J. P. S.; Morsyleide, de, F, R. A comprehensive approach for obtaining cellulose nanocrystal from coconut fiber.Part I: Proposition of technological pathways. *Ind. Crops Prod.* **2016**, *93*, 66–75.

22. Alemdar, A.; Sain, M. Isolation and characterization of nanofibers from agricultural residues-wheat straw and soy hulls. *Bioresour. Technol.* **2008**, *99*, 1664–1671.

23. Shahabi-Ghahafarrokhi, I.; Khodaiyan, F.; Mousavi, M.; Yousefi, H. Preparation and characterization of nanocellulose from beer industrial residues using acid hydrolysis/ultrasound. *Fibers Polym.* **2015**, *16*, 529–536.

24. Kamphunthong, W.; Hornsby, P.; Sirisinha, K. Isolation of cellulose nanofibers from para rubberwood and their reinforcing effect in poly (vinyl alcohol) composites. *J. Appl. Polym. Sci.* **2012**, *125*, 1642–1651.

25. Deepa, B.; Abraham, E.; Cordeiro, N.; Mozetic, M.; Mathew, A. P.; Oksman, K.; Faria, M.; Thomas, S.; Pothan, L. A. Utilization of various lignocellulosic biomass for the production of nanocellulose: A comparative study. *Cellulose* **2015**, *22*, 1075–1090.

26. Tang, Y.; Yang, S.; Zhang, N.; Zhang, J. Preparation and characterization of nanocrystalline cellulose via low-intensity ultrasonic-assisted sulphuric acid hydrolysis. *Cellulose* **2014**, *21*, 335–346.

27. Elanthikkal, S.; Gopalakrishnapanicker, U.; Varghese, S.; Guthrie, J. T. Cellulose microfibres produced from banana plant wastes: Isolation and characterization. *Carbohydr. Polym.* **2010**, *80*, 852–859.

28. Nishiyama, Y.; Johnson, G. P.; French, A. D. Diffraction from nonperiodic models of cellulose crystals. *Cellulose* **2012**, *19*, 319–336.

29. Borysiak, S.; Garbarczyk, J. Applying the WAXS method to estimate the supermolecular structure of cellulose fibres after mercerisation.

Fibres Text. East. Eur. **2003**, *11*, 104–106.

30. Soyekwo, F.; Zhang, Q. G.; Lin, X. C.; Wu, X. M.; Zhu, A. M.; Liu, Q. L. Facile preparation and separation performances of cellulose nanofibrous membranes. *J. Appl. Polym. Sci.* **2016**, 24, *133*.

31. Peng, Y.; Gardner, D. J.; Han, Y.; Kiziltas, A.; Cai, Z.; Tshabalala, M. A. Influence of drying method on the material properties of nanocellulose I: Thermostability and crystallinity. *Cellulose* **2013**, *20*, 2379–2392.

32. Lani, N, S.; Nagadi, N.; Johari, A.; Jusoh, M. Isolation, characterization, and application of nanocellulose from oil palm empty fruit bunch fiber as nanocomposites. *J. Nanomater.* **2014**, *2014*, 13.

33. Naduparambath, S.; Purushothaman, E. Sago seed shell: Determination of the composition and isolation of microcrystalline cellulose (MCC). *Cellulose* **2016**, *23*, 1803–1812.

34. OSullivan, A. C. Cellulose: The structure slowly unravels. *Cellulose* **1997**, *4*, 173–207.

35. John, M. J.; Anandjiwala, R. D. Recent developments in chemical modification and characterization of natural fiber-reinforced composites. *Polym. Compos.* **2008**, *29*, 187–207.

36. Abraham, E.; Deepa, B.; Pothan, L. A.; Jacob, M.; Thomas, S.; Cvelbar, U.; Anandjiwala, R. Extraction of nanocellulose fibrils from lignocellulosic fibres: A novel approach. *Carbohydr. Polym.* **2011**, *86*, 1468–1475.

37. Fortunati, E.; Puglia, D.; Monti, M.; Peponi, L.; Santulli, C.; Kenny, J. M.; Torre, L. Extraction of cellulose nanocrystals from phormium tenax fibres. *J.Polym. Env.* **2013**, *21*, 319–328.

38. Xiang, Q.; Lee, Y. Y.; Pettersson, P. O.; Torget, R. W. *Biotechnology for fuels and chemicals: The twenty-fourth symposium, heterogeneous aspects of acid hydrolysis of α-cellulose*; Humana Press: Totowa, NJ, 2003;

39. Segal, L.; Creely, J. J.; Martin, A. E.; Conrad, C. M. An empirical method for estimating the degree of crystallinity of native cellulose using the X-Ray diffractometer. *Text. Res. J.* **1959**, *29*, 786–794.

40. Azubuike, C. P.; Rodríguez, H.; Okhamafe, A. O.; Rogers, R. D. Physicochemical properties of maize cob cellulose powders reconstituted from ionic liquid solution. *Cellulose* **2012**, *19*, 425–433.

41. French, A. D.; Santiago Cintrón, M. Cellulose polymorphy, crystallite size, and the Segal crystallinity index. *Cellulose* **2013**, *20*, 583–588.

42. Korotkov, A. N.; Voskoboinikov, I. V.; Konstantinova, S. A.; Gal'braikh, L. S.; Mikhailov, A. I. Some observations on obtaining cellulose nanocrystals. *Fibre Chem.* **2012**, *43*, 339–343.

43. Teixeira, E. de M.; Bondancia, T. J.; Teodoro, K. B. R.; Corrêa, A. C.; Marconcini, J. M.; Mattoso, L. H. C. Sugarcane bagasse whiskers: Extraction and characterizations. *Ind. Crops Prod.* **2011**, *33*, 63–66.

44. Chen, Y.; Liu, C.; Chang, P. R.; Cao, X.; Anderson, D. P. Bionanocomposites based on pea starch and cellulose nanowhiskers hydrolyzed from pea hull fibre: Effect of hydrolysis time. *Carbohydr. Polym.* **2009**, *76*, 607–615.

45. Cheng, Q.; Wang, S.; Rials, T. G.; Lee, S. H. Physical and mechanical properties of poly (vinyl alcohol) and polypropylene composite materials reinforced with fibril aggregates isolated from regenerated cellulose fibers. *Cellulose* **2007**, *14*, 593–602.

46. Jiang, F.; Hsieh, Y. L. Chemically and mechanically isolated nanocellulose and their self-assembled structures. *Carbohydr. Polym.* **2013**, *95*, 32–40.

47. Kargarzadeh, H.; Ahmad, I.; Abdullah, I.; Dufresne, A.; Zainudin, S. Y.; Sheltami, R. M. Effects of hydrolysis conditions on the morphology, crystallinity, and thermal stability of cellulose nanocrystals extracted from kenaf bast fibers. *Cellulose* **2012**, *19*, 855–866.

48. Lu, P.; Hsieh, You, L. Preparation and characterization of cellulose nanocrystals from rice straw. *Carbohydr. Polym.* **2012**, *87*, 564–573.

49. Martínez-Sanz, M.; Lopez-Rubio, A.; Lagaron, J. M. Optimization of the nanofabrication by acid hydrolysis of bacterial cellulose nanowhiskers. *Carbohydr. Polym.* **2011**, *85*, 228–236.

50. Wang, Y.; Wei, X.; Li, J.; Wang, F.; Wang, Q.; Chen, J.; Kong, L. Study on nanocellulose by high pressure homogenization in homogeneous isolation. *Fibers Polym.* **2015**, *16*, 572–578.

51. Paul B. Filson; Benjamin E; Dawson, A. Sono-chemical preparation of cellulose nanocrystals from lignocellulose derived materials. *Bioresour. Technol.* **2009**, *100*, 2259–2264.

52. Wang, N.; Ding, E.; Cheng, R. Thermal degradation behaviors of spherical cellulose nanocrystals with sulphate groups. *Polym.* **2007**, *48*, 3486–3493.

53. Berg, O. van den; Capadona, J. R.; Weder, C. Preparation of homogeneous dispersions of tunicate cellulose whiskers in organic solvents. *Biomacromolecules* **2007**, *8*, 1353–1357.

54. Mandal, A.; Chakrabarty, D. Isolation of nanocellulose from waste sugarcane bagasse (SCB) and its characterization. *Carbohydr. Polym.* **2011**, *86*, 1291–1299.

55. Samir, M. A. S. A.; Alloin, F.; Dufresne, A. Review of recent research into cellulosic whisker, their properties and their application in nanocomposites field. *Biomacromolecules* **2005**, *6*, 612–626.

56. Salim Khouri. Experimental characterization and theoretical calculations of responsive polymeric systems. M.Sc. dissertation, University of Waterloo, Waterloo, Canada. **2010**.

57. Morais, J. P. S.; Rosa, M. D. F.; De Souza Filho, M. D. S. M.; Nascimento, L. D.; Do Nascimento, D. M.; Cassales, A. R. Extraction and characterization of nanocellulose structures from raw cotton linter. *Carbohydr. Polym.* **2013**, *91*, 229–235.

58. Li, Y.; Liu, Y.; Chen, W.; Wang, Q.; Liu, Y.; Li, J.; Yu, H. Facile extraction of cellulose nanocrystals from wood using ethanol and peroxide solvothermal pretreatment followed by ultrasonic nanofibrillation. *Green Chem.* **2015**, *18*, 1010–1018.

59. Faradilla, R. H. F.; Lee, G.; Rawal, A.; Hutomo, T.; Stenzel, M. H.; Arcot, J. Nanocellulose characteristics from the inner and outer layer of banana pseudo-stem prepared by TEMPO-mediated oxidation. *Cellulose* **2016**, *23*, 3023–3037.

60. Levan. Thermal degradation, concise encyclopedia of wood &wood-based materials. *Pergamon Press. Elmsford, NY* **1989**, 271–273.

61. Morán, J. I.; Alvarez, V. A.; Cyras, V. P.; Vázquez, A. Extraction of cellulose and preparation of nanocellulose from sisal fibers. *Cellulose* **2008**, *15*, 149–159.

62. de Morais Teixeira, E.; Corrêa, A. C.; Manzoli, A.; de Lima Leite, F.; de Ribeiro Oliveira, C.; Mattoso, L. H. C. Cellulose nanofibers from white and naturally colored cotton fibers. *Cellulose* **2010**, *17*, 595–606.

63. Roman, M.; Winter, W. T. Effect of sulphate groups from sulphuric acid hydrolysis on the thermal degradation behaviour of bacterial cellulose. *Biomacromolecules* **2004**, 1671–1677.

CHAPTER 7

DEVELOPMENT OF BIO-NANOCOMPOSITS OF POLY (VINYL ALCOHOL) REINFORCED WITH CELLULOSE NANOCRYSTALS ISOLATED FROM SAGO SEED SHELLS

Abstract

The present chapter deals with the optimisation of cellulose nanocrystals isolated from sago seed shells, being used as reinforcement in PVA matrix. The bio-nanocomposite films developed were characterized by FTIR, ATR-FTIR, XRD, DSC, TG, UV-Visible, SEM, and AFM. Mechanical and biodegradability studies were also carried out. FTIR & ATR-FTIR analyses show the incorporation CNCs into the PVA matrix. This is further supported by XRD and DSC. TG analysis shows a slight increase in thermal stability for lower concentration of CNCs. UV-visible spectra exhibited no reduction in the transparency of composite film compared to neat PVA film. SEM and AFM further support the distribution of CNCs into the matrix. Among the composites 0.75 wt.% CNCs showed the highest tensile strength. Biodegradation through weight loss, tensile strength and SEM show increase in biodegradability of bio-nanocomposites compared to neat PVA.

7.1 INTRODUCTION

Composites having desirable properties have been used in diverse fields in many applications. Traditionally composites are filled with macro sized fillers like carbon black, silica, glass fibres, natural fibres etc. Nanocomposites are multi-phase materials, in which one of the constituents has dimension less than 100 nm, thus nanoparticles give ample opportunities for the development of high performance composites [1]. Polymer nanocomposites consist of thermoplastics, thermosets or elastomers, reinforced with small quantities of nano sized particles. Due to the high specific surface area, nanocomposites present a large volume of interphase, with properties different from those of the bulk, which can impart remarkable properties to composites [2]. Thus the uniform distribution of nanoparticles leads to a very large matrix-filler interfacial area, changing the molecular motion, relaxation behaviour and thus ensuring better thermal and mechanical properties [3,4]. Therefore, replacement of traditional composites by nanocomposite materials has grown up during the last two decades to overcome the limitations of the traditional composites.

Cellulose is one of the most abundant natural biopolymers, can produce nanomaterials like microfibrillated cellulose (MFC) or nanofibrillated cellulose (NFC) by mechanical force and naocellulose or nanowhiskers by acid hydrolysis. The impressive mechanical properties, reinforcing capability, abundance, low weight, crystalline cellulose having axial elastic modulus than Kevlar, reactive surface -OH groups, amenable for modification and biodegradability make them ideal candidates for the processing of polymer nanocomposite at low filler loadings [5,6]. Bio-nanocomposites are composites reinforced with renewable nanoparticles like cellulose whiskers or MFC and petroleum-derived polymers like PP, PE,

epoxies, etc., or biopolymers like PLA and PHA reinforced with synthetic or inorganic nanofillers like carbon nanotubes, nanoclay etc [1,7]. When both the matrix and nano reinforcement are biodegradable, we can also have green bio-nanocomposites.

As already discussed in previous chapters, PVA is a well-known synthetic polymer of great industrial value with many desirable characteristics. PVA degrades in microbial active environments within 5–6 weeks [8]. PVA and PVA-based composites are used in a wide range of applications, including filtration materials [9], paper coatings [10], films [11,12], mats [13] and packaging materials [14], as well as in medical field [15]. However, the low mechanical strength and integrity of PVA demand the use of reinforcing agents, for example, carbon nanotubes, cellulose nano fibres, chitin whiskers etc [8]. Since PVA is biodegradable, the growing emphasis on environmental awareness and search for new material focus on eco-friendly materials which are renewable, recyclable, sustainable and triggered biodegradable [16].

PVA and CNCs being hydrophilic both can be processed in an aqueous medium. Interaction between matrix and filler gets improved, dispersion of filler will be easy and moreover, the composite will be environmental friendly.

Ramaraj and Poomalai 2005 prepared PVA composites reinforced with different wt.% of coconut shell powder by aqueous mixing. Weight loss measurements showed that the biodegradability increased as the filler content increases [17]. Bana and Banthia 2007 studied the effect of Piyasal wood waste as filler in PVA containing glutaraldehyde as crosslinking agent, the biodegradability tests showed that wood dust increased the biodegradability of composites [18]. The same authors in 2011 added maleic anhydride-

modified wood dust as reinforcement in PVA by solvent casting, and studied their properties. The results also showed that the presence of wood dust enhanced the biodegradability of polymer composites [19].

Cellulose whiskers were isolated from cotton linter using acid hydrolysis by Roohani et al.2008 and used as filler in PVA. The effect of PVA having different molecular weights and degree hydrolysis on whisker addition was studied by conditioning the composite at various moisture contents. The results showed that reinforcing effect increased when the degree of hydrolysis of the matrix increases. This leads to an increase in the glass transition temperature, decrease of both the melting point and degree of crystallinity of the polymeric matrix in dry atmosphere. But increase in T_g was observed under humid condition on whiskers addition irrespective of degree of hydrolysis [20]. The effect of spherical nanocellulose, isolated from cotton linter and linen was studied by Ibrahim *et al*.2010, as reinforcement in PVA. Nanocomposite containing 20% of nanocellulose particles from linen increased the mechanical properties, while 40 and 60% resulted decreases in the tensile strength. The elongation at break of nanocomposite from linen is in the range 26.8–108.53% , but at 40% nanocellulose content, composites showed lower value than neat PVA [21].

Zhang *et al*.2011 used pan milling process to separate cellulose from bleached hardwood pulp fibers, used as reinforcement in PVA along with water and formamide as plasticizer. The tensile strength of cellulose/PVA composites increased from 8.8 MPa to 16.4 MPa, while elongation at break increased from 76.8% to 374%, when pan-milling cycles of cellulose increased. The composite exhibited enhanced thermal stability and better biodegradability [22]. Commercial MCC was used to isolate nanocellulose by Cho and Park in 2011 and used as reinforcement in PVA. The results showed

that as nanocellulose increases, tensile modulus and strength improved, but decreased for 7 wt.% of nanocellulose. DMA analysis showed improvement in storage modulus at 3 wt.% of nanocellulose. Thermal stability of the nanocomposite improved as the nanocellulose content increased up to 7 wt.% [23].

Ooi *et al*.2012 prepared films reinforced with Rambutan skin waste flour in PVA by solution casting, with and without cross linker in presence of glycerol as a plasticizer. Biodegradability through weight loss showed that, weight loss of non-cross linked films was higher than those of cross linked films [24]. Lexmeshwar *et al*.2012 studied the effect of modified cellulose using 2-(trifluromethyl) benzoylchloride by base catalysed reaction in PVA matrix. Soil burial test showed that composites have good biodegradation behaviour [25]. Zoltan *et al*.2012 prepared composites of PVA containing bacterial cellulose (BC) and chitosan (CTS) as fillers. Biodegradation results showed a relative high degradation of the BC/CTS/PVA film than BC/PVA [26].

Fortunati *et al*.2013 isolated CNC from Okra bahmia (*Abelmoschus Esculentus*) bast fibres and used as reinforcement in PVA. UV-visible spectra between 300 and 450 nm exhibited reduction in transmission, while at 650 nm showed constant transmission level of about 92%. TG indicated that maximum degradation rate was reduced with the addition of CNC to the PVA matrix up to 5 wt.% content. Moreover, at 5 wt.% cellulose content there was direct mechanical interaction between the PVA and cellulose structures [27]. Corn cob was used to isolate CNC using sulphuric acid at 45 ^{0}C for different times by Alves *et al*.2013 and studied their reinforcing capability in PVA. The composite containing nanocellulose with 60 minute hydrolysis duration showed an increase in tensile strength of 140.2% with 9 wt.% of CNC.

Moreover, visually the incorporation of CNC did not affected the transparency or homogeneity of the polymeric matrix [28]. Fortunati *et al* .2013 prepared PVA bio-nanocomposites reinforced with CNC extracted from commercial MCC and from natural fibres, Phormium tenax and Flax. Thermal analysis of composites showed that, CNC promotes the crystallization of the PVA matrix and TG showed that maximum degradation rate reduced with the addition of 5 wt.% CNC. Moreover, CNCs resulted in an increase in tensile strength of about 45% for MCC derived CNC-PVA and flax derived CNC-PVA composites compared to the PVA matrix. All CNC-PVA composites remain transparent and showed saturation level after the first 18–24 h of water absorption [29].

Mizanur *et al*.2014 isolated cellulose crystals (CC) from jute by chemical treatment followed by hydrolysis with 40% sulphuric acid and used as reinforcement in PVA. The tensile strength and modulus increased with CC up to 9% and decreased at higher loading [30]. Commercial MCC was used by Voronova *et al*.2015 to isolate CNC and used as reinforcement in PVA. The results showed that thermal stability of CNC-PVA composites enhanced with CNC content of 8–12 wt.%, decreased when more than 12 wt.% CNCs content was used [31].

Since the morphologies of cellulose nanocrystals depend to a large extent on the source and method of preparation, this in turn determines the reinforcing ability of nano particle. Cellulose nanocrystals prepared from other sources can be tried to check its reinforcing ability. Fillers will have large impact on the physio-chemical properties of composite when the reinforcing ability changes. Therefore, the main objective of the present chapter is to investigate the effect of cellulose nanocrystals as reinforcement in PVA by developing bio-nanocomposites.

7.2 RESULTS AND DISCUSSION

7.2.*1 Fabrication of bio-nanocomposite film*

Solution casting technique was used for the fabrication of bio-nanocomposites. Since cellulose nanocrystals contain negative charges due to considerable grafting during sulphuric acid hydrolysis, they form stable suspension in aqueous medium. Therefore can be easily processed in water along with PVA, which is also water soluble. The detailed method of fabrication has already been given in **Chapter 3.2.5**. Bio-nanocomposites fabricated are listed in **Table 7.1**.

Table 7.1 Bio-nanocomposite films.

Wt. of PVA (g)	Wt. % of CNC relative to PVA (g)	Composite films
5	0	5PVA
5	0.5	5PVA-0.5CNC
5	0.75	5PVA-0.75CNC
5	1	5PVA-1CNC

7.2.2 *FTIR and ATR-FTIR analyses*

Figure 7.1 (a) shows the FTIR spectra of the PVA and **Figures 7.1** (b), (c) and (d) show ATR-FTIR spectra of bio-nanocomposite. From **Figure 7.1** (a) the frequency at 3404 cm^{-1} is due to the stretching vibration of its side hydroxyl groups, 2921 cm^{-1} is due to CH_2 group stretching vibrations, 1712 cm^{-1} is due to C=O from residual acetate group or oxidation during manufacturing process present in the PVA. Frequency at 1435 cm^{-1} is attributed to O-H or C-H bending, or CH_2 deformations. Frequency at 1093

cm^{-1} is due to C-O stretching vibrations and 844 cm^{-1} is due to skeletal and CH_2 rocking and they are characteristic of neat PVA.

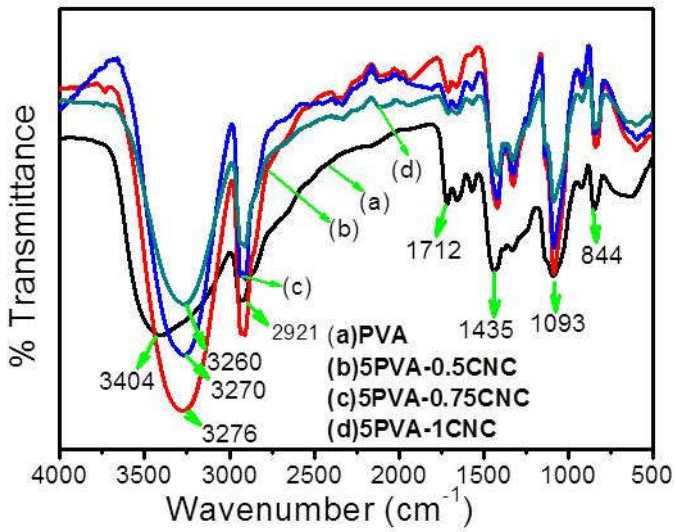

Figure.7.1 (a) FTIR spectra of PVA, (b) ATR-FTIR spectra of 5PVA-0.5CNC, (c) ATR-FTIR spectra of 5PVA-0.75CNC and (d) ATR-FTIR spectra of 5PVA-1CNC.

Comparing the **Figures 7.1** (a) with (b), (c) and (d), stretching frequency at 3404 cm^{-1} of neat PVA get shifted to 3276, 3270, 3260 cm^{-1} for PVA-0.5CNCs, 5PVA-0.75CNCs, 5PVA-1CNCs respectively, indicating the disruption of hydrogen bond existed in PVA film and possibility of formation of new hydrogen bond between -OH groups of PVA and CNCs due to sonication [27,29,32]. Moreover, the frequency at 1093 cm^{-1} does not make any shift, because the sulphuric acid hydrolysis will introduce sulphate group on cellulose nanocrystals, which in turn impart repulsive effect. The intensity of the band in the region of 1093 cm^{-1} increased with the addition of CNC to

the PVA matrix because of the contribution of C-O stretching from the cellulosic component [33].

7.2.3 *XRD analysis*

Figure 7.2 shows the XRD patterns of 5PVA film and 5PVA-CNC bio-nanocomposites. It was found that the XRD pattern **Figure 7.2** (a) of 5PVA film contains a narrow peak at $2\theta=19.4^0$ and peaks at $2\theta=22.0^0$ corresponding to the semi crystalline nature of pure PVA [34].

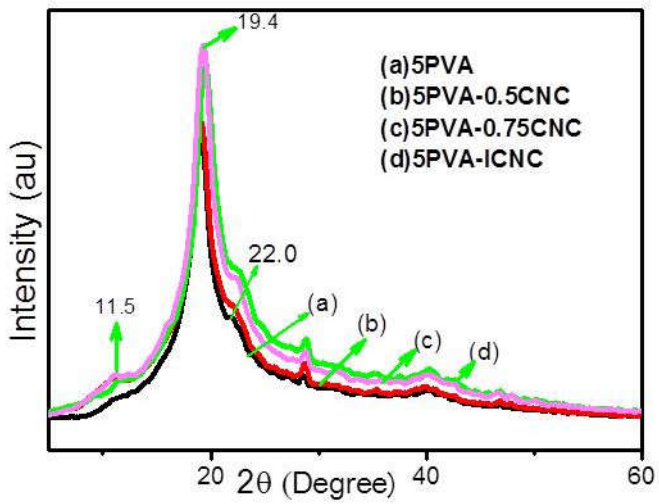

Figure 7.2 XRD patterns of (a) 5PVA film, (b) 5PVA-0.5CNC, (c) 5PVA-0.75CNC and (d) 5PVA-1CNC.

From **Figure 7.2** (b-d), it can be observed that diffractograms of the nanocomposite display the superposition of the characteristic peaks of the two components [31]. All the composites show strong peak at $2\theta=19.4$, 22.0 corresponding to PVA, suggesting that the crystal structure of PVA is essentially maintained even with the introduction of CNCs. Moreover, nanocomposites contains a diffraction peak at $2\theta=11.5^0$ due to the presence of

cellulose nanocrystals and becomes more pronounced when the CNCs concentration is increased [11,35]. The slight increase in crystallinity of PVA due to superposition of the peaks is further supported by DSC analysis.

7.2.4 *Differential scanning calorimetry (DSC)*

Figure 7.3 shows the DSC curves obtained for 5PVA film and 5PVA-CNCs bio-nanocomposites. Since PVA is a semi crystalline polymer, it has strong inter- and intra-chain interactions through hydrogen bonds in its structure [8]. Glass transition temperature (T_g), melting temperature (T_m) and heat of fusion (H_f) were determined for all the samples on the first heating scan. CNCs are highly crystalline and hence do not show any glass transition temperature (T_g) and no T_m for cellulose since it degrades prior to melting. As a result DSC thermogram mainly shows the PVA behaviour [36].

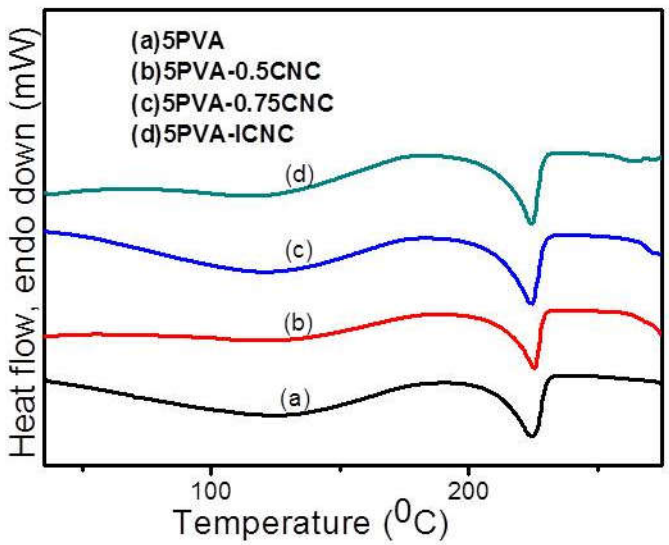

Figure 7.3 DSC curves of (a) 5PVA film, (b) 5PVA-0.5CNC, (c) 5PVA-0.75CNC and (d) 5PVA-1CNC

From **Figure 7.3** (a) 5PVA film exhibits sharp endothermic curve, with peak at 224.7 ^{0}C. There is also a specific heat increment observed around 75 ^{0}C, corresponding to T_g [11]. From **Figure 7.3** (b-d) T_g values of nanocomposites are 76 ^{0}C for 5PVA-0.5CNC, 76.5 ^{0}C for 5PVA-0.75CNC and 77 ^{0}C for 5PVA-1CNC respectively. The T_g values are slightly shifted to higher temperatures due to competitive interactions between PVA, water and CNC surface, ie., PVA/CNC and water/CNC interactions tend to shift T_g towards higher temperature [20,37]. From **Figure 7.3** (b-d) the melting temperatures are found to be 224.5, 224.2, and 224.1 ^{0}C for 5PVA-0.5CNC, 5PVA-0.75CNC and 5PVA-1CNC respectively. As the CNCs content increases the melting temperatures show a slight decrease indicating the incorporation of CNCs into the PVA matrix due to interactions between the CNCs and polymer matrix [8,20,31]. Crystalline domains are formed, by restriction in the polymer chains due to the interactions between CNCs and matrix [11,31]. This may lead to changes in crystallinity of host polymer matrix, because CNCs are able to promote the crystallization of the PVA matrix acting as heterogeneous nucleating agents [29]. The degree of crystallinity (X_p) of the composites was calculated using the **Equation 7.1**

$$X_p\ (\%) = \Delta H_f \times 100 / (w \times \Delta H^0_f) \text{ ----------} \textbf{7.1}\ [38]\textbf{.}$$

Where (ΔH_f) obtained from the area under the melting endotherms of each sample and w is the weight fraction of the polymer in the composite. The value 161.6 Jg^{-1} was used for the heat of fusion of 100% crystalline PVA (ΔH^o_f) [20]. T_g, T_m and the degree of crystallinity (X_p) are presented in **Table 7.2.** The degree of crystallinity was found to be slightly increased with the increase in CNC content [39].

Table 7.2 T_g, T_m and degree of crystallinity (X_p) of 5PVA and PVA-CNC bio-nanocomposites.

Polymer/ bio-nanocomposite	T_g (^{0}C)	T_m (^{0}C)	H_f Jg^{-1}	X_p (%)
5PVA	75	224.7	54.3	33.6
5PVA-0.5CNC	76	224.5	56.0	34.87
5PVA-0.75CNC	76.5	224. 2	58.04	36.17
5PVA-1CNC	77	224.1	58.25	36.04

7.2.5 *Thermogravimetry (TG)*

TG was used to study the thermal performance of 5PVA film and PVA-CNC bio-nanocomposite. All the films exhibited three distinct weight losses, initial weight loss in the region 70-140 ^{0}C is due to evaporation of water, consistent with similar observations [11,31].

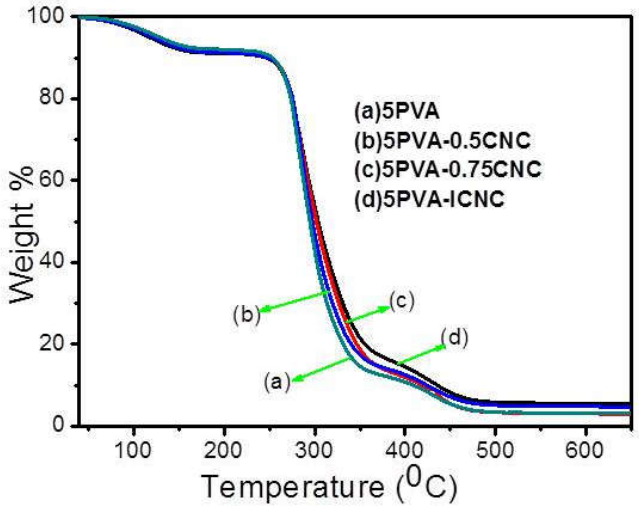

Figure 7.4 TG curves of (a) 5PVA film, (b) 5PVA-0.5CNC, (c) 5PVA-0.75CNC and (d) 5PVA-1CNC.

From **Figure 7.4** (a) for neat 5PVA, the second stage degradation occurs at the range of 254-340 ^{0}C, due to decomposition of side chain of PVA mainly involving dehydration reactions and the formation of volatile products. From **Figure 7.4** (b-d), the second stage degradation temperatures for nanocomposites are in the range of 257-346, 260-350, and 258-346 ^{0}C for 5PVA-0.5CNC, 5PVA-0.75CNC, and 5PVA-1CNC respectively. The onset thermal decomposition temperature (T_{on}) of PVA-CNC composites shifted slightly towards higher temperature, suggesting that the composite films had higher thermal stability mainly because of the presence of the crystal structure and interaction between CNCs and PVA [23,31,37]. The formation of additional hydrogen bonds between PVA and CNC, improves the decomposition temperature T_{on} in the second stage decomposition of composites. Among nanocomposite 5PVA-0.75CNC has slightly higher T_{on} due to higher interaction between CNCs and matrix. This is further supported by tensile strength measurement also. Above 500 ^{0}C, TG curves of all samples became flat, and mainly the residue remains. The third stage decomposition for 5PVA and for composites was found to be almost the same, which can be well understood from the DTG curves. The results obtained are presented in **Table 7. 3.**

Figure 7.5 shows the **DTG** curves of 5PVA and bio-nanocomposites. From **Figure 7.5** (b-c) the DTG_{max} of the PVA-CNCs composites shifted slightly to a higher temperature compared to that of pure PVA [**Figure 7.5** (a)]. But for 5PVA-1CNC, the DTG_{max} was found to be slightly lower than the 5PVA-0.75CNC may be due to reduced interfacial adhesion accounting possible agglomeration. The DTG curve temperature can also be used as a measure of thermal stability, as all the DTG_{max} of composites move to higher temperatures after the addition of CNCs, indicating that CNCs improve the thermal stability of the composites [23,35].

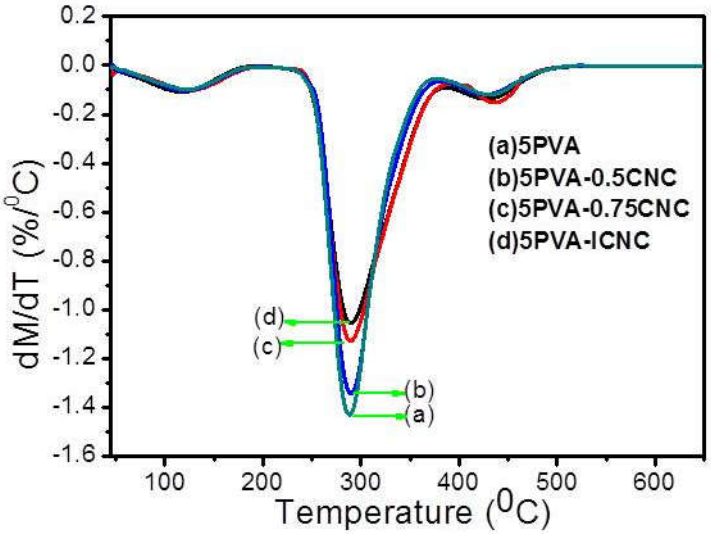

Figure 7.5 DTG curves of (a) 5PVA film (b) 5PVA-0.5CNC, (c) 5PVA-0.75CNC and (d) 5PVA-1CNC

The decomposition temperature corresponding to the maximum weight loss shows that the thermal decomposition behaviour of the composites is similar to that of the pure PVA. DTG results of 5PVA and bio-nanocomposites are also presented in **Table 7. 3**

Table 7.3 TG and DTG results of 5PVA and PVA-CNC bio-nanocomposites

Polymer/ Bio-nanocomposite	Second stage decomposition			Third stage decomposition	
	T_{on} (^{0}C)	T_{max} (^{0}C)	DTG_{max} (^{0}C)	T_{on} (^{0}C)	T_{max} (^{0}C)
5PVA	254	340	286	350	460
5PVA-0.5CNC	257	346	288	350	460
5PVA-0.75CNC	260	350	289	355	461
5PVA-1CNC	258	346	287	355	459

7.2.6 *UV-Visible spectra*

The light transmittance (Tr) of the composite films were studied by recording the UV-Visible spectra from 200 to 900 nm, which are shown in **Figure 7.6**. The bio-nano composites films exhibited higher Tr values at the visible region (400–800 nm) than the ultraviolet region (200–400 nm). The Tr values of 5PVA and bio-nanocomposite films are 80-85% in the region 400 to 900 nm, indicating their good transparency.

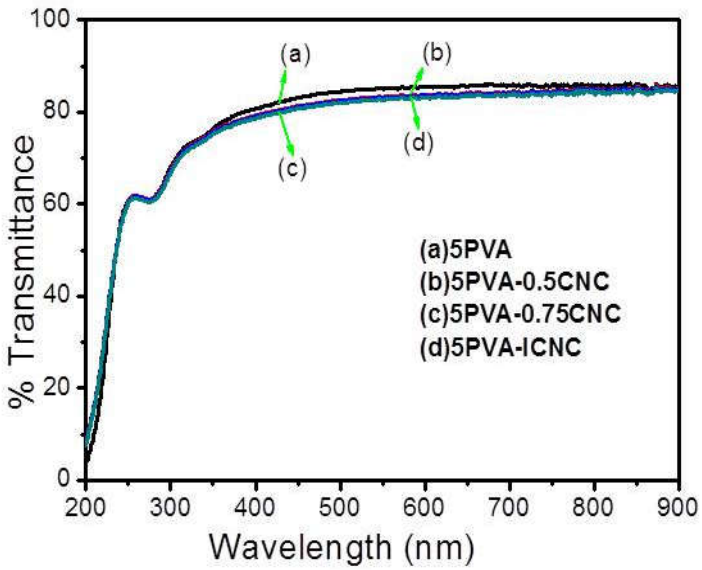

Figure 7.6 UV-Visible spectra of (a) 5PVA film, (b) 5PVA-0.5CNC, (c) 5PVA-0.75CNC and (d) 5PVA-1CNC.

From **Figure 7.6** (b-d) it can be clearly observed that there is no much reduction in transparency of composites films especially in 400-900 region, because particles are too small to scatter visible light [27,29]. Moreover, bio-nanocomposites have shown no shift in bands, indicating no

charge transfer or chemical change takes place during the incorporation of CNCs [40].

7.2.7 SEM analysis

Figure 7.7(a) shows fractured surface image of 5PVA, (b) 5PVA-0.75CNC and (c) 5PVA-1CNC. The fracture surface morphological character of the prepared pure 5PVA film and 5PVA-CNC composites have been investigated by SEM analysis by dipping in liquid nitrogen and the images are shown as **Figure 7.7**.

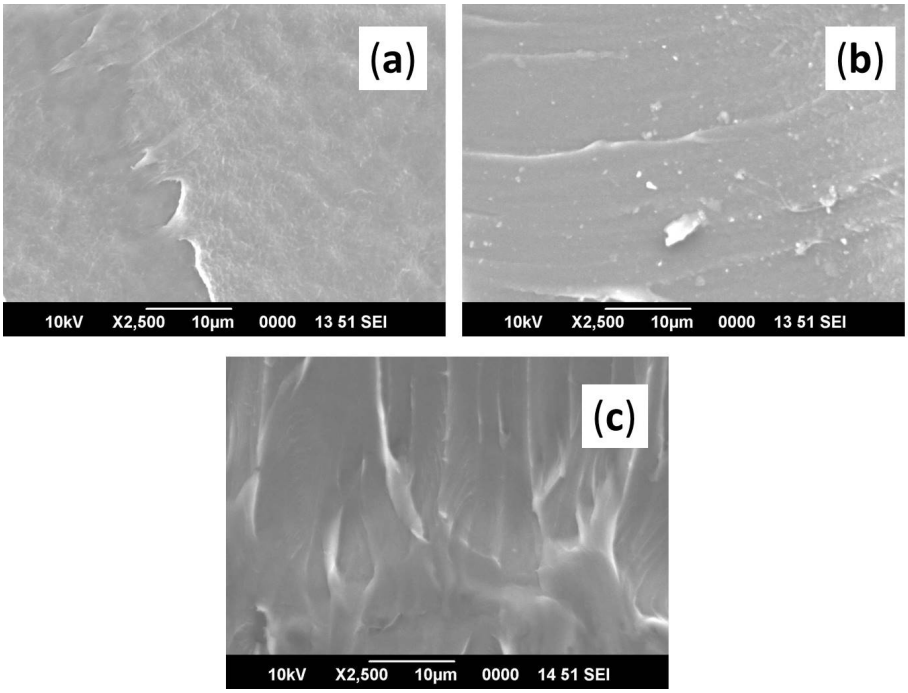

Figure 7.7 Fractured surface SEM images of (a) 5PVA, (b) 5PVA-0.75 CNCs and (c) 5PVA-1CNC.

From **Figure 7.7** (a) homogenous structure with smooth surface is observed for PVA film. From **Figure 7.7** (b) evidences for uniform

dispersion can be observed. The small CNCs appear as white dots, which are distributed evenly throughout the matrix, but rough texture was observed at higher CNC concentration for 5PVA-1CNC [**Figure 7.7** (c)] [11,20,41].

7.2.8 AFM analysis

Figures 7.8 (a-d) exhibit the AFM height images of 5PVA film and 5PVA-CNC bio-nanocomposites.

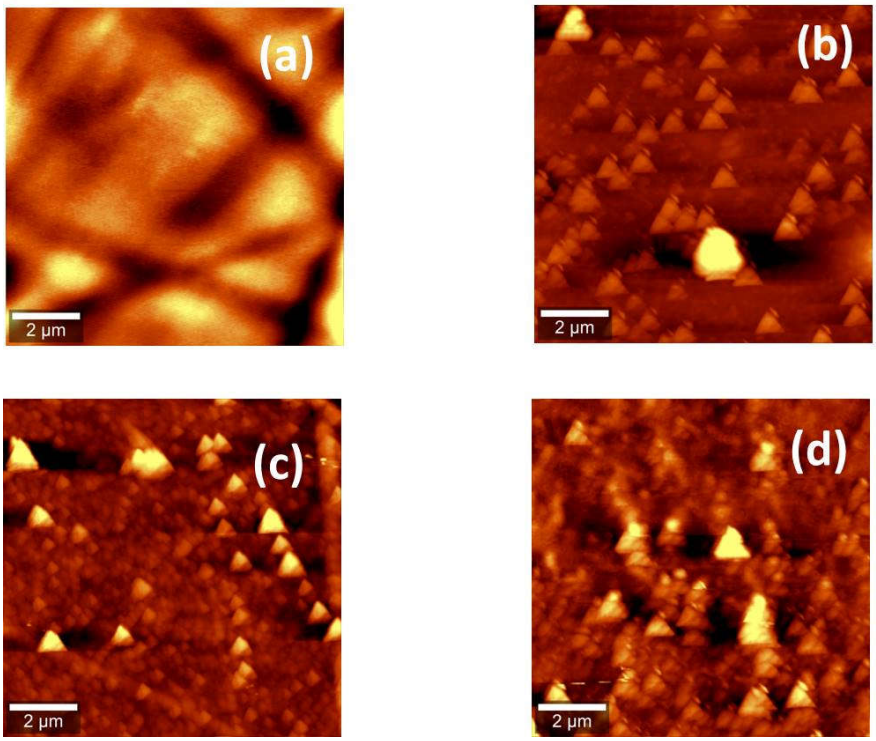

Figure 7.8 AFM height images (a) 5PVA film, (b) 5PVA-0.5CNC, (c) PVA-0.75CNC and (d) 5PVA-1CNC.

Figure 7.8 (a) AFM height image of 5PVA has light coloured regions which corresponds to crystalline regions and dark coloured corresponding to amorphous regions, indicating its semi crystalline nature,

which may arise from the random distribution of polymeric chains in an amorphous matrix [42]. **Figures 7.8** (b-d) show some bright coloured spots and it becomes more pronounced when CNC concentration increases. This clearly reveals the surface morphological change during the incorporation of CNC into PVA.

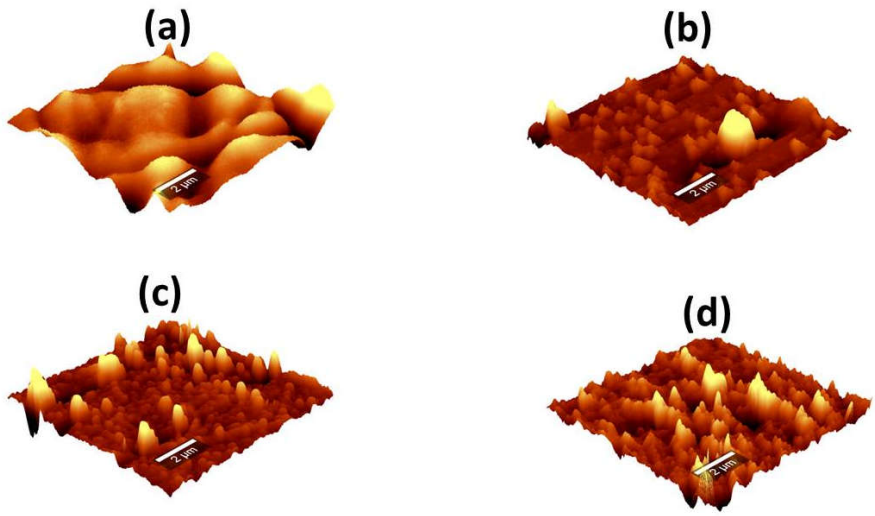

Figure 7.9 AFM 3D images (a) 5PVA film (b) 5PVA-0.5CNC (c) PVA-0.75CNC and (d) 5PVA-1CNC

Figures 7.9 (a-d) represents the AFM 3D images of 5PVA film and bio-nanocomposites. **Figure 7.9** (a), shows the AFM 3D image of 5PVA film, contains both amorphous and crystalline regions. Surface morphological changes of bio-nanocomposite films are visible in **Figure 7.9** (b-d). As the concentration of CNC increases there is remarkable change in the surface due to the incorporation of CNC. For 5PVA-1CNC, from **Figure 7.9** (d) more agglomerated structures were observed, which is further supported by SEM image **Figure 7.8** (c)

7.2.9 Mechanical properties

7.2.9.1 Tensile strength

The mechanical behaviour of 5PVA film and bio-nanocomposites were evaluated, the tensile strength values are graphically represented in **Figure 7.10**. It is well known that the mechanical properties of composites depend on nature of the matrix, reinforcement and on their interfacial adhesion. Pure film gives an average tensile strength of 32 MPa. Among the bio-nanocomposite 5PVA-0.75CNC has the highest tensile strength of 55 MPa, at higher loading the tensile strength is found to be decreasing. The enhancement in tensile strength is due to uniform distribution and better filler matrix interaction. Increase in tensile strength of PVA reinforced with nanocellulose has been reported in number of earlier studies [11,21,28,35,43,44].

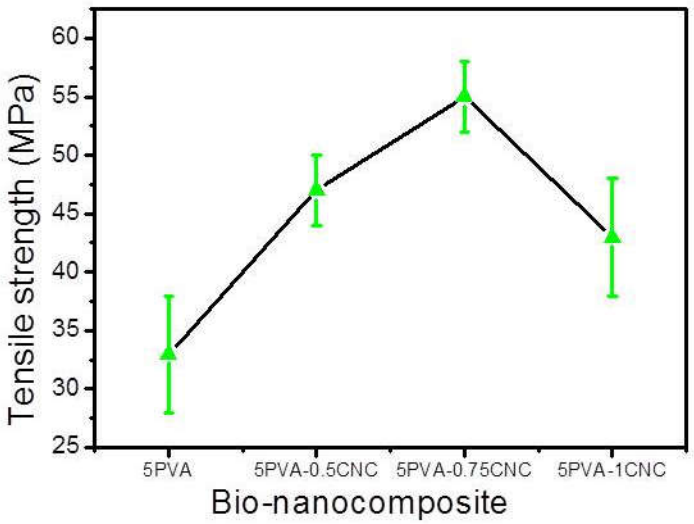

Figure 7.10 Tensile strength of 5PVA film and bio-nanocomposites.

The uniform distribution is further supported by SEM analysis also [**Figure 7.7** (b)]. Since PVA is hydrophilic in nature, there is a strong interfacial bonding between hydroxyl groups of CNCs with polymer, resulting in an increase in tensile strength of the composite film. The reinforcing ability of CNCs is attributed to the formation of rigid CNC networks, in which stress transfer is facilitated by hydrogen bonding between the CNCs. Van der Waal's interactions also shown to play a significant role. But CNC-CNC interactions can also lead to aggregation during the nanocomposite fabrication [45]. Therefore, at higher filler loading the tensile strength decreases. The formation of rigid network resulting from strong interactions between adjacent whiskers through hydrogen bonding was responsible for the mechanical behaviour of cellulose whiskers reinforced composites or the percolation of network held by hydrogen bonds. As degree of hydrolysis of PVA increases more –OH group in PVA chain results in the stronger PVA-CNC interaction [46].

7.2.9.2 Elongation at break

Figure 7.11 exhibits the elongation at break of 5PVA and bio-nanocomposites. The elongation at break is affected by the volume fraction of the added reinforcement, the dispersion in the matrix, and the interaction between the reinforcement and the matrix.

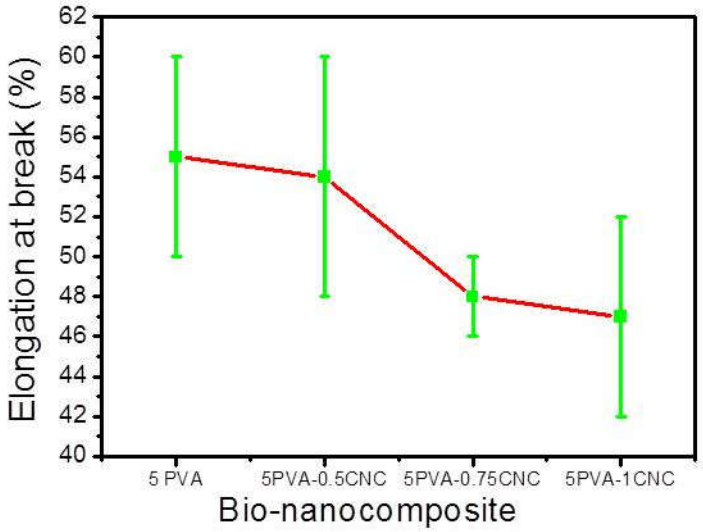

Figure 7.11 Elongation at break of 5PVA film and 5PVA- CNC bio-nanocomposites

It can be seen from the graph as the CNC content increases the elongation at break decreases [46]. The reduced elongation at break with the addition of filler in the polymer, is a common phenomenon observed in thermoplastic composites [27].

7.2.10 Biodegradation studies

7.2.10.1 Weight loss

Biodegradability evaluation is very important for eco-friendly materials for their commercial application. There are methods like enzymatic, microbial and soil burial which are used for monitoring the biodegradation. Evaluation by soil burial is mostly based on the weight loss of materials referring to the erosion of molecules from the solid phase. The indoor soil burial test carried out in plastic trays sprinked with water helps the microorganism to grow and degrade the bio-nanocomposites. The molecules

leached from the bio-nanocomposite films might be CNCs or PVA metabolites such as low molecular organic acids and ketonic compounds. These molecules can be easily degraded by microorganisms. **Figure 7.12** shows the weight loss of 5PVA and bio-nanocomposite after soil burial for 60 days.

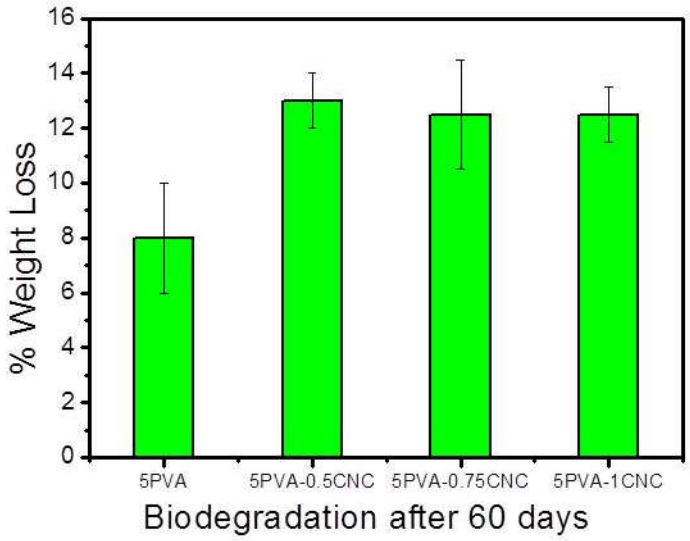

Figure 7.12 Weight losses during biodegradation of 5PVA and bio-nanocomposites

As shown in **Figure 7.12** all the bio-nanocomposites exhibited increased weight loss than neat PVA, indicating their better biodegradability [19,22]. Since cellulose component in the nanocomposites films is consumed by the microorganisms faster than PVA there is faster disintegration of bio-nanocomposites [47]. The soil burial test provides indirect indications of biodegradation. Since the number of micro-organism that degrades PVA were limited, microbial attack occurs, especially in environments containing continuous contamination by the polymer [48]. Eventhough, soil burial is an

easy and efficient method, the difficulties in removing the soil adhered on the surface and inside the sample, which are difficult to extract without damaging the specimens may cause error in assessing the residual mass [49].

7.2.10.2 Tensile strength

Figure 7.13 shows the tensile strength values of 5PVA and bio-nanocomposites before and after soil burial.

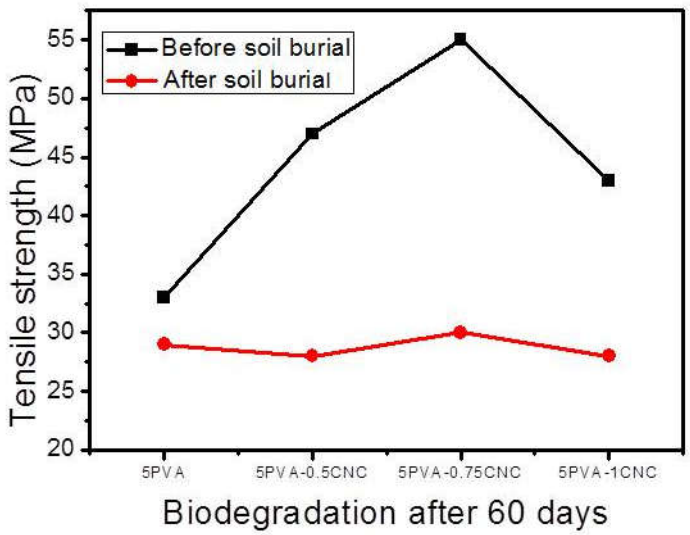

Figure 7.13 Tensile strength of 5PVA film, bio-nanocomposites before and after soil burial

It has been found that invariably there is decrease in tensile strength of neat 5PVA film and bio-nanocomposites after soil burial. The reduction in tensile strength is due to the erosion of filler particle due to biodegradation and physical deterioration of the composites.

7.2.10.3 SEM analysis

The surface morphological characters of the neat 5PVA film and bio-nanocomposites have been investigated by SEM analysis and the images are shown **Figure 7.14**. SEM images after biodegradation is a useful method to analyse the level and extent of biodegradation.

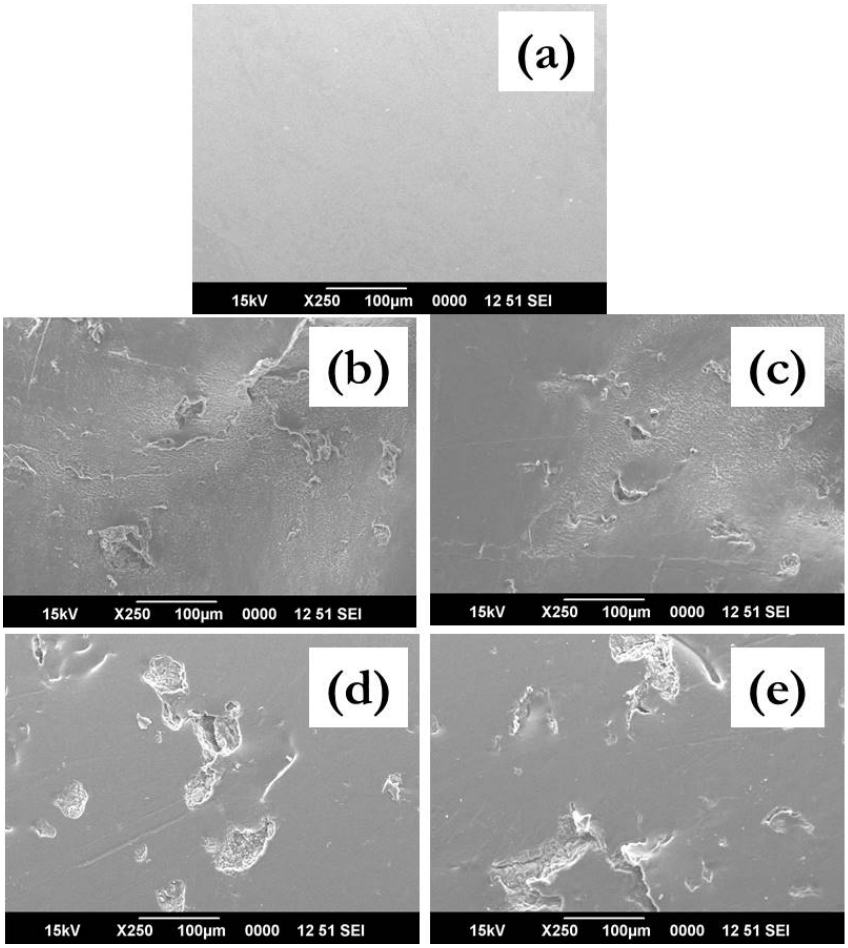

Figure 7.14 (a) SEM surface images of 5PVA before soil burial, (b) 5PVA film after soil burial, (c) 5PVA-0.5CNC after soil burial, (c) 5PVA-0.75CNC after soil burial and (d) 5PVA-1CNC after soil burial.

From **Figure 7.13** (a), the surface SEM image of neat 5PVA film exhibit homogenous with smooth surface having no characteristic surface defects. From **Figure 7.14** (b) that of 5PVA after soil burial shows evidences for biodegradation, due to heterogeneous and uneven surface. All bio-nanocomposites presented morphological modifications after the soil burial test. In comparison with the surface images of the neat PVA films, bio-nanocomposites are considerably destroyed which can be clearly observed from **Figures 7.14** (c-e). The microbial attack on the sample surface leads to massive surface erosion, increase in surface roughness, formation of cracks, grooves and voids seen, which increase as the CNC concentration increases [50–52]. The SEM micrographs add testimony to the results obtained from tensile strength after biodegradation.

7.3 CONCLUSION

Bio-nanocomposites reinforced with cellulose nanocrystals isolated from sago seed shells have been developed and optimised for better properties. The FTIR and ATR-FTIR give evidence for the incorporation of CNCs into the PVA matrix through hydrogen bonding, having lower –OH stretching frequency than PVA. XRD shows the super position of peaks for bio-nanocomposites. DSC analysis of bio-nanocomposite shows that, there is slight increase in crystallinity due to interaction between PVA and CNC. Moreover, they show marginal increase in glass transition temperature and slight decrease in melting temperatures. XRD and DSC results support each other. The uniform distribution is supported by SEM and surface morphological changes during the reinforcement with different amount of CNC were shown by AFM analysis. TG data reveals the increased thermal stability in the second stage decomposition for 5PVA-0.75CNC and almost same stability for bio-nanocomposites at the third stage. Among the bio-

nanocomposites 5PVA-0.75CNC has shown highest mechanical strength and showed 71.8% increase in tensile strength than neat PVA film. The improved mechanical properties of the composites have been attributed to the uniform distribution of cellulose nanocrystals in PVA matrix and decreased at higher concentration due to possible agglomeration. Moreover, bio-nanocomposites film showed good transparency and there is no reduction in the transparency by the addition of CNCs. The biodegradability studies through weight loss, tensile strength and SEM analysis show that, bio-nanocomposites have better biodegradability than neat PVA.

REFERENCES

1. Oksman, K.; Mathew, A. P.; Bondeson, D.; Kvien, I. Manufacturing process of cellulose whiskers/poly (lactic acid) nanocomposites. *Compos. Sci. Technol.* **2006**, *66*, 2776–2784.

2. Siqueira, G.; Bras, J.; Dufresne, A. Cellulosic bionanocomposites: A review of preparation, properties and applications. *Polym.* **2010**, *2*, 728–765.

3. Azeredo, H. M. C. De Nanocomposites for food packaging applications. *Food Res. Int.* **2009**, *42*, 1240–1253.

4. Schadler, L. S.; Brinson, L. C.; Sawyer, W. G. Polymer Nanocomposites: A small part of the story. *Nanocompsite Mater.* **2007**, 53–60.

5. Dufresne, A. Processing of polymer nanocomposites reinforced with polysaccharide nanocrystals. *Molecule* **2010**, *15*, 4111–4128.

6. Moon, R. J.; Martini, A.; Nairn; Simonsen, J.; Jeff, Y. Cellulose nanomaterials review: Structure, properties and nanocomposites. *Chem. Soc. Rev.* **2011**, *40*, 3941–3994.

7. Darder, B. M.; Aranda, P.; Ruiz-hitzky, E. Bionanocomposites: A new concept of ecological, bioinspired, and functional hybrid materials. *Adv. Mater.* **2007**, *19*, 1309–1319.

8. Virtanen, S.; Vartianen, J.; Tammelin, T.; Vuoti, S. Modified nanofibrillated cellulose–poly (vinyl alcohol) films with improved mechanical performance. *RSC Adv.* **2014**, *4*, 11343–11350.

9. Shang, Y.; Peng, Y. Research of a PVA composite ultrafiltration membrane used in oil-in-water. *Desalination* **2007**, *204*, 322–327.

10. Flieger, M.; Antorová, M. K.; Prell, A.; Rezanka, T.; Votruba, J. Biodegradable plastics from renewable sources. *Folia Microbiol.* **2003**, *48*, 27–44.

11. Lu, J.; Wang, T.; Drzal, L. T. Preparation and properties of microfibrillated cellulose poly (vinyl alcohol) composite materials. *Compos. Part A. Appl. Sci. Manuf.* **2008**, *39*, 738–746.

12. Tang, C.; Liu, H. Cellulose nanofiber reinforced poly (vinyl alcohol) composite film with high visible light transmittance. *Compos. Part A* **2008**, *39*, 1638–1643.

13. Peresin, M. S.; Habibi, Y.; Zoppe, J. O.; Pawlak, J. J.; Rojas, O. J. Nanofiber composites of poly (vinyl alcohol) and cellulose nanocrystals: Manufacture and characterization. *Biomacromolecules* **2010**, *11*, 674–681.

14. Bai, H.; Li, Y.; Wang, W.; Chen, G.; Rojas, O. J.; Dong, W.; Liu, X. Interpenetrated polymer networks in composites with poly (vinyl alcohol), micro- and nano-fibrillated cellulose (M/NFC) and poly HEMA to develop packaging materials. *Cellulose* **2015**, *22*, 3877–3894.

15. Karimi, A.; Navidbakhsh, M. Mechanical properties of PVA material for tissue engineering applications. *Mater. Technol. Adv. Perform. Mater.* **2014**, *29*, 90–100.

16. Satyanarayana, K. G.; Arizaga, G. G. C.; Wypych, F. Biodegradable composites based on lignocellulosic fibers-An overview. *Prog. Polym. Sci.* **2009**, *34*, 982–1021.

17. Ramaraj, B.; Poomalai, P. Ecofriendly poly (vinyl alcohol) and coconut shell powder composite films: Physico-mechanical, thermal properties, and swelling studies. *J. Appl. Polym. Sci.* **2005**, *102*, 3862–3867.

18. Bana, R.; Banthia, A. K. Green composites: Development of poly (vinyl alcohol)- wood dust composites. *Polym. Plast. Technol. Eng.* **2007**, *46*, 821–829.

19. Bana, R.; Banthia, A. K. Mechanical and dynamic analysis of poly (vinyl alcohol)-modified wood dust nanocomposite. *Polym. Plast. Technol. Eng.* **2011**, *50*, 667–673.

20. Roohani, M.; Habibi, Y.; Belgacem, N. M.; Ebrahim, G.; Naghi, A.; Dufresne, A. Cellulose whiskers reinforced poly (vinyl alcohol) copolymers nanocomposites. *Eur. Polym. J.* **2008**, *44*, 2489–2498.

21. Ibrahim, M. M.; El-zawawy, W. K.; Nassar, M. A. Synthesis and characterization of poly (vinyl alcohol)/nanospherical cellulose particle films. *Carbohydr. Polym.* **2010**, *79*, 694–699.

22. Zhang, W.; Yang, X.; Li, C.; Liang, M.; Lu, C.; Deng, Y. Mechanochemical activation of cellulose and its thermoplastic poly (vinyl alcohol) ecocomposites with enhanced physico-chemical properties. *Carbohydr. Polym.* **2011**, *83*, 257–263.

23. Cho, M.; Park, B. Tensile and thermal properties of nanocellulose-reinforced poly (vinyl alcohol) nanocomposites. *J. Ind. Eng. Chem.* **2011**, *17*, 36–40.

24. Ooi, Z. X.; Ismail, H.; Bakar, A. A.; Aziz, N. A. A. Properties of the crosslinked plasticized biodegradable poly (vinyl alcohol)/rambutan skin waste flour blends. *J. Appl. Polym. Sci.* **2012**, *125*, 1127–1135.

25. Laxmeshwar, S. S.; Kumar, D. J. M.; Viveka, S.; Nagaraja, G. K. Preparation and properties of biodegradable film composites using modified cellulose fibre-reinforced with PVA. *ISRN Polym. Sci.* **2012**, *2012*, 1–8.

26. Csaba, Zoltan, K. S.; Stroescu, M.; Stoica-Guzum, A.; Jinga, S. I.; Szilveszter, S.; Jipa, I.; Dobre, T. Biodegradation behavior of composite films with poly (vinyl alcohol) matrix. *J .Polym. Environ.* **2012**, *20*, 422–430.

27. Fortunati, E.; Puglia, D.; Monti, M.; Santulli, C.; Maniruzzaman, M.; Kenny, J. M. Cellulose nanocrystals extracted from Okra fibers in PVA nanocomposites. *J. Appl. Polym. Sci.* **2013**, *128*, 3220–3230.

28. Alves, H.; Pires, W.; Neto, F.; Oliveira, N.; Pasquini, D. Extraction and characterization of cellulose nanocrystals from corncob for application as reinforcing agent in nanocomposites. *Ind. Crops Prod.* **2013**, *44*, 427–436.

29. Fortunati, E.; Puglia, D.; Luzi, F.; Santulli, C.; Kenny, J. M.; Torre, L. Binary PVA bio-nanocomposites containing cellulose nanocrystals extracted from different natural sources: Part I. *Carbohydr. Polym.* **2013**, *97*, 825–836.

30. Mizanur, M, R.; Sanjida, A.; Haque, P. Characterization of crystalline cellulose of jute reinforced poly (vinyl alcohol) (PVA) biocomposite film for potential biomedical applications. *Prog. Biomater.* **2014**, *23*, 1–9.

31. Voronova, M. I.; Surov, O. V; Guseinov, S. S.; Barannikov, V. P.; Zakharov, A. G. Thermal stability of poly (vinyl alcohol)/nanocrystalline cellulose composites. *Carbohydr. Polym.* **2015**, *130*, 440–447.

32. Hema, M.; Selvasekerapandian, S.; Sakunthala, A.; Arunkumar, D.; Nithya, H. Structural, vibrational and electrical characterization of PVA-NH4Br polymer electrolyte system. *Phys. B* **2008**, *403*, 2740–2747.

33. Qua, E. H.; Hornsby, P. R.; Sharma, H. S. S.; Lyons, G.; McCall, R. D. Preparation and characterization of poly (vinyl alcohol) nanocomposites made from cellulose nanofibers. *J. Appl. Polym. Sci.* **2009**, *113*, 2238–2247.

34. Ricciardi, R.; Finizia, A.; Rosa, C.; Lauprêtre, F. X-ray diffraction analysis of poly (vinyl alcohol) hydrogels, obtained by freezing and thawing techniques. *Macromolecules* **2004**, *37*, 1921–1927.

35. Zhang, W.; He, X.; Li, C.; Lu, C.; Zhang, X.; Deng, Y. High performance poly (vinyl alcohol)/cellulose nanocrystals nanocomposites manufactured by injection molding. *Cellulose* **2014**, *21*, 485–494.

36. Qiu, K.; Netravali, A. N. Fabrication and characterization of biodegradable composites based on microfibrillated cellulose and poly (vinyl alcohol). *Compos. Sci. Technol.* **2012**, *72*, 1588–1594.

37. Liu, D.; Sun, X.; Tian, H.; Maiti, S.; Ma, Z. Effects of cellulose nanofibrils on the structure and properties on PVA nanocomposites. *Cellulose* **2013**, *20*, 2981–2989.

38. Azizi Samir, M. A. S.; Alloin, F.; Sanchez, J. Y.; Dufresne, A. Cellulose nanocrystals reinforced poly (oxyethylene). *Polym.* **2004**, *45*, 4149–4157.

39. Baheti, V.; Militky, J. Reinforcement of wet milled jute nano/micro particles in poly (vinyl alcohol) films. *Fibers Polym.* **2013**, *14*, 133–137.

40. Chen, Y.; Cao, X.; Chang, P. R.; Huneault, M. A. Comparative study on the films of poly (vinyl alcohol)/pea starch nanocrystals and poly (vinyl alcohol)/native pea starch. *Carbohydr. Polym.* **2008**, *73*, 8–17.

41. Paralikar, S. A.; Simonsen, J.; Lombardi, J. Poly (vinyl alcohol)/cellulose nanocrystal barrier membranes. *J. Memb. Sci.* **2008**, *320*, 248–258.

42. Sreeja, S.; Sreedhanya, S.; Smijesh, N.; Philip, R.; Muneera, C. I. Organic dye impregnated poly (vinyl alcohol) nanocomposite as an efficient optical limiter: Structure, morphology and photophysical properties. *J. Mater. Chem. C* **2013**, *1*, 3851–3861.

43. Peng, J.; Ellingham, T.; Sabo, R.; Turng, L.-S.; Clemons, C. M. Short cellulose nanofibrils as reinforcement in poly (vinyl alcohol) fiber. *Cellulose* **2014**, *21*, 4287–4298.

44. Bhatnagar, A.; Sain, M. Processing of cellulose nanofiber-reinforced composites. *J. Reinf. Plast. Compos.* **2005**, *24*, 1259–1267.

45. Capadona, J. R.; Kadhiravan, S.; Trittschuh, S.; Seidel, S.; Rowan, S. J.; Weder, C. Polymer nanocomposites with nanowhiskers isolated from microcrystalline cellulose. *Biomacromolecules* **2009**, *10*, 712–716.

46. Roohani, M.; Habibi, Y.; Belgacem, N. M.; Ebrahim, G.; Naghi, A.; Dufresne, A. Cellulose whiskers reinforced poly vinyl alcohol copolymers nanocomposites. *Eur. Polym. J.* **2008**, *44*, 2489–2498.

47. Bras, J.; Hassan, M. L.; Bruzesse, C.; Hassan, E. A.; El-wakil, N. A.; Dufresne, A. Mechanical, barrier, and biodegradability properties of bagasse cellulose whiskers reinforced natural rubber nanocomposites. *Ind. Crops Prod.* **2010**, *32*, 627–633.

48. Chiellini, E.; Corti, A.; Solaro, R. Biodegradation of poly (vinyl alcohol) based blown films under different environmental conditions. *Polym. Degrad. Stab.* **1999**, *64*, 305–312.

49. Goheen, S. M.; Wool, R. P. Degradation of polyethylene-starch blends in soil. *J. Appl. Polym. Sci.* **1991**, *42*, 2691–2701.

50. Campos, A. de; Marconato, J. C.; Martins-franchetti, S. M. Biodegradation of blend films PVA/PVC, PVA/PCL in soil and soil with landfill leachate. *Brazilian Arch. Biol. Technol.* **2011**, *54*, 1367–1378.

51. Raghul, S. S.; Bhat, S. G.; Chandrasekaran, M.; Francis, V.; Thachil, E. T. Biodegradation of poly (vinyl alcohol)-low linear density polyethylene-blended plastic film by consortium of marine benthic vibrios. *Int. J. Environ. Sci. Technol.* **2013**, *11*, 1827–1834.

52. Ooi, Z. X.; Chan, K. L.; Ewe, C. Y.; Muniyandi, M.; Teoh, Y. P.; Ismail, H. Evaluation of water affinity and soil burial degradation of thermoplastic film derived from oil palm ash-filled Polyvinyl alcohol. *Bioresour. com* **2015**, *12*, 4111–4122.

CHAPTER 8
DEVELOPMENT OF BIO-NANOCOMPSITES AS BARRIER MEMBRANE FOR PACKAGING APPLICATIONS

Abstract

This chapter presents the development of bio-nanocomposites as barrier membrane for packaging applications. The barrier properties like, water vapour transmission rate, moisture uptake and gas barrier were examined. Water vapour transmission rate and moisture uptake were found to be decreased as the CNC concentration increases. On contrary to this, nanocomposite film showed increase in oxygen transmission rate as the CNC increases.

8.1 INTRODUCTION

Packaging materials are used for protection of consumer goods against physical, biochemical, and microbiological attack. They should provide enough barriers against oxygen, water vapour, grease, and microorganisms etc [1]. Majority of manufactured plastics are used as packaging material due to their desirable properties like high specific strength, lightness, resistance to water and water-borne microorganisms, long durability, transparency, availability in large quantities at low cost, tear strength, good barrier properties to O_2 and aroma compounds and heat sealability [2,3]. Therefore, they are replaced by the conventional packaging materials like glass, metals, and ceramics in many fields. However, unlike materials such as glass or metals, polymers such as polyolefin, polyesters, polyamides, etc., which have been used mainly as packaging materials are permeable to gases, water vapour and volatile organic compounds like hydrocarbons or food flavors etc [4]. Eventhough, these are credited with many desirable properties they are nonbiodegradable.

The indiscriminate use of plastics in our daily life resulted in generation of huge amount of plastic wastes and disposal of these become serious concern as well as strong regulations and criteria for cleaner and safer environment, have directed the search for eco-friendly materials [5]. Biopolymers like starch, cellulose, PHA, PLA etc, obtained from renewable sources are alternative to synthetic nonbiodegradable polymers. Another way to increase the biodegradability is to incorporate biopolymers like starch, cellulose, or lignocellulosic material into the synthetic polymer matrix. Eventhough, starch is an abundant biopolymer; it has no physico-mechanical characteristics and processing properties good enough to allow the whole replacement of the composite materials based on synthetic polymers. The

products from starch are mostly water soluble and brittle. Some properties of starch can be improved by blending with synthetic polymers [6–8]. Cellulose is another abundant biopolymer used in packaging industry, but unfortunately common paper made from lignocelluloses does not provide sufficient barrier for water, oxygen or oil [1]. Therefore, biopolymer films have disabilities to obtain wide commercial applications. Moreover, the barrier properties of the biopolymers are not as good as conventional packaging materials derived from petroleum based polymers like PP, PE etc [9].

Since PVA has excellent chemical resistance, optical, physical properties and film forming ability, they find use in a number of fields. To enhance the barrier and performance, PVA is usually reinforced with polymer or fillers. Incorporation of naturally occurring polymers or fillers like cellulose or starch improves the eco-friendliness [6,10]. Eventhough, PVA has good oxygen barrier properties and mechanical properties in dry state; due to moisture sensitivity its applications are limited in this field. High moisture uptake and fast moisture transmission due to hydroxyl groups restricts its potential use in many applications. In order to widen the application of PVA, improvement in the water resistance properties of PVA is necessary and fillers have been incorporated to improve the water resistance properties [11].

The ability of a film to form a barrier is critical in the packaging industry and the most important properties are the oxygen transmission rate (OTR) and the water vapour transmission rate (WVTR). Water vapour and oxygen are two main permeates studied extensively in packaging applications, because they get transferred through the packaging material from internal or external environment, changing the quality of the product and shelf-life [12]. The factors which affect the barrier properties are nature of the permeant molecule like size, shape, polarity etc., temperature,

concentration of the permeate in the polymer and the nature of the polymer chain like flexibility, crystallinity, polarity etc [13].

Choi and Simonsen 2006 isolated cellulose nanocrystals (CNXLs) from Whatman 1 filter paper, used as filler in carboxymethyl cellulose (CMC) containing glycerine as plasticizer and compared the properties to that containing MCC. The results showed that the composites containing CNXLs improved the strength and stiffness than MCC. Moreover, nanocomposite become water resistant after heat treatment [14].

Cellulose nanocrystals (CNXL) isolated from Whatman 1 filter paper was studied as reinforcement in PVA along with Poly (acrylic acid) (PAA) as the cross linking agent by Paralikar *et al*. in 2008. Moisture transport gets reduced by the presence of CNXLs and PAA. The improvements in barrier performance were minimum for composites containing modified CNXL [15]. Fukuzumi *et al.* in 2008 prepared cellulose nano fibres by TEMPO mediated oxidation (TOCN). The results indicates that a thin layer of TOCN on the PLA film drastically decreased oxygen permeability of PLA film [16].

Avella *et al*. in 2012 prepared PVA based foams containing pulp cellulose fibres and microfibrillated cellulose (MFC). Foams containing pulp cellulose fibres showed reduction in water vapour absorption. Different swelling behaviour was observed for foams containing pulp cellulose and MFC fibres [17]. Fortunati *et al*.2012 isolated cellulose nanocrystals from MCC, modified by using surfactant (s-CNC) and used as reinforcement in PLA. Water permeability showed a reductions of 34% for films containing 1 wt.% of s-CNC, while composites containing 1 wt.% and 5 wt.% of modified and unmodified cellulose nanocrystals showed good oxygen barrier properties [18]. Chen *et al*.2012 isolated cellulose nanocrystals from potato peel and used as reinforcement in PVA along with thermoplastic starch.

Water vapour transmission measurements showed a marginal reduction in water permeability for the PVA composite, but starch composites showed no effect [19].

Abraham *et al*.2013 isolated nanocellulose from banana fibre by the steam explosion and used as the reinforcing filler in natural rubber (NR) latex. The transport of nonpolar organic solvents through composites decreased and the resistance increased with increasing the nanofibre content. Diffusion coefficient and the equilibrium solvent absorption was also found to be decreased with the addition of nanocellulose [20]. Lani *et al*.2014 isolated nanocellulose from oil palm empty fruit bunch fibre and studied their reinforcing effect in PVA/starch blend films. Good properties were shown by composites containing 5% (v/v) of nanocellulose. Water absorption of nanocellulose reinforced films was found to be lower than starch-PVA blend films [21]. Liu *et al*.2014 prepared foams of PVA reinforced with cellulose nanofibrils (CNF) through unidirectional freeze drying technology. Results showed that the incorporation of CNF at a weight ratio of 30 wt.% greatly enhanced the mechanical strength, modulus, water resistance, and dimensional stability of the composites [22]. Pereira *et al*.2014 isolated CNC from banana pseudostems fibres, and studied their effect as fillers in PVA. The Water vapour permeability (WVP) results showed that the incorporation of 5 wt.% CNCs decreased the WVP of pure PVA films from 0.61 ± 0.04 g.mm/kPa.h.m^2 to 0.44 ± 0.01 g.mm/kPa.h.m^2 [23].

Lim *et al*.2015 prepared PVA blend films by cross linking with boric acid (BA). As BA content increase up to 5% the oxygen transmission rate (OTR) of pure PVA decreased from 5.96 to 0.15 cc/m^2 day but water resistant pressure and tensile strength increased [11]. Lim *et al*.2016 also prepared poly (acrylic acid) cross linked PVA blend films. The oxygen transmission

rate of pure PVA decreased from 5.91 to 1.59 cc $m^{-1}day^{-1}$ with increasing PAA ratio and water resistance also increased [24].

Since no known pure polymer exhibits all the desired mechanical and barrier properties, they are often modified by using plasticizers, cross-linking agents, fillers and compatibilizers [25]. Nano clays have also been used in polymeric materials to improve the barrier properties [2]. No systematic studies have been reported on the barrier properties of bio-nanocomposites, especially on PVA containing CNCs without any cross linking agent. Therefore, the main objective of the present chapter is to study the barrier properties of PVA containing CNC with special emphasis on packaging application.

8.2 RESULTS AND DISCUSSION

8.2.1 Fabrication of barrier membranes

Solution casting technique was used for the fabrication of bio-nanocomposites as barrier membrane. Barrier membranes fabricated are listed in **Table 8.1.** The detailed method of fabrication has already been given in **Chapter 3.2.6.** The prepared membranes were labelled as 5PVA-0.5CNC, 5PVA-0.75CNC, 5PVA-1CNC, which contains 0.5, 0.75 and 1 wt.% of CNC respectively.

Table 8.1 Bio-nanocomposite as barrier membranes

Wt. of PVA (g)	Volume of solution used (mL)	Wt. % of CNC relative to PVA (g)	Barrier membrane
5	25	0	5PVA
5	25	0.5	5PVA-0.5CNC
5	25	0.75	5PVA-0.75CNC
5	25	1	5PVA-1CNC

8.2.2 Water vapour transmission rate (WVTR)

Table 8.2 shows the WVTR of bio-nanocomposites. The amount of the mass exchange between the packaged material and the external environment determines the permeability of packaging material. The weight loss when water molecule transferred is plotted against time, dividing the slope of this graph with area in m^2 gives WVTR of bio-nanocomposites in g h^{-1} m^{-2} **[Chapter 3.3.9.1]**. The transport of permeate molecules through polymeric materials is determined by the potential capacity of a polymer matrix to sorb the permeate molecules and the ability of those molecules to diffuse through the polymeric material [26]. WVTR is the measure of ability of moistures to cross the film. The values of WVTR are given in **Table 8.2.**

Table 8.2 WVTR values of 5PVA and bio-nanocomposite membranes

Polymer/ bio-nanocomposite membranes	WVTR (g h^{-1} m^{-2})
5PVA	16.5±0.5
5PVA-0.5CNC	16±0.2
5PVA-0.75CNC	15.7±0.2
5PVA-1CNC	15.4±0.3

As shown in **Table 8.2** all composite films exhibited slightly lower WVTR values compared to neat PVA film. When the CNC content increases, due to interaction between CNC and PVA, segmental motion and hence porosity in the polymer surface are reduced leading to low water vapour transmission. High degree of crystallinity of cellulose nanocrystals supplemented with composite structure formed due to rigid hydrogen bonded network were responsible for the slight reduction in WVTR by decreasing the effective diffusion and to increase tortuosity of the permeation path for water molecules [15,27]. The barrier properties get improved due to interactions

between water and CNCs, resulting in rearrangements of water molecules in the matrix, leading to lowering of plasticizing effect and improving the barrier properties of the material [19,28].

8.2.3 Moisture uptake (MU)

Figure 8.3 Illustrates the percentages of the MU for 5PVA and bio-nanocomposites at different periods of time calculated using the **Equation 3.1.** Eventhough, PVA is one of the important biodegradable polymers its poor resistance to water absorption limits its wide applications. Addition of fillers is an effective way of decreasing its moisture uptake [29].

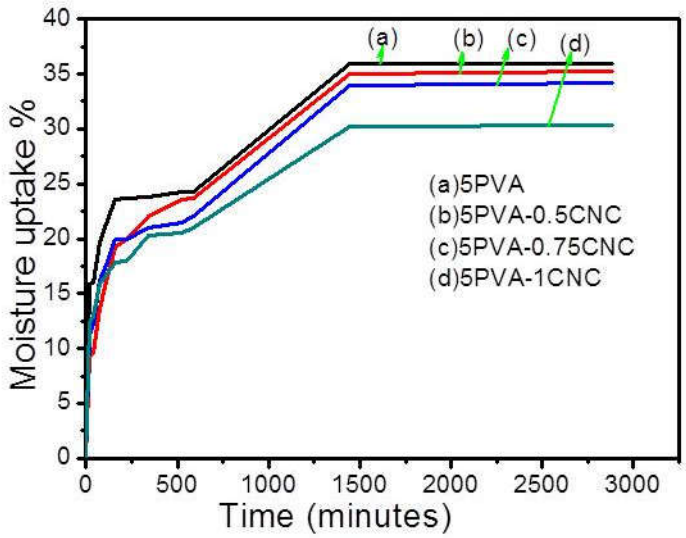

Figure 8.2 Moisture uptakes of (a) 5PVA, (b) 5PVA-0.5CNC (c) 5PVA-0.75CNC and (d) 5PVA-1CNC.

From **Figure 8. 2** it can be clearly observed that initially moisture uptake is rapid, then slowly increases and almost reach equilibrium in 48 hours. As the CNCs content increases MU % decreases. The hydroxyl group of cellulose nanocrystals with a compact chemical structure and having high

crystallinity are less accessible, therefore it would be expected to show only lower water uptake compared to PVA, leading to reduced moisture uptake [21,22,30,31]. Absorbed water molecules can accumulate in cellulose nanocrystals and at the polymer/cellulose nanocrystals interface. Since crystalline cellulose does not absorb significant amounts of water leaving only the CNC/polymer interface to accommodate most part of absorbed water molecules at equilibrium [32]. The formation of the network structure between the cellulose nanocrystals and PVA can also prevent the water molecules leading to improvement in the water resistance of the film [21].

8.2.4 Oxygen transmission rate (OTR)

Table 8.3 shows the OTR values of 5PVA and bio-nanocomposites. Hydrophobic polyolefin like polypropylene and polyethylene are characterised by low WVTR but high OTR, but cellophane, nanocellulose like cellulosic films have low OTR but have a very high WVTR [33].

Table 8.3 OTR values of 5PVA and bio-nanocomposite.

Polymer/bio-nanocomposite membranes	OTR (cm^3/m^2.24 hrs at 0.1 Mpa)
5PVA	10.729
5PVA-0.5CNC	11.849
5PVA-0.75CNC	12.125
5PVA-1CNC	14.065

From the **Table 8.3** it can be observed that the bio-nanocomposites shown slight increase in OTR values on the addition of CNCs. Contrary, CNC addition is not affected the oxygen transmission rate of bio-nanocomposites. For hydrophilic polymer like PVA, increasing the humidity

from 0 up to 100%, increases the oxygen permeability by a factor 2500 [34]. The barrier properties of hydrophilic polymers can be seriously affected by the presence of organic vapours and liquids that penetrate and plasticize the polymer. Moreover, polymers that contain hydroxyl groups like cellophane and amide groups like nylon 6, nylon 6,6, etc., show large increase in permeability as they absorb water [26]. The deterioration of oxygen barrier under humid conditions is therefore the main drawback, limiting the use of these polymers and composites in food packaging, especially for packaging high moisture foods or food which will lose quality when in contact with moisture or oxygen [34]. But for packaging fresh fruits and vegetables, high barriers to migration or gas diffusion are undesirable because shelf life is dependent on the availability of continued supply of oxygen for sustained cellular respiration. OTR values lower than 20 mL m^{-2} day^{-1} has been recommended for packaging applications. Since there are differences in the morphology of prepared cellulose nanocrystals the slight increase in the OTR values reveals the poor connectivity of the pores in the composite film [35]. Polymers such as polyethylene and polyethylene terephthalate do not change their barrier resistance when allowed to come into contact with moisture because the hydrophobic polymers do not absorb enough water to plasticize the polymer chains to cause an increase in gas permeability.

Nanocomposite containing bentonite has shown reduction in the permeability of the PLA while the MCC nanocomposite drastically increased the oxygen permeability of the PLA [36]. But there are reports on reduction in oxygen transmission rate on PLA by addition of cellulose nanocrytal [18]. The transport properties of gases through polymer films are governed by the tortuosity of their path, shape and aspect ratio of the filler, degree of exfoliation or dispersion, filler loading, orientation, adhesion to the matrix, moisture activity, filler induced crystallinity, polymer chain immobilization,

filler induced solvent retention and porosity [37]. However, to the best of our knowledge there are no prior literatures related to OTR values of the bio-nanocomposites of PVA reinforced with CNCs. The newly developed bio-nanocomposite materials, could find application in packaging industry in fields such as consumer and agriculture, like carriers for chemicals, fertilizers, pesticides etc. Many packaging applications demand certain barrier properties as well as mechanical resistance, therefore 5PVA-0.75CNC found to be better.

8.3 CONCLUSION

Bio-nanocomposite has been developed as barrier membrane with a view to using them for packaging application. The barrier properties of the membrane like, water vapour transmission rate, moisture uptake and oxygen transmission rate of these membranes were therefore examined. Water vapour transmission rate and moisture uptake were found to be decreased as the CNC concentration increases, which show resistance to moisture. However bio-nanocomposite films exhibit a slight increase in oxygen transmission rate. Since many packaging applications demand certain barrier properties as well as mechanical resistance, the bio-nanocomposites developed 5PVA-0.75CNC can be effectively used in place of PVA for better packaging application in consumer and agricultural fields.

REFERENCES

1. Nair, S. S.; Zhu, J. Y.; Deng, Y.; Ragauskas, A. J. High performance green barriers based on nanocellulose. *Sustain. Chem. Process* **2014**, *23*, 1–7.

2. Majeed, K.; Jawaid, M.; Hassan, A.; Bakar, A. A.; Khalil, H. P. S. A.; Salema, A. A.; Inuwa, I. Potential materials for food packaging from nanoclay/natural fibres filled hybrid composites. *Mater. Des.* **2013**, *46*, 391–410.

3. Tharanathan, R. N. Biodegradable films and composite coatings: Past, present and future. *Trends Food Sci. Technol.* **2003**, *14*, 71–78.

4. Amberg Schwab, S.; Hoffmann, M.; Bader, H.; Gessler, M. Inorganic-organic polymers with barrier properties for water vapor, oxygen and flavors. *Sol-Gel Sci. Technol.* **1998**, *2*, 141–146.

5. Bledzki, A. K.; Gassan, J. Composites reinforced with cellulose based fibres. *Prog. Polym. Sci.* **1999**, *24*, 221–274.

6. Debiagi, F.; Kobayashi, R. K. T.; Nakazato, G.; Panagio, L. A.; Mali, S. Biodegradable active packaging based on cassava bagasse, poly (vinyl alcohol) and essential oils. *Ind. Crops Prod.* **2014**, *52*, 664–670.

7. Kuchaiyaphum, P.; Punyodom, W.; Watanesk, S.; Watanesk, R. Composition optimization of poly (vinyl alcohol)/rice starch/silk fibroin-blended films for improving its eco-friendly packaging properties. *J. Appl. Polym. Sci.* **2013**, *129*, 2614–2620.

8. Jayasekara, R.; Harding, I.; Bowater, I.; Christie, G. B. Y.; Lonergan, G. T. Preparation, surface modification and characterisation of solution cast starch PVA blended films. *Polym. Test.* **2004**, *23*, 17–27.

9. Kim, J.; Shim, B. S.; Kim, H. S.; Lee, Y.; Min, S.; Jang, D.; Abas, Z.; Kim, J. Review of nanocellulose for sustainable future materials. *Int. J. Precis. Eng. Mnufacturing-Green Technol.* **2015**, *2*, 197–213.

10. Parvin, F.; Rahman, M. A.; Islam, Jahid, M, M.; Khan, M. A.; Saadat, A. H. M. Preparation and characterization of starch/PVA blend for biodegradable packaging material. *Adv. Mater. Res.* **2010**, *123*, 351–354.

11. Lim, M.; Kwon, H.; Kim, D.; Seo, J.; Han, H.; Khan, S. B. Highly-enhanced water resistant and oxygen barrier properties of cross-linked

poly (vinyl alcohol) hybrid films for packaging applications. *Prog. Org. Coatings* **2015**, *85*, 68–75.

12. Siracusa, V.; Rocculi, P.; Romani, S.; Rosa, M. D. Biodegradable polymers for food packaging: A review. *Trends Food Sci. Technol.* **2008**, *19*, 634–643.

13. Gordon, G. A.; Abraham, R. Oxygen transmission through highly crosslinked polymers. *Polym. Eng. Sci.* **1980**, *20*, 70–77.

14. Choi, Y.; Simonsen, J. Cellulose nanocrystal-filled carboxymethyl cellulose nanocomposites. *J. Nanosci. Technol.* **2006**, *6*, 633–639.

15. Paralikar, S. A.; Simonsen, J.; Lombardi, J. Poly (vinyl alcohol)/cellulose nanocrystal barrier membranes. *J. Memb. Sci.* **2008**, *320*, 248–258.

16. Fukuzumi, H.; Saito, T.; Iwata, T.; Kumamoto, Y.; Isogai, A. Transparent and high gas barrier films of cellulose nanofibers prepared by TEMPO-mediated oxidation. *Biomacromolecules* **2008**, *10*, 162–165.

17. Avella, M.; Cocca, M.; Errico, M. E.; Gennaro, G. Poly (vinyl alcohol) biodegradable foams containing cellulose fibres. *J. Cell. Plast.* **2012**, *48*, 459–470.

18. Fortunati, E.; Peltzer, M.; Armentano, I.; Torre, L.; Jiménez, A.; Kenny, J. M. Effects of modified cellulose nanocrystals on the barrier and migration properties of PLA nano-biocomposites. *Carbohydr. Polym.* **2012**, *90*, 948–956.

19. Chen, D.; Lawton, D.; Thompson, M. R.; Liu, Q. Biocomposites reinforced with cellulose nanocrystals derived from potato peel waste. *Carbohydr. Polym.* **2012**, *90*, 709–716.

20. Abraham, E.; Thomas, M. S.; John, C.; Pothen, L. A.; Shoseyov, O.; Thomas, S. Green nanocomposites of natural rubber/nanocellulose: Membrane transport, rheological and thermal degradation characterisations. *Ind. Crops Prod.* **2013**, *51*, 415–424.

21. Lani, N, S.; Nagadi, N.; Johari, A.; Jusoh, M. Isolation, characterization, and application of nanocellulose from oil palm empty fruit bunch fiber as nanocomposites. *J. Nanomater.* **2014**, *2014*, 13.

22. Liu, D.; Ma, Z.; Wang, Z.; Tian, H.; Gu, M. Biodegradable poly (vinyl alcohol) foams supported by cellulose nano fibrils: Processing, structure, and properties. *Langmiur* **2014**, *30*, 9544–9550.

23. Pereira, A. L. S.; Nascimento, D. M. do; Filho, M. de sá M. S.; Morais, J. P. S.; Vasconcelos, N. F.; Feitosa, J. P. A.; Brígida, A. I. S.; Rosa, M. de F. Improvement of poly (vinyl alcohol) properties by adding nanocrystalline cellulose isolated from banana pseudostems. *Carbohydr. Polym.* **2014**, *112*, 165–172.

24. Lim, M.; Kim, D.; Seo, J. Enhanced oxygen-barrier and water-resistance properties of poly (vinyl alcohol) blended with poly (acrylic acid) for packaging applications. *Polym. Int.* **2016**, *65,* 400-406.

25. Priya, B.; Kumar, V.; Pathania, D.; Singha, A. S. Synthesis, characterization and antibacterial activity of biodegradable starch/PVA composite films reinforced with cellulosic fibre. *Carbohydr. Polym.* **2014**, *109*, 171–179.

26. Zhang, Z.; Britt, I. J.; Tung, M. A. Permeation of oxygen and water vapor through EVOH films as influenced by relative humidity. *J. Appl. Polym. Sci.* **2001**, *82*, 1866–1872.

27. Saxena, A.; Ragauskas, A. J. Water transmission barrier properties of biodegradable films based on cellulosic whiskers and xylan. *Carbohydr. Polym.* **2009**, *78*, 357–360.

28. Roohani, M.; Habibi, Y.; Belgacem, N. M.; Ebrahim, G.; Naghi, A.; Dufresne, A. Cellulose whiskers reinforced poly (vinyl alcohol) copolymers nanocomposites. *Eur. Polym. J.* **2008**, *44*, 2489–2498.

29. Laxmeshwar, S. S.; Kumar, D. J. M.; Viveka, S.; Nagaraja, G. K. Preparation and properties of biodegradable film composites using modified cellulose fibre-reinforced with PVA. *ISRN Polym. Sci.* **2012**, *2012*, 1–8.

30. Cheng, Q.; Wang, S.; Rials, T. G. Poly (vinyl alcohol) nanocomposites reinforced with cellulose fibrils isolated by high intensity ultrasonication. *Compos. Part A* **2009**, *40*, 218–224.

31. Cao, X.; Chen, Y.; Chang, P. R.; Stumborg, M.; Huneault, M. A. Green composites reinforced with Hemp nanocrystals in plasticized starch. *J. Appl. Polym. Sci.* **2008**, *109*, 3804–3810.

32. Fortunati, E.; Puglia, D.; Luzi, F.; Santulli, C.; Kenny, J. M.; Torre, L. Binary PVA bio-nanocomposites containing cellulose nanocrystals extracted from different natural sources: Part I. *Carbohydr. Polym.* **2013**, *97*, 825–836.

33. Aspler, J. O. E.; Bouchard, J.; Hamad, W.; Berry, R.; Beck, S.; Drolet, F.; Zou, X. *Biopolymer nanocomposites: Processing, properties, and applications*; John Wiley & Sons, Inc, 2013;

34. Johansson, C.; Clegg, F. Hydrophobically modified poly (vinyl alcohol) and bentonite nanocomposites thereof: Barrier, mechanical, and aesthetic properties. *J. Appl. Polym. Sci.* **2015**, *13*, 132.

35. Chinga-carrasco, G.; Syverud, K. On the structure and oxygen transmission rate of biodegradable cellulose nanobarriers. *Nanoscale Res. Lett.* **2012**, *7*, 192.

36. Petersson, L.; Oksman, K. Biopolymer based nanocomposites: Comparing layered silicates and microcrystalline cellulose as nanoreinforcement. *Compos. Sci. Technol.* **2006**, *66*, 2187–2196.

37. Sanchez-garcia, M. D.; Gimenez, E.; Lagaron, J. M. Morphology and barrier properties of solvent cast composites of thermoplastic biopolymers and purified cellulose fibers. *Carbohydr. Polym.* **2008**, *71*, 235–244.

CHAPTER 9
SUMMARY AND OUTLOOK

Abstract

The major findings of the investigations on sago seed shells such as its composition, isolation of microcrystalline cellulose and cellulose nanocrystals have been summarised in this chapter. The fabrication of green composites of PVA reinforced with microcrystalline cellulose, bio-nanocomposites reinforced with cellulose nanocrystals and their characterisation using spectral, thermal, X-ray diffraction, morphological, mechanical properties and biodegradation have been consolidated. The utilization of bio-nanocomposites as barrier membrane has also been summarized. The scope for future studies based on the results of the present work has also been discussed.

Biomasses have been serving the civilisation from time immemorial in a number of fields, now investigated and exploited for the development of nanomaterials in diverse application. Biomasses are composed of polymers, oligomers, monomers, and other nonpolymerisable simple organic compounds, metallic salts etc. The major constituents present are cellulose, hemicellulose, lignins, pectins, extractives, inorganic compounds etc. Therefore, they are also referred as lignocellulosics. Among this cellulose, which is the most abundant biopolymer attracted much attention in recent years. The outstanding aspect of bio-mass or lignocellulosic material is their wide varieties which give ample opportunities in diverse fields. Traditionally they find use in households, production of charcoal, isolation various compounds and potential reinforcement in composites. Composite industries use different parts of plants and fruits of many agricultural crops as fillers. This gives non-food commercial applications to underutilized renewable materials. Another commercially important product obtained is microcrystalline cellulose (MCC) used in a number of fields. Since each application needs specific requirement, compositional analysis of biomass gains much momentum.

Synthetic polymers are considered to be the important gift of modern sciences and technology to mankind. They become unavoidable in our life owing to their wide range of applications in many fields such as packaging, agriculture, food, consumer products, medical appliances, building materials, industry, aerospace materials etc. However, the non-biodegradability has become the serious concern and severe environmental problems, including the difficulties in waste disposal have raised serious concerns all over the world. Therefore, the search for biodegradable polymer gains importance. Unfortunately, the degradable polymers available are associated with inferior

physical properties in terms of strength and dimensional stability, and above all most of them are expensive.

Therefore, there has been increasing demand for environment friendly materials with high performance at affordable costs in recent years with emphasis on renewable, recyclable, sustainable and triggered biodegradability. Since polymer alone cannot meet all the desirable properties they are often blended to achieve the required properties giving composites. Composites containing nanoparticle is another thrust area, they exhibit improved strength and stiffness, reduced gas and water vapour permeability and other intriguing desirable properties, opening opportunities for new high performance materials. Bio-nanocomposites, nanocomposites having biodegradable fillers like cellulose nanomaterials brought revolutions in material science in past few years.

Since PVA is the only carbon-carbon backbone polymer which is water soluble and biodegradable under both aerobic and anaerobic conditions, has the potential of being used as the matrix to produce biodegradable composites. Any source containing cellulose can be used for the isolation cellulose nanomaterials. There are two categories of cellulosic nanomaterials including microfibrillated cellulose and cellulose nanocrystals (CNC). The main objective of this study is to explore the possibility of using underutilised agricultural waste material sago *(Cycas circinalis)* seed shells for the isolation of MCC and CNC. Moreover, MCC and CNC can be potentially used as filler in PVA to fabricate green and bio-nanocomposite.

Chapter 1 gives an account of general background of composites, natural fiber reinforced composites and nanocomposites. Special reference is given to cellulose nanomaterials and use of PVA as the matrix. Chapter 2 covers a review on MCC reinforced composites, isolation of nanocellulose

and cellulose nanomaterial reinforced composites. The materials and various experimental techniques used in the investigations are briefly discussed in Chapter 3.

Since there are no report on the composition of the sago seed shells, establishing the composition is necessary to decide the feasibility of getting cellulose in reasonable amount. Chapter 4 gives an account of establishing the composition of sago seed shells, isolation of microcrystalline cellulose and their characterisation. ASTM methods were employed to establish the composition of sago seed shells, extractives were determined by ASTM D1107-96, klason lignin was determined by ASTM D1106-96, holocellulose was isolated by method described by Wise *et al* 1946, α-cellulose determined as per ASTM D 1103-60, hemicellulose by difference between holocellulose and α-cellulose and Ash content by T 211 om 02. The results obtained are presented in the table below

Name of component	Extractives	Klason lignin	Holo-cellulose	α-Cellulose	Hemi-cellulose	Ash content
Weight %	8.2±1	23.6±0.8	59.0±1.2	36.5±1	22.5±1	9.2±0.2

Analyses show that it has reasonably good lignin content and high cellulose, therefore sago seed shells can be used as a potential source for the extraction of cellulose.

FTIR spectra show the presence of lignin, holocellulose and α-cellulose. TG also reveals the presence of holocellulose and α-cellulose. Sago seed shells are having reasonably good α-cellulose content compared with other agricultural waste materials. Therefore, α-cellulose isolated has been converted into MCC by treating with 2.5N HCl. α-Cellulose and MCC exhibited similar FTIR spectra, but –OH stretching frequency was found to

be slightly less for MCC. TG shows similar decomposition temperatures for MCC and α-cellulose, but a well-defined curve was obtained for MCC. XRD pattern of α-cellulose exhibited cellulose I structure, but small amount of cellulose II was also present in MCC and the degree of crystallinity was found to be increased due to the removal amorphous regions. SEM analysis of MCC reveals the presence of aggregated and non-aggregated fibres, further supported by TEM. AFM analysis of MCC shows the presence of some spherical shapes with non-uniform and rough surfaces. TEM and AFM results reveal the microstructural behaviour of isolated MCC.

Since MCC is hydrophilic in nature and only very few reports are available on MCC reinforced composites, composites are fabricated using MCC as the filler. Therefore, PVA which is hydrophilic, water soluble and biodegradable is the most suitable matrix to form composite with MCC. The development of green composites of MCC reinforced PVA and their optimisations for better properties are presented in chapter 5. Green composites of PVA reinforced with MCC have been developed by solution casting into a glass plate and their composition was optimised for better properties. The prepared film was labelled as 5PVA-1MCC, 5PVA-2MCC, 5PVA-3MCC, which contains 1, 2 and 3 weight % of MCC relative to PVA weight. The FTIR, ATR-FTIR, XRD and DSC analyses supports the incorporation of MCC into the matrix. TG also substantiates the incorporation by showing increased onset thermal decomposition temperature for 5PVA-1MCC than neat PVA. The tensile strength of 5PVA-1MCC composite films increased slightly due to uniform distribution of particles in the polymer matrix and decreased at higher loading due to possible agglomeration. The uniform distribution and agglomeration are further supported by SEM and AFM analysis. The composites have good transparency, however slightly lower than glass.

The morphology of cellulose nanomaterials depends on the nature of source and method of preparation. Eventhough, large number of sources have been used for the isolation of CNC, there are only very few reports for their isolation from seed shells. Isolation of cellulose nanocrystals from sago seed shells and their characterisations are given in Chapter 6. CNCs have been successfully isolated from sago seed shells by sulphuric hydrolysis. FTIR spectra of CNCs reveal similar frequencies as that of α-cellulose. XRD pattern shows the co-existence of cellulose I and cellulose II with crystallite size of 9.4 nm. TEM analysis showed that the isolated CNCs contain networked structures and almost spherical shaped particles having 10-15 nm in size. The reductions in size during acid hydrolysis were revealed by SEM. The size of nanoparticle from AFM analysis was found to be approximately 50 nm, containing almost spherical shape and other shaped CNCs. DLS measurement shows that the CNCs have an average particle size of 50.4±3.1nm and zeta potential of -37.8 mV. CNCs exhibited lower onset decomposition temperature and different degradation behaviour compared to α-cellulose as shown by TG.

The fabrication of bio-nanocomposites of PVA reinforced with CNCs and their properties are presented in Chapter 7. Since CNCs have very high modulus they can be effectively used as reinforcement in polymers to fabricate bio-nanocomposites. Bio-nanocomposites were fabricated by solution casting into a glass plate and optimised for better properties. The prepared film was labelled as 5PVA-0.5CNC, 5PVA-0.75CNC, 5PVA-1CNC, which contains 0.5, 0.75 and 1 wt.% of CNC relative to PVA weight. The FTIR and ATR-FTIR show the interaction of CNC with the matrix through hydrogen bonding. XRD pattern shows the super position of peaks for bio-nanocomposites. DSC analysis of bio-nanocomposites shows that, there is slight increase in crystallinity of PVA due to interaction between

PVA and CNCs. 5PVA-0.75CNC exhibited slight increase in onset decomposition temperature as revealed by TG. The uniform distribution was also supported by SEM. The surface morphological changes during the reinforcement were shown by AFM analysis. Among the bio-nanocomposites 5PVA-0.75CNC has shown highest mechanical strength of 55 MPa, while neat film has 32 MPa. Improvement in mechanical properties of the bio-nanocomposite is due to the uniform distribution of CNCs in PVA matrix. The tensile strength decreased at higher concentration due to agglomeration. Moreover, there was no reduction in the transparency of bio-nanocomposite by the addition of CNCs. The biodegradability studies by weight loss, tensile strength and SEM analysis show that bio-nanocomposites have better biodegradability than neat PVA.

The development of bio-nanocomposites as barrier membrane for packaging application is explored in chapter 8. Bio-nanocomposite has been developed as barrier membrane for packaging applications. The barrier properties of the membrane like water vapour transmission rate, moisture uptake and gas barrier properties were examined. Water vapour transmission rate and moisture uptake were found to be decreased as the CNC concentration increases, which show the resistance to moisture. However, bio-nanocomposite shown slight increase in oxygen transmission rate. Since the bio-nancomposites meet the packaging requirements, the fabricated barrier membranes can be effectively used in place of PVA for better packaging application in consumer and agricultural fields. Many packaging applications demand certain barrier properties as well as mechanical resistance, therefore 5PVA-0.75CNC found to be better.

OUTLOOK

The present work gives opportunities for future investigators to look many aspects of green composites and bio-nanocomposites. Some recommendations for future research include:

- The oxygen transmission rate of bio-nanocomposites can be improved using hydrophobic nanoparticles. Moreover, this may also leads to further increase in water resistance while maintaining the other desirable properties like mechanical, thermal and biodegradability.
- Further investigations can be carried out on another cellulose source which has not been so far exploited.
- Cellulose can be isolated by other methods, since method of isolation has influence on the property of cellulose, MCC and CNC.
- MCC and CNC can be successfully used as filler in other hydrophilic matrices.
- MCC and CNC can be suitably modified and used as filler in different hydrophobic matrices.

APPENDIX

Refereed Journals

1. **Subair Naduparambath** and E. Purushothaman. Sago seed shell: Determination of the composition and isolation of microcrystalline cellulose (MCC). **Cellulose** (**2016**) **23**:1803–1812

2. **Subair Naduparambath**, M. P. Sreejith, T. V. Jinitha, V. Shaniba, K. B. Aparna, E. Purushothaman. Development of Green Composites of Poly (Vinyl Alcohol) Reinforced with Microcrystalline Cellulose Derived from Sago Seed Shells, **Polymer composites**, **2017 DOI;10.1002/pc.24307**

3. **Subair Naduparambath**, Jinitha T.V., Shaniba V., Sreejith M.P., Aparna K. Balan, Purushothaman. E. Isolation and characterisation of cellulose nanocrystals from sago seed shells. **Carbohydrate Polymers**, **2017, DOI;10.1016/j.carbpol.2017. 09.088**

4. Aparna K. Balan, Sreejith M.P., Shaniba V., Jinitha T.V., **Subair N**., Purushothaman E. Coconut shell powder reinforced thermoplastic polyurethane/natural rubber blend-composites: effect of silane coupling agents on the mechanical and thermal properties of the composites. Journal of Materials Science, 2017;52(11), 6712-6725.

Conference Proceedings

1. Aparna K. Balan., Sreejith M.P., Shaniba V., Jinitha T.V., **Subair N**., Purushothaman E. Transport behavior of aromatic hydrocarbons through coconut shell powder filled thermoplastic polyurethane/natural rubber blend-composites. ***AIP Conference Proceedings***, 2017; 1849 (1), 020046.

2. Shaniba V., Aparna K. Balan., Sreejith M.P, Jinitha T.V, **Subair N**., Purushothaman E. Effect of filler loading and silane modification on the biodegradability of SBR composites reinforced with peanut shell powder. ***AIP Conference Proceedings***, 2017; 1849 (1), 020049.

3. Sreejith M.P., Aparna K. Balan, Shaniba V., Jinitha T.V., **Subair N**., Purushothaman E. Biodegradation behavior of styrene butadiene rubber (SBR) reinforced with modified coconut shell powder. ***AIP Conference Proceedings***, 2017; 1849 (1), 020047.

Presentations

1. **Subair Naduparambath.**, M.P Sreejith., Shaniba V., Aparna K. Balan., Jinitha T.V. Green composites of poly (vinyl alcohol) and Microcrystalline cellulose". International conference on "Advanced materials (SCICON 16)" at Amrita Vishwa Vidyapeetham, Coimbatore19-21 December 2016 (ISBN: 978-93-86176-47-9)

2. **Subair Naduparambath.**, Jinitha T. V., Shaniba V., Aparna K Balan., Sreejith M. P. and Purushothaman E. Green nanocomposites of poly (vinyl alcohol) reinforced with cellulose nanocrystals isolated from sago seed shells". National conference "Biomaterials in Medicinal Chemistry" (BMC-2017), at Madurai Kamaraj University on 12-13 April 2017 (ISBN: 978-93-86568-01-4)